MIT-CTP 4375
LA-UR-13-20960

Using 1-Jettiness to Measure 2 Jets in DIS 3 Ways

Daekyoung Kang,[1] Christopher Lee,[2] and Iain W. Stewart[1]

[1] *Center for Theoretical Physics, Massachusetts Institute of Technology, Cambridge, MA 02139, USA*
[2] *Theoretical Division, MS B283, Los Alamos National Laboratory, Los Alamos, NM 87545, USA*

We predict cross sections in deep inelastic scattering (DIS) for the production of two jets—one along the proton beam direction created by initial state radiation (ISR) and another created by final state radiation after the hard collision. Our results include fixed order corrections and a summation of large logarithms up to next-to-next-to-leading logarithmic (NNLL) accuracy in resummed perturbation theory. We make predictions for three versions of a DIS event shape 1-jettiness, each of which constrains hadronic final states to be well collimated into two jets along the beam and final-state jet directions, but which differ in their sensitivity to the transverse momentum of the ISR from the proton beam. We use the tools of soft collinear effective theory (SCET) to derive factorization theorems for these three versions of 1-jettiness. The sensitivity to the ISR gives rise to significantly different structures in the corresponding factorization theorems—for example, dependence on either the ordinary or the generalized $k_\perp$-dependent beam function. Despite the differences among 1-jettiness definitions, we show that the leading nonperturbative correction that shifts the tail region of their distributions is given by a single universal nonperturbative parameter Ω_1, even accounting for hadron mass effects. Finally, we give numerical results for Q^2 and x values explored at the HERA collider, emphasizing that the target of our factorization-based analyses is to open the door for higher-precision jet phenomenology in DIS.

PACS numbers: 12.38.Cy,12.39.St,13.87.-a

Contents

I. INTRODUCTION

Deep inelastic scattering (DIS) of an energetic lepton from a proton target at large momentum transfer probes the partonic structure of the proton and the nature of the strong interaction, and was an important ingredient in the development of the theory of Quantum Chromodynamics (QCD) [1–6]. Modern DIS experiments at HERA and Jefferson Lab continue to illuminate the internal partonic structure of hadrons, yielding information on parton distribution functions of all types, as well as the value of the strong coupling α_s itself (see *e.g.* [7]). The precision of α_s extractions from DIS jet cross sections is currently limited by the availability of theoretical predictions only at NLO [7].

Predicting the dependence of such cross sections on jet algorithms, sizes, and vetoes to high accuracy currently presents a formidable challenge. The dependence on more "global" observables characterizing the jet-like structure of final states can often be predicted to much higher accuracy. Indeed, some of the most precise extractions of α_s today come from hadronic event shapes in e^+e^- collisions, for which theoretical predictions in QCD exist to N^{3}LL accuracy in resummed perturbation theory matched to N^{3}LO fixed-order results [8–14], along with a wealth of data from LEP. Using event shapes to describe jet-like final states in QCD in a global manner holds the potential to improve the description of jet production in DIS to the same high level of precision.

Thrust distributions in DIS were considered in [15] and calculated to NLL accuracy in resummed perturbation theory, matched to $\mathcal{O}(\alpha_s)$ fixed-order results analytically and compared to $\mathcal{O}(\alpha_s^2)$ fixed-order results calculated numerically [16, 17]. Since then the improvement of theoretical predictions for DIS event shapes beyond these orders of accuracy has not received much attention. The introduction of soft collinear effective theory (SCET) [18–22] has brought about a revolution in methods to achieve higher-order resummation in a variety of applications in QCD, leading, for example, to the N^{3}LL resummation of thrust [12] and heavy jet mass [13] in e^+e^- collisions mentioned above . SCET has been used to predict a wide variety of event shapes in e^+e^- collisions [23–25] and pp collisions [26–29], going beyond the resummed accuracy previously available. A wealth of data now exists on event shapes in DIS from measurements at HERA by the ZEUS and H1 collaborations [30–35]. To take advantage of these data, for instance to achieve high-precision extractions of α_s, requires commensurate accuracy in theoretical predictions. Thanks to advances already made in tools and calculations for e^+e^- and pp event shapes, the time is ripe to extend the accuracy of DIS event shape predictions beyond NLL. (DIS in the endpoint region, $x \to 1$, has been studied with SCET in [36–40].)

Traditional ways to define jet cross sections involve the use of a jet algorithm (such as k$_\mathrm{T}$-type recombination algorithms or infrared-safe cone algorithms [41–46]), and often a jet veto as well. Predicting the dependence on jet algorithms, sizes, and vetoes to high accuracy is currently a formidable theoretical problem in QCD. In particular, non-global logarithms (NGLs) [47, 48] can arise and complicate resummation beginning at NLL order for observables that probe soft radiation with different measures in sharply divided regions of phase space, as occurs with some jet vetoes, for instance [49–55]. Similar clustering logs due to the way algorithms cluster soft gluons can also spoil resummation beginning at NLL order [52, 53, 56–59]. NGLs and clustering logs limit the precision one can achieve in theoretical predictions for jet cross sections in QCD. A great deal of progress has been made to resum NGLs numerically in the large-N_C limit [47, 48], to understand the origin and structure of NGLs in the framework of effective field theory [54, 60–62], and to find ways to minimize their numerical impact (*e.g.* [29, 63]), but a generic approach to obtain NNLL and higher order predictions does not yet exist. These complications due to non-global methods of measuring jets provide a strong motivation to use *global* measurements of hadronic final states that still probe their jet-like structure and are resummable to arbitrarily high accuracy in QCD perturbation theory. The first steps needed for higher order resummation in DIS are the derivations of appropriate factorization theorems.

Precisely such a global measure of jet-like structure of hadronic final states is the N-jettiness introduced in [27]. N-jettiness τ_N is global event shape that is a generalization of thrust [64] and can be used in any type of collision to constrain the final state to contain $N+N_B$ jets, where N_B is the number of initial-state hadronic "beam" directions. In e^+e^- collisions, events with small τ_N contain N jets in the final state; in pp collisions, they contain $N+2$ jets, with two along the beam directions from initial state radiation (ISR). In DIS, small τ_N constrains events to have $N+1$ jets, with one jet along the beam direction from ISR from the proton.

In this paper we will predict a special case of N-jettiness cross sections in DIS, the 1-jettiness. We define a whole class of DIS 1-jettiness observables by

$$\tau_1 = \frac{2}{Q^2} \sum_{i \in X} \min\{q_B \cdot p_i, q_J \cdot p_i\}\,, \tag{1}$$

where q_B is a four-vector along the incident proton beam direction and q_J is another four-vector picking out the direction of the additional final-state jet we wish to measure. Particles i in the final state X are grouped into regions, according to which vector $q_{B,J}$ they are closer to as measured by the dot products in Eq. (1). Different choices of $q_{B,J}$ give different definitions of the 1-jettiness. In this paper we consider three such choices:

$$\tau_1^a: \qquad q_B^a = xP\,, \qquad q_J^a = \text{jet axis} \tag{2a}$$

$$\tau_1^b: \qquad q_B^b = xP\,, \qquad q_J^b = q + xP \tag{2b}$$

$$\tau_1^c: \qquad q_B^c = P\,, \qquad q_J^c = k\,, \tag{2c}$$

where P and k are the initial proton and electron momenta, and Q and x are the usual DIS momentum trans-

fer and the Björken scaling variable. The three versions of τ_1 in Eq. (2) are named for one of their distinctive properties: τ_1^a *aligns* the vector q_J^a with the physical jet axis as identified by a jet algorithm or by minimization of the sum in Eq. (1) over possible directions of q_J^a, see for example Ref. [65]. This jet axis is almost but not quite equal to $q+xP$, which is used as the vector q_J^b in τ_1^b. The measurement of τ_1^b groups final state particles in Eq. (1) into exact back-to-back hemispheres in the *Breit* frame. Finally, τ_1^c groups particles into exact back-to-back hemispheres in the *center-of-momentum* frame.

Note that the three τ_1's in Eq. (2) are physically distinct observables. Each one of them can be defined in any reference frame, but the definitions may be simpler in one frame versus another. The DIS 1-jettiness τ_1^a coincides with the version of 1-jettiness recently considered in [66] at NLL order, and is closest in spirit to the original N-jettiness event shape in [27]. No factorization theorems so far exist for either τ_1^b or τ_1^c.

There are in fact a number of DIS event shapes that have been measured by experiments at HERA. Two versions of thrust [64] were measured by the H1 Collaboration [30–32], and by the ZEUS collaboration [33–35]. The DIS thrust variables $\tau_{\hat{n}E}$ are all based on hemispheres in the Breit frame where the thrust axis $\hat{n}$ is either frozen to $\hat{z}$ (along the virtual γ or weak boson), or determined from a minimization. They have been computed to NLL+$\mathcal{O}(\alpha_s)$ [15, 48]. The $\tau_{\hat{n}E}$ measure particles from only one hemisphere, and the choice of normalization E determines whether they are global or non-global [48] (where the non-global variables were used for the experimental measurements). Our 1-jettiness event shapes defined in Eqs. (1) and (2) are global variables, avoiding NGLs by including information from all particles in the final state. We will demonstrate that our DIS 1-jettiness variable τ_1^b actually exactly coincides with the DIS thrust $\tau_Q \equiv \tau_{\hat{z}Q}$, computed in [15] at NLL+$\mathcal{O}(\alpha_s)$.

It would be interesting to re-analyze HERA data to measure global 1-jettiness or thrust variables. For such measurements, one may be concerned about the contribution of the proton remnants to Eq. (1). However, the remnants remain close to the q_B axis, so their contributions to the sum giving τ_1 are exponentially suppressed [67]. It is only the larger-angle soft radiation and ISR in the beam region and the collision products in the q_J region that need to be measured. In fact, we will show below that one *can* measure $\tau_1^{a,b,c}$ only from the products in the q_J region, obtaining the q_B-region contributions by momentum conservation (however for τ_1^a this is true only in the two-jet region $\tau_1^a \ll 1$).

We will give predictions for cross sections in the three versions of τ_1 in Eq. (2) accurate for small τ_1. We will also prove factorization theorems for all three variables $\tau_1^{a,b,c}$. The structure of these factorization theorems will differ because $\tau_1^{a,b,c}$ each probe initial- and final-state radiation in DIS differently. Besides grouping final-state hadrons into different regions, each version has a different sensitivity to the transverse momentum of ISR. For τ_1^b and τ_1^c, the nonzero $k_\perp$ of ISR causes the final-state jet momentum to deviate from the q_J axis by an amount $\simeq k_\perp$ due to momentum conservation. This affects the measurement of τ_1^b or τ_1^c at leading order. For τ_1^a, q_J^a is always aligned with the physical jet momentum and so is insensitive to the $k_\perp$ of ISR at leading order. This leads to different structures in the factorization theorems for $\tau_1^{a,b,c}$.

We will prove that the cross sections in all three variables factorize as special cases of the form:

$$\begin{aligned}\frac{d\sigma}{dx\,dQ^2\,d\tau_1} &= \frac{d\sigma_0}{dx\,dQ^2}\sum_\kappa H_\kappa(Q^2,\mu)\int dt_J dt_B dk_S d^2\mathbf{p}_\perp \\ &\quad\times J_q(t_J-(\mathbf{q}_\perp+\mathbf{p}_\perp)^2,\mu)\,\mathcal{B}_{\kappa/p}(t_B,x,\mathbf{p}_\perp^2,\mu) \\ &\quad\times S_{\rm hemi}(k_S,\mu)\,\delta\Big(\tau_1-\frac{t_J}{s_J}-\frac{t_B}{s_B}-\frac{k_S}{Q_R}\Big)\,, \end{aligned} \tag{3}$$

where κ runs over quark and antiquark flavors, s_J, s_B, Q_R are normalization constants given in Eqs. (54) and (58) that depend on the choice of observable τ_1 in Eq. (2). σ_0 is the Born cross section, H_κ is a hard function arising from integrating out hard degrees of freedom from QCD in matching onto SCET, J_q is a quark jet function describing collinear radiation in the final-state jet, and $\mathcal{B}_{\kappa/p}$ is a quark beam function containing both perturbative collinear radiation in a function $\mathcal{I}_{\kappa j}$ as well as the proton parton distribution function (PDF) $f_{j/p}$:

$$\mathcal{B}_{\kappa/p}(t,x,\mathbf{p}_\perp^2,\mu) = \sum_j \int_x^1 \frac{dz}{z}\,\mathcal{I}_{\kappa j}\Big(t,\frac{x}{z},\mathbf{p}_\perp^2,\mu\Big)\,f_{j/p}(z,\mu). \tag{4}$$

This beam function depends on the transverse virtuality t_B of the quark κ as well as the transverse momentum $\mathbf{p}_\perp$ of ISR. $S_{\rm hemi}$ in Eq. (3) describes soft radiation from both the proton beam and the final-state jet. Despite the fact that the 1-jettiness Eq. (1) may not divide the final state into hemispheres, we will nevertheless show that the soft function for any 1-jettiness in DIS is related to the hemisphere soft function $S_{\rm hemi}$. Finally, $\mathbf{q}_\perp$ is the transverse momentum of the momentum transfer q in the DIS collision with respect to the jet and beam directions.

We briefly discuss differences in the factorization theorem for $\tau_1^{a,b,c}$. For τ_1^a, the jet axis is aligned so that the argument of the jet function $t_J-(\mathbf{q}_\perp+\mathbf{p}_\perp)^2 \to t_J$ with zero transverse momentum, and $\mathbf{p}_\perp$ then gets averaged over in Eq. (3), removing the dependence on this variable in the beam function and yielding the ordinary beam function of Ref. [67]. For τ_1^b, τ_1^c, the convolution over $\mathbf{p}_\perp$ remains and thus they are sensitive to transverse momentum of ISR. Thus for τ_1^b, τ_1^c results depend on generalized $\mathbf{p}_\perp$-dependent beam function introduced in Ref. [68]. The final difference is that $\mathbf{q}_\perp$ is identically zero for τ_1^b, while it is nonzero for τ_1^c, causing these observables to differ and inducing additional complications in the convolution over $\mathbf{p}_\perp$ for τ_1^c. In particular the cross section for τ_1^c does not start at $\tau_1^c = 0$, but rather at

$\tau_1^c = \mathbf{q}_\perp^2/Q^2$ due to the nonzero $\mathbf{q}_\perp$ injected into the collision and the choice here for the jet axis.

The ingredients in the factorization theorem Eq. (3) depend on an arbitrary scale μ that arises due to integrating out degrees of freedom from QCD, matching onto a theory of collinear and soft modes, and then integrating out collinear degrees of freedom and matching onto just soft modes. The resulting hard, jet, beam, and soft functions each depend on logs of μ over physical variables. Renormalization group (RG) evolution allows us to evolve each function from a scale $\mu_{H,J,B,S}$ where these logs are minimized to the common scale μ. This evolution resums logs of $\tau_1^{a,b,c}$ to all orders in α_s, to a given order of logarithmic accuracy determined by the order to which we know the anomalous dimensions for the RG evolution. We will use this technology to resum logs of 1-jettiness in DIS to NNLL accuracy for $\tau_1^{a,b,c}$.

The factorized cross section in Eq. (3) accurately predicts the τ_1 distribution in the peak region and for the tail to the right of the peak, where $\tau_1 \ll 1$ and logs of τ_1 are large. To be accurate for larger τ_1, the prediction of Eq. (3) must be matched onto predictions of fixed-order QCD perturbation theory to determine the "nonsingular" terms. In this paper we do not perform the matching onto the $\mathcal{O}(\alpha_s)$ and $\mathcal{O}(\alpha_s^2)$ tail of the τ_1 distributions, leaving that to future work. However, by comparing the unmatched predictions of Eq. (3) integrated over τ_1 to the QCD total cross section at x, Q^2 we can estimate the small size of these missing corrections at large τ_1. We emphasize that Eq. (3) accurately captures the distribution for smaller τ_1 near the peak region.

The factorization theorem Eq. (3) also allows us to account for nonperturbative effects—not only in the parton distributions $f(x,\mu)$, but also through a shape function that appears in the soft function S. In e^+e^- collisions, the leading nonperturbative corrections from this shape function have been shown to be universal for different event shapes and collision energies [69–72] (for earlier work see [73–75]). The same conclusions hold for the soft shape function in Eq. (3), endowing it with real predictive power. We will analyze the dominant effects of the nonperturbative soft shape function on the DIS 1-jettiness. For the peak region we include a simple nonperturbative model function to show the impact these corrections have and how they modify the perturbatively calculated distribution. For the tail region the leading shape function power correction is a simple dimension-1 parameter $\Omega_1^{a,b,c}$ that induces a shift to $\tau_1^{a,b,c}$, and is defined by a matrix element of a soft Wilson line operator. For our observables we will prove that there is universality for this correction, namely that $\Omega_1^a = \Omega_1^b = \Omega_1^c$. This follows from a general analysis we carry out for how the direction of axes affect nonperturbative matrix elements for two-jet soft Wilson line operators.

The paper is organized as follows: In Sec. II we review the kinematics of DIS in several commonly used reference frames, laying out the notation for our subsequent analyses. In Sec. III we define the three versions of 1-jettiness in DIS that we will use in this paper and consider their physics in some detail. In Sec. IV we follow the usual formalism for calculating the DIS cross section in QCD, and introduce an additional measurement of the 1-jettiness into the hadronic tensor that appears therein. Sec. V is the technical heart of the paper. Here we present the elements of the SCET formalism that we need and give a detailed proof of the factorization theorems for the generic DIS 1-jettiness in Eq. (1) and the three specializations we give in Eq. (2) . In particular we derive in each factorization theorem how the observable depends on the transverse momentum of ISR through the beam function, and also show that by rescaling arguments we can always use the hemisphere soft function for each version of 1-jettiness.

In Sec. VI we use the factorization theorems from Sec. V to give predictions for the singular terms in the τ_1 distributions at fixed order $\mathcal{O}(\alpha_s)$, and also enumerate the results for the hard, jet, beam, and soft functions that we will need to perform the RG evolution in the next section. In Sec. VII we perform the RG evolution and give our resummed predictions to NNLL accuracy. We compare our predictions for τ_1^b to those of [15] at NLL. We also explain the "profiles" for the individual hard, jet, beam, and soft scales which we use to perform the RG evolution [14, 28, 76]. These profiles allow for a smooth transition from the tail region into the peak region where the soft scale becomes nonperturbative, and into the far tail region where the resummation of logarithms must be turned off. Then we explain how we incorporate nonperturbative hadronization corrections into our predictions through a soft shape function and discuss the Ω_1 parameters. We show that the shifts $\Omega_1^{a,b,c}$ to the tail region of all three versions of the 1-jettiness distributions obey universality.

In Sec. VIII we present numerical results for our predictions to NNLL for the $\tau_1^{a,b,c}$ cross sections, including also their x and Q^2 dependence. We consider both integrated (cumulant) and differential cross sections. The particular results we present are for x, Q^2 values studied at HERA [32, 35]. However, the analytic results we give in Sec. VII can just as easily be used for other experiments at different kinematics, such as at Jefferson Lab (JLab) [77], or for nuclear states other than the proton, such as those at the future Electron-Ion Collider (EIC) [78] and Large Hadron Electron Collider (LHeC) [79].

In Sec. IX we conclude. In several Appendices we collect various technical details that are used in the main body of the paper. In particular, in App. D we collect the anomalous dimensions we need to get to NNLL accuracy in the τ_1 cross sections, and in App. F we give the resummed cross sections in an alternative formalism [38, 80] to that used in Sec. VII [14, 76]. In Sec. VII we use a formalism that expresses the result of the RG evolution of Eq. (3) entirely in momentum space, while in App. F we use a formalism that expresses the RG evolution through Laplace space objects. These two approaches give identical analytic results at each order in

resummed perturbation theory, but since both are commonly used in the SCET literature we provide both results for people who prefer one or the other. Indeed, all of our numeric results have been cross checked between two codes which each use one of these two approaches.

The reader mainly interested in the phenomenology of DIS 1-jettiness and our numerical predictions may read Secs. I–III and then skip to Sec. VIII. For those interested in details of the factorization and resummation, we provide these in Secs. IV–VII and the Appendices.

II. KINEMATICS OF DIS

In this section we define the kinematic variables in DIS that we will use throughout the paper. We also consider three reference frames—center-of-momentum (CM), target rest frame, and Breit frame—and describe the picture of the events in each of these frames.

A. Kinematic variables

In DIS, an incoming electron with momentum k and a proton with momentum P undergo hard scattering by exchange of a virtual boson (photon or Z) with a large momentum q, and outgoing electron k'. The boson momentum q can be determined from the initial- and final-state electron momenta,

$$q = k - k'. \tag{5}$$

In inclusive DIS, the final states from the hard scattering are inclusively denoted as X and their total momentum is denoted as p_X. Using Eq. (5) momentum conservation $k + P = k' + p_X$ can be written as

$$q + P = p_X. \tag{6}$$

The momentum scale Q of the hard scattering is defined by the virtuality of the exchanged gauge boson. Because the boson has a spacelike (negative) virtuality, one defines the positive definite quantity Q^2 by

$$Q^2 \equiv -q^2. \tag{7}$$

where we will be interested in $Q \gg \Lambda_{\rm QCD}$. Next one defines dimensionless Lorentz invariant variables. The Björken scaling variable x is defined by

$$x = -\frac{q^2}{2P\cdot q} = \frac{Q^2}{2P\cdot q}, \tag{8}$$

where x ranges between $0 \le x \le 1$. Another Lorentz-invariant quantity y is defined by

$$y = \frac{2P\cdot q}{2P\cdot k} = \frac{Q^2}{xs}, \tag{9}$$

where the total invariant mass $s = (P+k)^2 = 2P\cdot k$ and y ranges from $0 \le y \le 1$. The variable y measures the energy loss of the electron in the target rest frame. For a given s Eq. (9) relates x, y, and Q^2 to one another, allowing one of the three variables to be eliminated. The invariant mass of the final state in terms of the above variables is

$$p_X^2 = \frac{1-x}{x}Q^2 = (1-x)ys\,. \tag{10}$$

In the classic DIS region one has $p_X^2 \sim Q^2$ for generic x. In the endpoint region $1 - x \sim \Lambda_{\rm QCD}/Q$, the final state is a single narrow jet with momentum of order Q in the virtual boson direction (and studied with SCET in Refs. [36–40]). The resonance region where $1 - x \sim \Lambda_{\rm QCD}^2/Q^2$ cannot be treated with inclusive perturbative methods.

In this work we are interested in the classic region where $1 - x \gg \Lambda_{\rm QCD}/Q$ i.e., $x \sim 1 - x < 1$. In this region one can have more than a single jet. Below, we will make an additional measurement that picks out *two*-jet-like final states.

B. Center-of-momentum frame

A two-jet-like event in the CM frame is illustrated in Fig. 1. An incoming electron and proton collide and produce in the final state an outgoing electron and hadrons. The hadrons, mostly collimated into two jets with additional soft particles elsewhere, are grouped into two regions $\mathcal{H}_B$ and $\mathcal{H}_J$, and p_J and p_B are the total momenta of particles in the each region. The regions $\mathcal{H}_{B,J}$ are not necessarily hemispheres in this frame, though we drew them as such in Fig. 1. The definitions of the regions are described in Sec. III A. As shown in Fig. 1, the electron direction is defined to be the $+z$ direction and the proton direction to be the $-z$ direction. In the CM frame the initial electron and proton momenta are

$$k^\mu = \sqrt{s}\,\frac{n_z^\mu}{2}\,, \qquad P^\mu = \sqrt{s}\,\frac{\bar n_z^\mu}{2}\,, \tag{11}$$

where the light cone vectors are

$$n_z = (1\,,0\,,0\,,1)\,, \qquad \bar n_z = (1\,,0\,,0\,,-1). \tag{12}$$

They satisfy $n_z\cdot\bar n_z = 2$ and $n_z\cdot n_z = \bar n_z\cdot\bar n_z = 0$. An arbitrary four vector V^μ can be written as

$$V^\mu = V^+\frac{\bar n_z^\mu}{2} + V^-\frac{n_z^\mu}{2} + V_T^\mu\,, \tag{13}$$

where $V^+ \equiv V\cdot n_z$ and $V^- \equiv V\cdot\bar n_z$ and $V_T^2 = -\mathbf{V}_T^2 < 0$. In this frame x, y take the values

$$x = \frac{Q^2}{\sqrt{s}\,\bar n_z\cdot q}\,, \quad y = \frac{\bar n_z\cdot q}{\sqrt{s}}\,. \tag{14}$$

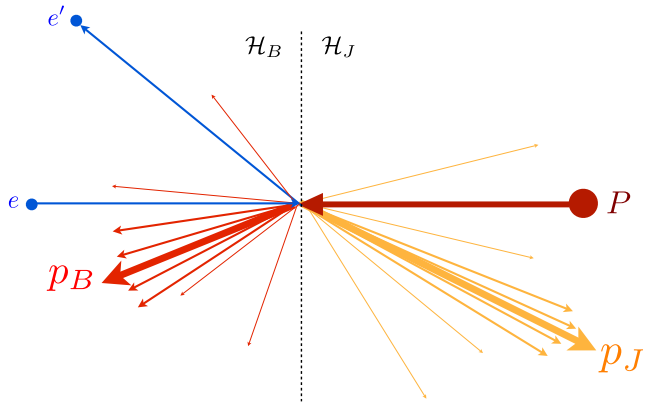

FIG. 1: Two-jet like event in center-of-momentum frame, in which one jet is produced by initial state radiation from the proton, and the other by the hard collision with the electron. Particles are grouped into two regions $\mathcal{H}_{J,B}$ with total momenta $p_{J,B}$ in each region. Different choices of "1-jettiness" observables will give different boundaries for the two regions.

and so q is given by

$$q^\mu = y\sqrt{s}\,\frac{n_z^\mu}{2} - x\sqrt{s}\left(1 - \frac{\mathbf{q}_T^2}{Q^2}\right)\frac{\bar{n}_z^\mu}{2} + q_T^\mu\,, \tag{15}$$

which satisfies $Q^2 = -q^2 = xys$. Here q_T is a four-vector transverse to $n_z, \bar{n}_z$ and satisfies $q_T^2 = -\mathbf{q}_T^2 < 0$.

C. Target rest frame

The same two-jet like event in Fig. 1 is illustrated as it would appear in the target rest frame in Fig. 2. The proton is at rest. The regions in Fig. 2 are transformed from those in Fig. 1 because of the boost along the proton direction. In this frame, the initial electron and proton momenta are

$$k^\mu = \frac{s}{M}\frac{n_z^\mu}{2}\,, \quad P^\mu = M\frac{n_z^\mu + \bar{n}_z^\mu}{2}\,, \tag{16}$$

satisfying $2k\cdot P = s$. Here M is the proton mass. We reach this frame by a boost of momenta p^μ in the CM frame along the z direction,

$$n_z\cdot p \to \frac{M}{\sqrt{s}}\,n_z\cdot p\,, \quad \bar{n}_z\cdot p \to \frac{\sqrt{s}}{M}\,\bar{n}_z\cdot p\,. \tag{17}$$

Therefore, in this frame, q^μ in Eq. (15) is boosted to become

$$q^\mu = \frac{Q^2}{xM}\frac{n_z^\mu}{2} - xM\left(1 - \frac{\mathbf{q}_T^2}{Q^2}\right)\frac{\bar{n}_z^\mu}{2} + q_T^\mu\,, \tag{18}$$

and x, y are given by

$$x = \frac{Q^2}{2M(E-E')}\,, \quad y = \frac{E-E'}{E}\,. \tag{19}$$

Here E and E' are the energies of the incoming and outgoing electron, respectively, measured in the target rest frame. Here y is the fractional electron energy loss.

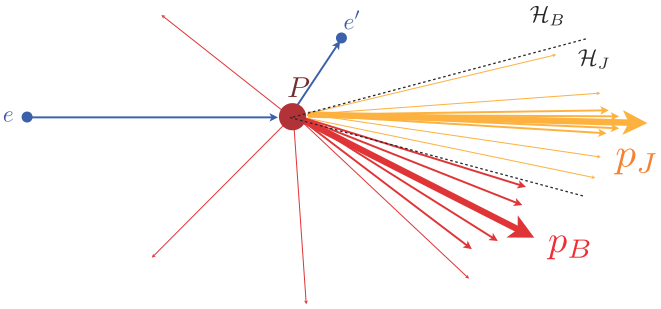

FIG. 2: Two-jet like event in target rest frame. The regions $\mathcal{H}_{J,B}$ and directions of the total momenta $p_{J,B}$ in these regions are boosted from the CM frame in Fig. 1. Both jets go forward, but those in $\mathcal{H}_J$ are more highly collimated.

D. Breit Frame

In the Breit frame, the virtual boson with momentum q^μ and proton with momentum P^μ collide along the z direction. This frame is useful because the proton initial state radiation moving along the proton direction can be relatively well separated from other scattering products. One might worry that an ISR jet, which we want to measure in this paper, could be contaminated by the proton remnants which are difficult to separate from ISR. However, the 1-jettiness observable in Sec. III A that we use to measure the jets in the final state is actually insensitive to this contamination since contributions from the region of the beam remnant give exponentially suppressed contributions to the variable. The contributions from the beam region are by far dominated by the initial state radiation at larger angles. The picture of the two-jet like event in the Breit frame is similar to Fig. 1 with incoming electron replaced by virtual boson and with the outgoing electron removed.

The Breit frame is defined as that in which the momentum transfer q is purely spacelike:

$$q^\mu = Q\frac{n_z^\mu - \bar{n}_z^\mu}{2}\,, \tag{20}$$

where we align $\bar{n}_z$ to be along the proton direction:

$$P^\mu = \frac{Q}{x}\frac{\bar{n}_z^\mu}{2}\,. \tag{21}$$

The incoming electron has momentum

$$k^\mu = \frac{Q}{y}\frac{n_z^\mu}{2} + Q\frac{1-y}{y}\frac{\bar{n}_z^\mu}{2} + k_T^\mu\,, \tag{22}$$

where $\mathbf{k}_T^2 = Q^2(1-y)/y^2$. The outgoing electron then has momentum

$$k'^\mu = Q\frac{1-y}{y}\frac{n_z^\mu}{2} + \frac{Q}{y}\frac{\bar{n}_z^\mu}{2} + k_T^\mu\,. \tag{23}$$

Unlike the CM and target rest frames, where for a fixed s the incident momenta are fixed, in the Breit frame the

incident momenta are functions of x, y. Thus each point in the differential cross section in x, y corresponds to a different Breit frame.

III. HADRONIC OBSERVABLES

A. N-jettiness

To restrict final states to be two-jet-like, we must make a measurement on the hadronic state and require energetic radiation to be collimated along two light-like directions. An observable naturally suited to this role is the N-jettiness [27]. In our case, with one proton beam, 1-jettiness τ_1 can be used to restrict final states to those that have *two* jets: one along the original proton direction (beam) from ISR and another produced from the hard scattering. Recalling the definition of τ_1 in Eq. (1):

$$\tau_1 = \frac{2}{Q^2} \sum_{i \in X} \min\{q_B \cdot p_i, q_J \cdot p_i\} \,, \tag{24}$$

where q_B, q_J are massless four-vectors chosen to lie along the beam and jet directions.

The minimum operator in Eq. (24) groups particles in X with the four-vector to which they are closest (in the sense of the dot product). We will call the region in which particles are grouped with the beam $\mathcal{H}_B$ and the region in which particles are grouped with the jet $\mathcal{H}_J$. We denote the total momentum in the beam region as p_B and total momentum in the jet region as p_J:

$$p_B = \sum_{i \in \mathcal{H}_B} p_i \,, \qquad p_J = \sum_{i \in \mathcal{H}_J} p_i \,. \tag{25}$$

These regions are illustrated for two examples in the CM and target rest frames in Fig. 1 and Fig. 2.

The 1-jettiness τ_1 can be expressed as the sum

$$\tau_1 = \tau_B + \tau_J \,, \tag{26}$$

where τ_B and τ_J are defined by

$$\tau_B = \frac{2 q_B \cdot p_B}{Q^2} \,, \qquad \tau_J = \frac{2 q_J \cdot p_J}{Q^2} \,. \tag{27}$$

The variables $\tau_{B,J}$ are projections of $p_{B,J}$ onto the references vector $q_{B,J}$. They can be thought as two independent observables, and τ_1 is one possible combination of them. Another combination gives a generalized rapidity gap and is discussed in App. A.

The reference vectors q_B and q_J can be expressed as

$$q_B^\mu = \omega_B \frac{n_B^\mu}{2} \,, \qquad q_J^\mu = \omega_J \frac{n_J^\mu}{2} \,, \tag{28}$$

for light-like vectors $n_{B,J}$ given by $n_{B,J} = (1, \mathbf{n}_{B,J})$, where $\mathbf{n}_{B,J}$ are unit 3-vectors satisfying $\mathbf{n}_{B,J}^2 = 1$. Below we will use the vectors $n_{B,J}$ to define the directions of the collinear fields in SCET which we use for the degrees of freedom that describe fluctuations collimated in the beam and jet regions. Refs. [27, 65] discussed the possibility of also minimizing over possible vectors $q_{B,J}$ to give the smallest possible τ_1 in Eq. (24), and Ref. [65] developed a fast algorithm to carry out this minimization. Here we will take $q_{B,J}$ to be fixed vectors. We will discuss several possible choices for $q_{B,J}$ below, each giving a different definition of τ_1.

Measuring τ_1 to be small means the final state has at most two collimated jets, one in the q_B direction and one in the q_J direction (irrespective of the exact definition of q_B and q_J). For power counting purposes we will use $\tau_1 \sim \lambda^2$ which defines a small parameter $\lambda \ll 1$ in which we will perform the expansion to obtain the leading-order factorization theorem for DIS 1-jettiness cross sections.

1. τ_1^a: 1-jettiness aligned with the jet axis

The first version of 1-jettiness that we consider is τ_1^a, which is defined by choosing the beam reference vector q_B^a in Eq. (24) to be proportional to the proton momentum, and the jet reference vector q_J^a to be the jet momentum as given by a jet algorithm such as anti-k_T [46]:

$$\tau_1^a = \frac{2}{Q^2} \sum_{i \in X} \min\{q_B^a \cdot p_i, q_J^a \cdot p_i\} \,. \tag{29}$$

These reference vectors are given by the values

$$q_B^{a\,\mu} = x P^\mu \,, \qquad q_J^{a\,\mu} = q^\mu + x P^\mu + q_J^{\perp\,\mu} \,, \tag{30}$$

where $q_J^\perp$ is $\mathcal{O}(Q\lambda)$. This is because xP is the longitudinal momentum of the parton that hard scatters from the virtual photon of momentum q, which would produce a jet of momentum $q + xP$, but the colliding parton may also have a transverse momentum of order $Q\lambda$. It cannot be larger, otherwise it would cause τ_1 to be larger than $\mathcal{O}(\lambda^2)$. Various jet algorithms give the same value of q_J^a up to negligible power corrections of $\mathcal{O}(Q\lambda^2)$, and the cross section does not actually depend on which of these algorithms is used. Here it would also be equivalent to leading power to define τ_1^a by minimizing the sum in Eq. (29) with respect to $\hat{n}_J$ in q_J^a. The total momentum of particles in the jet region $\mathcal{H}_J$ is $p_J = q_J^a + k$ for a soft momentum k of $\mathcal{O}(Q\lambda^2)$. Thus, to the order we are working, the sum over particles in the jet region $\mathcal{H}_J$ in Eq. (29) gives the total invariant mass of those particles, $2 q_J^a \cdot p_J = p_J^2 = m_J^2$ (for more discussion of this see Refs. [29, 81]).

We will show below that in deriving the correct factorization theorem for the τ_1^a cross section, we must use the fact that $q_J^\perp$ is chosen to make the relative transverse momentum between q_J^a and the actual jet momentum p_J be zero (technically the dominant $\mathcal{O}(Q\lambda)$ part must be zero and a small $\mathcal{O}(Q\lambda^2)$ part is still allowed). That is, q_J^a is *aligned* with the jet, hence the name τ_1^a. This is also important for experimentally measuring τ_1^a. Nevertheless, once this factorization theorem is known, $q_J^\perp$ is

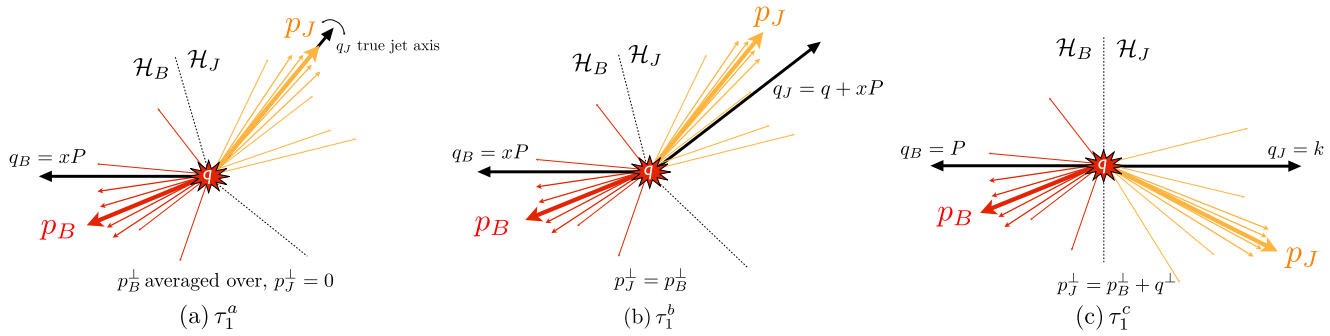

FIG. 3: (a) 1-jettiness τ_1^a measures the small light-cone component of the momentum in the jet region $\mathcal{H}_J$ along the "true" jet axis q_J^a, which is proportional to the jet invariant mass and is thus insensitive at leading order in λ to the transverse momentum $p_B^\perp$ of ISR. Thus $p_B^\perp$ gets averaged over in calculating the τ_1^a cross section. (b) 1-jettiness τ_1^b measures the small light-cone component of p_J along the fixed axis $q_J^b = q + xP$. This projection *is* sensitive to and balances the transverse momentum $p_B^\perp$ of ISR. The transverse momenta of p_B and p_J get convolved together in calculating the cross section. Both τ_1^a and τ_1^b divide the final state into hemispheres in the Breit frame. (c) 1-jettiness τ_1^c divides event into back-to-back hemispheres in the CM frame and projects beam and jet momenta onto $n_z, \bar{n}_z$ axes. These projections are sensitive to the transverse momentum $p_B^\perp$ of ISR. The momentum transfer q has a nonzero transverse component in these coordinates, and the jet and beam momenta are convolved in $p_B^\perp$ in calculating the cross section.

not directly required for calculating the objects such as hard and soft functions that appear in the factorization theorem. For the other versions of 1-jettiness we consider below, the reference vector q_J is not aligned exactly with the jet, and the transverse momentum between q_J and the jet momentum p_J will be nonzero, as illustrated in Fig. 3. This will change the structure of the corresponding factorization theorems, introducing convolutions over the transverse momenta of radiation from the beam and from the final-state jet.

2. τ_1^b: *hemisphere 1-jettiness in the Breit frame*

A second way to define 1-jettiness in DIS is

$$\tau_1^b = \frac{2}{Q^2} \sum_{i \in X} \min\{q_B^b \cdot p_i, q_J^b \cdot p_i\}\,, \tag{31}$$

where

$$q_B^{b\,\mu} = xP^\mu\,, \quad q_J^{b\,\mu} = q^\mu + xP^\mu\,. \tag{32}$$

In this case, q_J^b is given exactly by the quantity $q + xP$ which can be constructed from the electron and proton momenta k, k', P, and needs no information about the jet momentum given by any jet-finding algorithm. Thus in general q_J^b differs by a transverse momentum $q_J^\perp \sim Q\lambda$ from the vector q_J^a used in the τ_1^a definition of 1-jettiness we introduced above in Eq. (29). Note that since $q = q_J^b - q_B^b$, q itself has zero tranverse momentum $q_\perp$ with respect to the directions n_J^b, n_B^b of q_J^b, q_B^b.

This choice of vectors is natural in the *Breit* frame (hence the name τ_1^b), in which it divides the final state into back-to-back hemispheres. In the Breit frame,

$$\tau_1^b \overset{\text{Breit}}{=} \frac{1}{Q} \sum_{i \in X} \min\{\bar{n}_z \cdot p_i, n_z \cdot p_i\}\,. \tag{33}$$

This definition directly corresponds to the thrust τ_Q in DIS defined in [15].

We will often work in the CM frame in intermediate stages of calculation below. Expressing $q_{B,J}^b$ in the CM frame, we find

$$\begin{aligned} q_B^{b\,\mu} &= x\sqrt{s}\,\frac{\bar{n}_z^\mu}{2}\,, \\ q_J^{b\,\mu} &= y\sqrt{s}\,\frac{n_z^\mu}{2} + x(1-y)\sqrt{s}\,\frac{\bar{n}_z^\mu}{2} + q_T^\mu\,, \end{aligned} \tag{34}$$

where $\mathbf{q}_T^2 = (1-y)Q^2$ and q_J^b is a massless vector. q_J^b in Eq. (34) can also be written in the form

$$q_J^{b\,\mu} = P_T e^Y \frac{n_z^\mu}{2} + P_T e^{-Y} \frac{\bar{n}_z^\mu}{2} + P_T\,\hat{n}_T^\mu\,, \tag{35}$$

where the jet transverse momentum and rapidity are

$$P_T = Q\sqrt{1-y}\,, \qquad Y = \frac{1}{2}\ln\frac{y}{x(1-y)}\,, \tag{36}$$

and $\hat{n}_T$ is a unit vector in the direction of q_T. These relations can be inverted to give

$$x = \frac{P_T\, e^{-Y}}{\sqrt{s} - P_T e^Y}\,, \qquad y = \frac{P_T\, e^Y}{\sqrt{s}}\,. \tag{37}$$

Equating the 0th components of Eqs. (28) and (35), we find that

$$\omega_J^b = 2P_T \cosh Y = [y + x(1-y)]\sqrt{s}\,. \tag{38}$$

Calculating τ_1^b in the CM frame groups particles into non-hemisphere-like regions. Particles with momenta p are grouped into the beam or jet regions according to which dot product is smaller:

$$\begin{aligned} \mathcal{H}_B &: \frac{x\sqrt{s}\,n_B^b \cdot p}{2} < \frac{\omega_J^b n_J^b \cdot p}{2}\,, \\ \mathcal{H}_J &: \frac{x\sqrt{s}\,n_B^b \cdot p}{2} > \frac{\omega_J^b n_J^b \cdot p}{2}\,. \end{aligned} \tag{39}$$

Using Eq. (38), we can write these conditions as

$$\mathcal{H}_B: \quad \frac{n_B^b\cdot p}{n_J^b\cdot p} < 1-y+\frac{y}{x}\,, \quad \mathcal{H}_J: \frac{n_B^b\cdot p}{n_J^b\cdot p} > 1-y+\frac{y}{x}\,. \tag{40}$$

In order to understand the regions defined by Eq. (40), let us consider simple case $y\sim 1$ and $x<y$. For this case q_J^b in Eq. (35) is n_z-collinear because in Eq. (36) P_T and Y are small and large, respectively. We can replace n_J^b and n_B^b in Eq. (40) by n_z and $\bar{n}_z$ and set $\bar{n}_z\cdot p/n_z\cdot p = 1/(\tan^2\theta/2)$ where θ is the polar angle of massless particle p. Then, the jet region is a symmetric cone around the n_z direction of opening angle given by

$$\tan^2\frac{R}{2}\approx\frac{x}{y}\,, \tag{41}$$

and the beam region is everything outside. For generic x and y, the jet region is not symmetric around the n_J^b.

As mentioned above in the description of τ_1^a, the vector $q_J^b = q+xP$ is the 4-momentum of a jet produced by scattering at momentum q on an incoming parton with momentum exactly equal to xP. In general the colliding incoming parton will have a nonzero transverse momentum due to ISR, causing the produced jet momentum to deviate by $\mathcal{O}(Q\lambda)$ from q_J^b. The scale $\mathcal{O}(Q\lambda)$ is perturbative and this transverse momentum is much larger than the intrinsic transverse momentum of partons in the proton. The observable τ_1^a differs from τ_1^b in that τ_1^a measures the true invariant mass m_J^2 of the jet while τ_1^b simply projects the jet momentum onto the fixed axis $q_J^b = q+xP$ which does not vary with the exact direction of the jet. The jet axis varies from q_J^b due to ISR from the beam before the hard collision. This subtle difference leads to a different structure in the factorization theorems for τ_1^a and τ_1^b.

For the 1-jettiness for DIS studied in [66], the procedure for determining the q_J was described as determining the jet axis from a jet algorithm. This makes their q_J correctly correspond with our q_J^a. However, they also used the formulas Eqs. (35) and (36) to describe their q_J, which yields $q_J = q+xP$, and this would correspond to our τ_1^b. This choice neglects the $\mathcal{O}(Q\lambda)$ transverse momentum between q_J and the jet momentum p_J, which taken literally would lead to an incorrect factorization theorem for the observable τ_1^a. However, after the correct form of the factorization theorem for τ_1^a is known (which was written in [66]), this approximation is valid for calculating the objects in that theorem to leading order in λ. Thus, the τ_1 in [66] is the same as our τ_1^a defined above in Eq. (29), where q_J is aligned along p_J.

3. τ_1^c: hemisphere 1-jettiness in the CM frame

A third way to define the 1-jettiness in DIS is with the proton and electron momenta

$$q_B^{c\,\mu} = P^\mu\,, \qquad q_J^{c\,\mu} = k^\mu\,. \tag{42}$$

1-jettiness	axis q_J	axis q_B
generic τ_1	$\omega_J\frac{n_J}{2}$	$\omega_B\frac{n_B}{2}$
τ_1^a	$xP+q+q_J^\perp$	xP
τ_1^b	$xP+q$	xP
τ_1^c	k	P

TABLE I: Reference vectors q_J and q_B defining the axes for various versions of 1-jettiness. For τ_1^a the q_J axis is defined to be the jet momentum q_J^a given by, e.g., the anti-kT algorithm. This axis is given by $q+xP$ up to transverse momentum corrections of order $q_J^\perp\sim\mathcal{O}(Q\lambda)$. The exact value of $q_J^\perp$ will not be needed for our calculation, only the fact that there is no relative transverse momentum larger than $\mathcal{O}(Q\lambda^2)$ between the momentum p_J in the jet region $\mathcal{H}_J$ and the axis q_J^a. This is in contrast to τ_1^b, for which the cross section will depend on the transverse momentum between p_J and $q_J^b = q+xP$, but where $q_\perp = 0$. Finally for τ_1^c we also have $q_\perp\neq 0$.

We use the superscripts c because this choice naturally divides the final state into hemispheres in the CM frame, mimicking the thrust defined in the CM frame for e^+e^- collisions [64].

In the CM frame the momenta k and P are along the z and $-z$ directions as in Eq. (11). In this frame the reference vectors $q_{J,B}$ are given by the light-cone directions $n_{B,J}^c$ and normalizations $\omega_{B,J}^c$:

$$n_B^{c\,\mu} = \bar{n}_z^\mu\,, \qquad n_J^{c\,\mu} = n_z^\mu\,, \tag{43}$$

and

$$\omega_B^c = \sqrt{s}\,, \qquad \omega_J^c = \sqrt{s}\,. \tag{44}$$

In this frame, τ_1 is then given by

$$\tau_1^c = \frac{1}{xy\sqrt{s}}\sum_{i\in X}\min\{\bar{n}_z\cdot p_i, n_z\cdot p_i\}\,. \tag{45}$$

The minimum here assigns particles to either the hemisphere containing the proton or electron. States with small τ_1 thus have two nearly back-to-back jets in this frame.

The essential differences among $\tau_1^a, \tau_1^b, \tau_1^c$ are illustrated in Fig. 3 drawn in the CM frame and summarized in Table I. τ_1^b and τ_1^c project the jet momentum onto a fixed axis, and are sensitive at leading order to the transverse momentum of initial state radiation from the incoming proton, while τ_1^a always projects the jet momentum onto the axis with respect to which it has no transverse momentum, and so measures the invariant mass of the jet which is insensitive at leading order to the transverse momentum of ISR. Table I summarizes the choices of reference vectors $q_{J,B}$ for the three versions of 1-jettiness defined in this section.

B. Versions of DIS Thrust

Several thrust DIS event shapes have been considered in the literature [82], and some of them have been measured by experiments. One version, called τ_Q in [15] but not yet measured, is defined in the Breit frame by

$$\tau_Q \overset{\text{Breit}}{=} 1 - \frac{2}{Q} \sum_{i \in \mathcal{H}_C} p_{z\,i}\,, \tag{46}$$

where $\mathcal{H}_C$ is the "current hemisphere" in the direction set by the virtual boson q. We will show below in section III D that τ_Q is equivalent to our τ_1^b.

Another version of thrust, used in [30, 33] and called τ_{tE} in [48], is defined using a thrust axis whose definition involves a maximization procedure over particles in the current hemisphere $\mathcal{H}_C = \mathcal{H}_J$ in the Breit frame:

$$\tau_{tE} = 1 - \max_{\mathbf{n}} \frac{\sum_{i \in \mathcal{H}_C} |\mathbf{p}_i \cdot \mathbf{n}|}{\sum_{i \in \mathcal{H}_C} |\mathbf{p}_i|}\,. \tag{47}$$

The maximization aligns the vector $\mathbf{n}$ with the direction of the jet in the current hemisphere, just like the q_J^a vector in our definition of τ_1^a. However, because the sums in both the numerator and denominator are limited to $\mathcal{H}_C$, the observable is actually non-global [48], cutting out radiation from the remnant hemisphere.[1] Thus it differs from our τ_1^a which sums over both hemispheres. It cannot be simply related to a global version of 1-jettiness as above. A global thrust event shape, τ_{tQ}, can be obtained by replacing the denominator in Eq. (47) by $Q/2$, but this version of the thrust event shape is also not related to our τ_1^a.

Yet another variation is τ_{zE} [30, 48] which is like Eq. (47) with the same normalization, but with respect to the $\mathbf{z}$-axis in the Breit frame. It is also not global [48]. H1 and ZEUS have measured τ_{zE} and τ_{tE} [32, 35]. It would be interesting to reanalyze the data to measure the global observables $\tau_1^{a,b,c}$ we predict in this paper at NNLL order.

C. Jet and Beam Momenta

1. *Jet and beam contributions to 1-jettiness*

The cross sections for the different versions of 1-jettiness in Sec. III A will all be expressed in terms of *beam*, *jet*, and *soft* functions that depend on the projections of the total momenta in the regions $\mathcal{H}_B$ and $\mathcal{H}_J$ onto the reference vectors $q_{B,J}$ in the definition of the 1-jettiness Eq. (24). These vectors point in the direction of light-cone vectors $n_B = \bar{n}_z$ and n_J, which varies for the three different versions of 1-jettiness $\tau_1^{a,b,c}$. The expression τ_1 in Eq. (26) can be written in terms of $n_J \cdot p_J$ and $n_B \cdot p_B$ as

$$\tau_1 = \frac{n_J \cdot p_J}{Q_J} + \frac{n_B \cdot p_B}{Q_B}\,, \tag{48}$$

where Q_J and Q_B are given by

$$Q_J = \frac{Q^2}{\omega_J}\,, \quad Q_B = \frac{Q^2}{\omega_B}. \tag{49}$$

Table II lists explicit expressions for $Q_{B,J}$ in the CM, Breit, and target rest frames for the three versions of 1-jettiness $\tau_1^a, \tau_1^b, \tau_1^c$.

For the three different cases $\tau_1^{a,b,c}$ of Eq. (48), the contributions $n_J \cdot p_J$ will be with respect to different vectors $n_J^{a,b,c}$, and $n_J \cdot p_J, n_B \cdot p_B$ will include momenta of particles in different regions $\mathcal{H}_{J,B}$ in the three cases. For τ_1^a, the differences between energies ω_J^b and ω_J^a and between unit vectors n_J^b and n_J^a are of order λ since the vectors q_J^b and q_J^a differ due to the transverse momentum of ISR of order $Q\lambda$. So using the same expression ω_J^b in Eq. (38) for ω_J^a is correct up to corrections suppressed by λ that can be neglected in computing τ_1^a. Nevertheless, the values of $n_J \cdot p_J$ in the equations for τ_1^b and τ_1^a do differ at leading power ($n_J \cdot p_J \sim Q\lambda^2$) because the $\mathcal{O}(\lambda)$ difference in the axes n_J^b and n_J^a is dotted the into transverse momentum in p_J which is of $\mathcal{O}(Q\lambda)$. This difference is reflected in the different factorization theorems for τ_1^a and τ_1^b.

The discussion on the jet and beam regions $\mathcal{H}_{J,B}$ in Sec. III A 2 can be done for a generic τ_1. For particles with momenta p grouped into the beam or jet region, the criteria $q_J \cdot p < q_B \cdot p$ and $q_B \cdot p < q_J \cdot p$ that define the regions $\mathcal{H}_{J,B}$, respectively, can be written

$$p \in \mathcal{H}_J : \quad \frac{n_J \cdot p}{\bar{n}_J \cdot p} < \frac{\omega_B n_J \cdot n_B}{2\omega_J} \equiv R_J^2\,, \tag{50a}$$

$$p \in \mathcal{H}_B : \quad \frac{n_B \cdot p}{\bar{n}_B \cdot p} < \frac{\omega_J n_J \cdot n_B}{2\omega_B} \equiv R_B^2\,. \tag{50b}$$

Here $\bar{n}_J$ and $\bar{n}_B$ are the normalized conjugate vectors to n_J and n_B, respectively. Their definitions are

$$\bar{n}_J^\mu \equiv \frac{2n_B^\mu}{n_J \cdot n_B}\,, \quad \bar{n}_B^\mu \equiv \frac{2n_J^\mu}{n_J \cdot n_B}\,, \tag{51}$$

chosen so that $n_J \cdot \bar{n}_J = n_B \cdot \bar{n}_B = 2$. The parameters $R_{J,B}$ characterize the sizes of the regions $\mathcal{H}_{J,B}$ into which the 1-jettiness Eq. (24) partitions final-state particles. The variables on the left-hand sides are analogous to the ratio of momenta related to rapidity: $n \cdot p / \bar{n} \cdot p = e^{-2Y}$ for back-to-back directions $n, \bar{n}$. They can be interpreted as a generalized rapidity, $e^{-2Y_{n_J \bar{n}_J}}$ or $e^{-2Y_{n_B \bar{n}_B}}$ as defined by Eq. (A2). These rapidities are defined in terms of 4-vectors $\bar{n}_{J,B}$ and $n_{J,B}$, which are not in general back-to-back. $R_{J,B}$ in Eq. (50) characterizes the range of these generalized rapidities that are included in each of the regions $\mathcal{H}_{J,B}$.

[1] The variable τ_{tE} is also not IR safe without a minimal energy constraint on the $\mathcal{H}_c$ hemisphere.

1-jettiness	frame	Q_J	Q_B	R_J	R_B	Q_R	s_J	s_B
generic τ_1		$\frac{Q^2}{\omega_J}$	$\frac{Q^2}{\omega_B}$	$\sqrt{\frac{\omega_B n_J\cdot n_B}{2\omega_J}}$	$\sqrt{\frac{\omega_J n_J\cdot n_B}{2\omega_B}}$	$\frac{Q^2}{\sqrt{2q_J\cdot q_B}}$	$\frac{q_B\cdot q}{q_B\cdot q_J}Q^2$	$-\frac{q_J\cdot q}{q_B\cdot q_J}Q^2$
$\tau_1^{a,b}$	CM	$\frac{\sqrt{xy}Q}{y+x(1-y)}$	$\sqrt{\frac{y}{x}}Q$	$\frac{\sqrt{xy}}{y+x(1-y)}$	$\sqrt{\frac{y}{x}}$	Q	Q^2	Q^2
	Breit	Q	Q	1	1			
	Target-rest	xM	$\frac{Q^2}{xM}$	$\frac{xM}{Q}$	$\frac{Q}{xM}$			
τ_1^{c}	CM	$\sqrt{xy}Q$	$\sqrt{xy}Q$	1	1	$\sqrt{xy}Q$	yQ^2	xyQ^2
	Breit	$\frac{yQ}{2-y}$	xQ	$\frac{\sqrt{y/x}}{2-y}$	$\sqrt{\frac{x}{y}}$			
	Target-rest	xyM	$\frac{Q^2}{M}$	$\frac{M}{\sqrt{s}}$	$\frac{\sqrt{s}}{M}$			

TABLE II: Kinematic variables characterizing 1-jettiness. Normalizations Q_J and Q_B in the expression Eq. (48) and sizes $R_{J,B}$ of the jet and beam regions $\mathcal{H}_{J,B}$ in Eq. (50) for the different versions of 1-jettiness, in three different reference frames described in Sec. II, and the Lorentz invariant combinations $Q_R \equiv Q_J/R_J = Q_B/R_B$ in Eq. (54) and $s_{J,B}$ given in Eq. (58).

2. *Invariants for 1-jettiness*

For later purposes we will express Eq. (48) in terms of separate n_J-collinear, n_B-collinear, and soft contributions:

$$\tau_1 = \frac{n_J\cdot(p_J^c + k_J)}{Q_J} + \frac{n_B\cdot(p_B^c + k_B)}{Q_B}\,, \qquad (52)$$

where p_J^c is the total momentum of all n_J-collinear modes, p_B^c is the total momentum of all n_B-collinear modes, and $k_{J,B}$ are the total momenta of soft modes in regions $\mathcal{H}_{J,B}$, respectively. These modes are defined by the scaling of their light-cone components of momentum:

$$\begin{aligned} &n_J\text{-collinear}: && (n_J\cdot p, \bar n_J\cdot p, p_\perp) \sim Q(\lambda^2, 1, \lambda)\\ &n_B\text{-collinear}: && (n_B\cdot p, \bar n_B\cdot p, p_\perp) \sim Q(\lambda^2, 1, \lambda)\\ &\text{soft}: && k \sim Q\lambda^2\,. \end{aligned} \qquad (53)$$

The normalization constants $Q_{J,B}$ in Eq. (52) are not Lorentz invariant (which for SCET corresponds to a reparameterization invariance [83, 84]), but by combining them with other kinematic quantities we can form invariants in terms of which we can express Eq. (52). One set of such combinations uses $R_{J,B}$ in Eq. (50). The sizes $R_{J,B}$ of the regions $\mathcal{H}_{J,B}$ are not Lorentz-invariant—they depend on the choice of frame. However, the ratios Q_J/R_J and Q_B/R_B *are* Lorentz/reparameterization invariant and, in fact, are equal:

$$Q_R \equiv \frac{Q_J}{R_J} = \frac{Q_B}{R_B} = \frac{Q^2}{\sqrt{2q_J\cdot q_B}}\,. \qquad (54)$$

Expressions for $R_{B,J}$ and Q_R for each case $\tau_1^{a,b,c}$ are given in Table II. (Strictly speaking, dot products with q_J^a are not Lorentz-invariant due to dependence on the jet algorithm, but for calculating Q_R and $s_{J,B}$ we can use the approximation $q_J^a = q_J^b = q + xP$ to leading order in λ, which does give Lorentz-invariant dot products.)

It is useful to re-express the soft contribution in Eq. (52) by rescaling the vectors $n_{J,B}$ by $n'_{J,B} = n_{J,B}/R_{J,B}$, which gives us

$$\tau_S \equiv \frac{n_J\cdot k_J}{Q_J} + \frac{n_B\cdot k_B}{Q_B} = \frac{n'_J\cdot k_J + n'_B\cdot k_B}{Q_R}\,. \qquad (55)$$

This relation will help us simplify the soft function in the factorized τ_1 cross sections later on. This is because rewriting the particle grouping in Eq. (50) in terms of $n'_{J,B}$ absorbs the factor $R_{J,B}$ giving $n'_J\cdot p/\bar n'_J\cdot p < 1$ and $n'_B\cdot p/\bar n'_B\cdot p > 1$. Hence with these variables the hemispheres $\mathcal{H}_{J,B}$ are symmetric, which makes it possible to connect our soft function to the usual hemisphere soft function.

We can also re-express the $n_{J,B}$ collinear contributions to τ_1 in Eq. (52) in terms of another set of Lorentz-invariant combinations involving $Q_{J,B}$. In the τ_1 factorization theorems we derive below, the arguments of the collinear jet and beam functions appearing therein will naturally depend on "transverse virtualities" $\bar n\cdot p\, n\cdot p$ of the n_J-collinear jet and of the struck parton in the proton, respectively. Relating the n_J-collinear contribution to τ_1 to the transverse virtuality t_J of the jet,

$$\tau_J^c \equiv \frac{n_J\cdot p_J^c}{Q_J} = \frac{\bar n_J\cdot p_J\, n_J\cdot p_J^c}{\bar n_J\cdot p_J\, Q_J} = \frac{t_J}{\bar n_J\cdot q\, Q_J} + \mathcal{O}(\lambda^4)\,, \qquad (56)$$

where in the middle step we simply multiplied top and bottom by the large component $\bar{n}_J \cdot p_J$ of the total collinear momentum in region $\mathcal{H}_J$, and in the last step we used in the denominator $\bar{n}_J \cdot p_J = \bar{n}_J \cdot q + \mathcal{O}(Q\lambda^2)$. The large component of the jet momentum can only come from the momentum transferred into the collision by the virtual boson of momentum q—the proton with which it collides only has a large component in the $n_J \cdot p$ component. Similarly, the n_B-collinear contribution to τ_1 is

$$\tau_B^c \equiv \frac{n_B \cdot p_B^c}{Q_B} = \frac{-\bar{n}_B \cdot p_x \, n_B \cdot p_x}{\bar{n}_B \cdot p_x \, Q_B} = \frac{t_B}{-\bar{n}_B \cdot q \, Q_B} + \mathcal{O}(\lambda^4)\,, \tag{57}$$

where p_x is the momentum of the parton that is struck by the virtual boson of momentum q. In the middle step we used that $n_B \cdot p_B^c = -n_B \cdot p_x$ since the struck parton recoils against the ISR and balances the small component of momentum in the n_B direction. In the last step, we defined the positive virtuality $t_B \equiv -\bar{n}_B \cdot p_x \, n_B \cdot p_x$ of the spacelike struck parton and in the denominator used that $\bar{n}_B \cdot p_x = -\bar{n}_B \cdot q + \mathcal{O}(Q\lambda^2)$. This is because the collision of the virtual boson and struck parton is the n_J-collinear jet which has no large momentum in the $n_B \cdot p$ component. Thus momentum conservation requires that the large components of $\bar{n}_B \cdot q$ and $\bar{n}_B \cdot p_x$ cancel.

The quantities in the denominators of the relations Eqs. (56) and (57) are Lorentz invariant:

$$s_J \equiv \bar{n}_J \cdot q \, Q_J = \frac{q_B \cdot q}{q_B \cdot q_J} \, Q^2\,, \tag{58a}$$

$$s_B \equiv -\bar{n}_B \cdot q \, Q_B = \frac{-q_J \cdot q}{q_B \cdot q_J} \, Q^2\,, \tag{58b}$$

where the minus sign in s_B makes it positive since $\bar{n}_B \cdot q < 0$. For the cases $\tau_1^{a,b,c}$, s_J and s_B take the special values given in Table II.

Using the definitions of Q_R and $s_{J,B}$ in Eqs. (54) and (58) these factors can be combined to give the transverse virtuality of the exchanged boson q:

$$\frac{s_J s_B}{Q_R^2} = -\bar{n}_B \cdot q \bar{n}_J \cdot q \frac{n_B \cdot n_J}{2} = Q^2(1 - \mathbf{q}_\perp^2/Q^2)\,, \tag{59}$$

where we used

$$q = \bar{n}_B \cdot q \frac{n_B}{2} + \bar{n}_J \cdot q \frac{n_J}{2} + q_\perp\,, \tag{60}$$

and $q^2 = -Q^2$. The transverse momentum $q_\perp$ is orthogonal to $n_{B,J}$. The relation Eq. (59) will be useful in evaluating the fixed-order τ_1 cross section in App. G. We will use that $\mathbf{q}_\perp^2/Q^2 \sim \lambda^2$ when 1-jettiness is measured to be small, $\tau_1 \sim \lambda^2$. A larger $\mathbf{q}_\perp$ cannot be transferred into the final state for this to be true, since particles have to be collimated along $q_{J,B}$ or be soft.

D. Momentum Conservation and the Beam Region

We noted earlier that the contribution of proton remnants to τ_1 is exponentially suppressed, by a factor $e^{-|\Delta Y|}$ of their rapidity with respect to q_B. Only the energetic ISR and soft radiation at larger angles in $\mathcal{H}_B$ contribute to τ_1. Although these contributions are easier to measure, one may still prefer to measure particles only in the $\mathcal{H}_J$ jet region in the direction of q_J. In general, such a restriction in the final state is non-global, and leads to NGLs. However, by momentum conservation, we can show that each of the global $\tau_1^{a,b,c}$ observables we consider can be rewritten in terms of momenta of particles only in the $\mathcal{H}_J$ region (for case a this is true only in the 2-jet region $\tau_1^a \ll 1$).

First, consider τ_1^b. In the Breit frame,

$$\begin{aligned}\tau_1^b &\overset{\text{Breit}}{=} \frac{1}{Q}\sum_{i\in X} \min\{n_z \cdot p_i, \bar{n}_z \cdot p_i\} \\ &= \frac{1}{Q}\Big[\sum_{i\in\mathcal{H}_J^b}(E_i - p_{z\,i}) + \sum_{i\in\mathcal{H}_B^b}(E_i + p_{z\,i})\Big] \\ &= \frac{1}{Q}\Big[\sum_{i\in X}(E_i + p_{z\,i}) - 2\sum_{i\in\mathcal{H}_J^b} p_{z\,i}\Big]\,,\end{aligned} \tag{61}$$

where $X = \mathcal{H}_J^b + \mathcal{H}_B^b$ denotes the entire final state. Note that in the Breit frame,

$$p_X = P + q = \Big(\frac{Q}{2x}, 0, 0, Q - \frac{Q}{2x}\Big)\,, \tag{62}$$

where $p_X^\mu \equiv \sum_{i\in X} p_i^\mu$. Thus, $E_X + p_{zX} = Q$, and we obtain

$$\tau_1^b \overset{\text{Breit}}{=} 1 - \frac{2}{Q}\sum_{i\in\mathcal{H}_J^b} p_{z\,i} \equiv \tau_Q\,, \tag{63}$$

where in the last equality we recall that Eq. (63) is precisely the definition in Eq. (46) of the DIS thrust variable called τ_Q in [15], where the hemisphere $\mathcal{H}_J^b$ in the Breit frame was called the "current hemisphere" $\mathcal{H}_C$. We will comment further on the relation between the results of [15] for τ_Q and our results for τ_1^b in Sec. VII B below. Eq. (63) shows that τ_1^b can always be computed just in terms of the measurements of momenta of particles in the current hemisphere $\mathcal{H}_C = \mathcal{H}_J^b$.

The same arguments as for τ_1^b in the Breit frame apply to τ_1^c in the CM frame. In the CM frame,

$$\begin{aligned}\tau_1^c &\overset{\text{CM}}{=} \frac{1}{xy\sqrt{s}}\sum_{i\in X} \min\{n_z \cdot p_i, \bar{n}_z \cdot p_i\} \\ &= \frac{1}{xy\sqrt{s}}\Big[\sum_{i\in X}(E_i + p_{z\,i}) - 2\sum_{i\in\mathcal{H}_J^c} p_{z\,i}\Big]\,.\end{aligned} \tag{64}$$

In this frame, we have that

$$\begin{aligned}p_X &= P + q \\ &= \frac{\sqrt{s}}{2}\Big(y+1-x\Big(1-\frac{\mathbf{q}_T^2}{Q^2}\Big), \frac{2\mathbf{q}_T}{\sqrt{s}}, y-1+x\Big(1-\frac{\mathbf{q}_T^2}{Q^2}\Big)\Big)\,,\end{aligned} \tag{65}$$

so

$$\tau_1^c \overset{\rm CM}{=} \frac{1}{x}\left(1 - \frac{2}{y\sqrt{s}}\sum_{i\in\mathcal{H}_J^c} p_{z\,i}\right). \tag{66}$$

Thus, τ_1^c also can be measured just from momenta of particles in the $\mathcal{H}_J$ hemisphere in the CM frame.

Finally, the above argument can be extended to apply also to the 1-jettiness τ_1^a, but only for the region where $\tau_1^a \ll 1$. τ_1^a can be written

$$\tau_1^a = \frac{2}{Q^2}\left[\sum_{i\in\mathcal{H}_J^a} q_J^a\cdot p_i + \sum_{i\in\mathcal{H}_B^a} q_B^a\cdot p_i\right]. \tag{67}$$

Now, $q_B^a = q_B^b$, while $q_J^a = q_J^b + \mathcal{O}(Q\lambda)$. Thus the regions $\mathcal{H}_{J,B}^a$ differ from those for τ_1^b, $\mathcal{H}_{J,B}^b$, by a change in the region boundary of $\mathcal{O}(\lambda)$. This does not affect the assignment of collinear particles to the two regions, since none of them change regions under this small change in boundary. An $\mathcal{O}(\lambda)$ fraction of the soft particles switch from one region to the other, but this then produces a correction suppressed by λ to the soft contribution τ_S in Eq. (55). Thus, Eq. (67) can be expressed

$$\begin{aligned}\tau_1^a &= \frac{2}{Q^2}\left[\sum_{i\in\mathcal{H}_J^b}(q_J^a - q_J^b)\cdot p_i + \sum_{i\in\mathcal{H}_J^b} q_J^b\cdot p_i + \sum_{i\in\mathcal{H}_B^b} q_B^b\cdot p_i\right] + \mathcal{O}(\lambda^3)\\ &= \tau_1^b + \frac{2}{Q^2}\sum_{i\in\mathcal{H}_J^b}(q_J^a - q_J^b)\cdot p_i + \mathcal{O}(\lambda^3),\end{aligned} \tag{68}$$

in the regime where $\tau_1 \sim \lambda^2 \ll 1$. This is the regime we aim to predict accurately in this paper. Thus, in this limit τ_1^a can also be computed just by measuring particles in the "current hemisphere" $\mathcal{H}_J^a = \mathcal{H}_C$ in the Breit frame, as long as both axes q_J^a and q_J^b are measured. For larger τ_1^a, both regions $\mathcal{H}_{J,B}^a$ would need to be measured, and we emphasize that the contribution of proton remnants is still exponentially suppressed.

In summary, for small τ_1 none of the three versions of 1-jettiness $\tau_1^{a,b,c}$ require direct measurement of particles from initial state radiation in the beam region. Furthermore, for larger τ_1 values the variables $\tau_1^{b,c}$ still do not require such measurements (though τ_1^a does). All three τ_1's are global observables since measurement of τ_1 by summing over the particles only in the $\mathcal{H}_J$ region is still affected by ISR from the proton beam through momentum conservation.

IV. CROSS SECTION IN QCD

In this Section we organize the full QCD cross section into the usual leptonic and hadronic tensors, but with an additional measurement of 1-jettiness inserted into the definition of the hadronic tensor. We express it in a form that will be easily matched or compared to the effective theory cross section we consider in the following section.

A. Inclusive DIS cross section

We begin with the inclusive DIS cross section in QCD, differential in the momentum transfer q,

$$\begin{aligned}\frac{d\sigma}{d^4q} = \frac{1}{2s}\int d\Phi_L \sum_X \left\langle |\mathcal{M}(eP\to LX)|^2\right\rangle \\ \times (2\pi)^4\delta^4(P+q-p_X)\delta^4(q-k+k'),\end{aligned} \tag{69}$$

where L is the final lepton state with momentum k', and X is the final hadronic state with momentum p_X. $d\Phi_L$ is the phase space for the lepton states, and the $\sum_X$ includes the phase space integrals for hadronic states. The squared amplitude $|\mathcal{M}|^2$ is averaged over initial spins, and summed over final spins. Recall that q (and x, y) can be determined entirely by measurements of the lepton momenta. Later in Sec. IV B we will insert additional measurements such as 1-jettiness on the state X.

We wish to express the cross section differential in the Lorentz-invariant variables Q^2, x using Eqs. (7) and (8). Although Q^2, x are Lorentz-invariant, at intermediate stages of integration we can work in a particular frame. In either the CM or Breit frame, the proton momentum is of the form $P = n_z\cdot P\,\bar n_z/2$. So we decompose q along the $n_z, \bar n_z$ directions, $q = n_z\cdot q\,\bar n_z/2 + \bar n_z\cdot q\,n_z/2 + q_T$. Then the delta functions defining Q^2, x take the form

$$\delta\left(x - \frac{Q^2}{n_z\cdot P\,\bar n_z\cdot q}\right)\delta\left(Q^2 + n_z\cdot q\,\bar n_z\cdot q - \mathbf{q}_T^2\right). \tag{70}$$

Inserting these into Eq. (69) and integrating over q^+ and q^-, we obtain

$$\begin{aligned}\frac{d\sigma}{dx\,dQ^2} = \frac{1}{4xs}\int d^2q_T \int d\Phi_L\delta^4(q-k+k') \\ \times\sum_X (2\pi)^4\delta^4(P+q-p_X)\langle|\mathcal{M}|^2\rangle,\end{aligned} \tag{71}$$

where q is now given by the value

$$q^\mu = \frac{Q^2}{xn_z\cdot P}\frac{n_z^\mu}{2} - xn_z\cdot P\left(1 - \frac{\mathbf{q}_T^2}{Q^2}\right)\frac{\bar n_z^\mu}{2} + q_T^\mu. \tag{72}$$

For a single electron final state $L = e(k')$ (which is all we have at the leading order in α_{em} at which we are working), the integral over Φ_L in Eq. (71) takes the form

$$\int\frac{d^3k'}{(2\pi)^3 2E_{k'}} = \int\frac{d^4k'}{(2\pi)^3}\delta(k'^2), \tag{73}$$

so, performing the k' integral, we obtain

$$\begin{aligned}\frac{d\sigma}{dx\,dQ^2} = \frac{1}{4(2\pi)^3\,xs}\int d^2q_T\delta((q-k)^2) \\ \times\sum_X (2\pi)^4\delta^4(P+q-p_X)\langle|\mathcal{M}|^2\rangle.\end{aligned} \tag{74}$$

To use the first delta function, we need to pick a particular frame in which to complete the q_T integration. In

the CM frame,

$$\delta((q-k)^2) = \delta(Q^2+2q\cdot k) = \frac{Q^2}{xs}\,\delta\left(\mathbf{q}_T^2 - \left(1-\frac{Q^2}{xs}\right)Q^2\right), \tag{75}$$

where we use Eq. (72), $k = \sqrt{s}\,n_z/2$ and $P = \sqrt{s}\,\bar{n}_z/2$. We use this delta function to perform the $\mathbf{q}_T^2$ integral in Eq. (74), and then use that the spin-averaged squared amplitude is independent of φ_q, to obtain

$$\frac{d\sigma}{dx\,dQ^2} = \frac{Q^2}{8(2\pi)^2\,x^2s^2}\sum_X (2\pi)^4\delta^4(P+q-p_X)\langle|\mathcal{M}|^2\rangle\,. \tag{76}$$

Here the integrand is evaluated in the CM frame with q now given by

$$q^\mu = y\sqrt{s}\,\frac{n_z^\mu}{2} - xy\sqrt{s}\,\frac{\bar{n}_z^\mu}{2} + \sqrt{1-y}\,Q\,\hat{n}_T^\mu\,, \tag{77}$$

where $\hat{n}_T = (0,1,0,0)$ in (n^0,n_1,n_2,n_3) coordinates.

The matrix element $\mathcal{M}$ is given by

$$\mathcal{M}(eP\to e'X) = \sum_{I=\gamma,Z}\langle e'X|J^\mu_{I,EW}(0)D^I_{\mu\nu}J^\nu_{I,QCD}(0)|eP\rangle, \tag{78}$$

where the sum over I is over photon and Z exchange, $J_{I,EW}$ is the appropriate electron electroweak current, $J_{I,QCD}$ is the quark electroweak current, and $D^I_{\mu\nu}$ is the γ or Z propagator. There is an implicit sum over quark flavors. The matrix element can be factored,

$$\mathcal{M}(eP\to e'X) = \sum_{I=\gamma,Z}\langle e'|J^\mu_{I,EW}D^I_{\mu\nu}|e\rangle\langle X|J^\nu_{I,QCD}|P\rangle\,. \tag{79}$$

More conveniently, we can express the sum over i as being over the vector and axial currents in QCD,

$$J^\mu_{Vf} = \bar{q}_f\gamma^\mu q_f\,, \qquad J^\mu_{Af} = \bar{q}_f\gamma^\mu\gamma_5 q_f\,. \tag{80}$$

The sum in Eq. (78) can then be expressed as

$$\mathcal{M} = \sum_{I=V,A}\sum_f L_{I\mu}\,\langle X|\,J^\mu_{If}\,|P\rangle\,, \tag{81}$$

defining the leptonic vector $L_{I\mu}$, which contains the electron matrix element, electroweak propagator, and electroweak charges of the quarks implicit in Eq. (78). The sum over f in Eq. (81) is over quark flavors.

Now the cross section in Eq. (76) can be written

$$\frac{d\sigma}{dx\,dQ^2} = \sum_{I,I'=V,A} L^{II'}_{\mu\nu}(x,Q^2)W^{II'\mu\nu}(x,Q^2)\,, \tag{82}$$

where

$$L^{\mu\nu}_{II'}(x,Q^2) = \frac{Q^2}{32\pi^2x^2s^2}L^{\mu\dagger}_I(x,Q^2)L^\nu_{I'}(x,Q^2)\,, \tag{83a}$$

$$W^{\mu\nu}_{II'}(x,Q^2) = \sum_X \langle P|\,J^{\mu\dagger}_I\,|X\rangle\,\langle X|\,J^\nu_{I'}\,|P\rangle \times(2\pi)^4\delta^4(P+q-p_X)\,. \tag{83b}$$

Here $L^{\mu\nu}_{II'}, W^{\mu\nu}_{II'}$ depend on x, Q^2 through the components of q given in Eq. (72). The average over initial electron and proton spins is implicit in Eq. (83), as is the sum over quark flavors in Eq. (83b).

1. Leptonic tensor

The leptonic tensor in Eq. (83a) is given by

$$L^{II'}_{\mu\nu ff'}(x,Q^2) = -\frac{\alpha_{em}^2}{2x^2s^2}\Big(L^{II'}_{gff'}(Q^2)g^T_{\mu\nu} + iL^{II'}_{\epsilon ff'}(Q^2)\epsilon^T_{\mu\nu}\Big), \tag{84}$$

where

$$g^T_{\mu\nu} = g_{\mu\nu} - 2\frac{k_\mu k'_\nu + k'_\mu k_\nu}{Q^2}\,, \quad \epsilon^T_{\mu\nu} = \frac{2}{Q^2}\epsilon_{\alpha\beta\mu\nu}k^\alpha k'^\beta\,, \tag{85}$$

where $k' = k - q$, with q given in Eq. (77) and

$$\begin{aligned}
L^{VV}_{gff'} &= Q_fQ_{f'} - \frac{(Q_fv_{f'}+v_fQ_{f'})v_e}{1+m_Z^2/Q^2} + \frac{v_fv_{f'}(v_e^2+a_e^2)}{(1+m_Z^2/Q^2)^2}\,,\\
L^{VV}_{\epsilon ff'} &= -a_e\frac{Q_fv_{f'}+v_fQ_{f'}}{1+m_Z^2/Q^2} + \frac{2a_ev_fv_{f'}v_e}{(1+m_Z^2/Q^2)^2}\,,\\
L^{AA}_{gff'} &= \frac{a_fa_{f'}(v_e^2+a_e^2)}{(1+m_Z^2/Q^2)^2}\,, \quad L^{AA}_{\epsilon ff'} = \frac{2a_fa_{f'}v_ea_e}{(1+m_Z^2/Q^2)^2}\,,\\
L^{AV}_{gff'} &= L^{VA}_{gf'f} = \frac{a_f}{1+m_Z^2/Q^2}\left[Q_{f'}v_e - \frac{v_{f'}(v_e^2+a_e^2)}{1+m_Z^2/Q^2}\right],\\
L^{AV}_{\epsilon ff'} &= L^{VA}_{\epsilon f'f} = \frac{a_fa_e}{1+m_Z^2/Q^2}\left(Q_{f'} - \frac{2v_{f'}v_e}{1+m_Z^2/Q^2}\right),
\end{aligned} \tag{86}$$

where we have made explicit the flavor indices f, f'. Q_f is the electric charge of the quark q_f in units of e; v_f, a_f are the weak vector and axial charges of q_f; and v_e, a_e the weak vector and axial charges of the electron. The vector and axial charges are given by:

$$\begin{aligned}
a_f &= \frac{T_f}{\sin 2\theta_W}, \qquad v_f = \frac{T_f - 2Q_f\sin^2\theta_W}{\sin 2\theta_W}\,,\\
a_e &= -\frac{1}{2\sin 2\theta_W}, \qquad v_e = \frac{-1+4\sin^2\theta_W}{2\sin 2\theta_W}\,,
\end{aligned} \tag{87}$$

where $T_f = 1/2$ for $f = u,c,t$ and $-1/2$ for $f = d,s,b$.

B. 1-jettiness cross section

To form the cross section differential in the 1-jettiness τ_1, we insert a delta function measuring τ_1 into the hadronic tensor Eq. (83b):

$$\frac{d\sigma}{dx\,dQ^2\,d\tau_1} = \sum_{I,I'=V,A} L^{II'}_{\mu\nu}(x,Q^2)W^{II'\mu\nu}(x,Q^2,\tau_1)\,, \tag{88}$$

where the τ_1-dependent hadronic tensor is

$$W^{\mu\nu}_{II'}(x,Q^2,\tau_1) = \sum_X \langle P|\,J^{\mu\dagger}_I\,|X\rangle\,\langle X|\,J^\nu_{I'}\,|P\rangle \times(2\pi)^4\delta^4(P+q-p_X)\delta(\tau_1-\tau_1(X))\,. \tag{89}$$

Here the 1-jettiness $\tau_1(X)$ of state X is defined by Eq. (24). The definition depends on the choices of reference vectors $q_{B,J}$.

The sum over states X in Eq. (89) can be removed by using an operator $\hat{\tau}_1$ which gives $\tau_1(X)$ when acting on the state X:

$$\hat{\tau}_1 \left|X\right\rangle = \tau_1(X) \left|X\right\rangle . \tag{90}$$

This operator can be constructed from a momentum-flow operator as in [85]. Explicitly,

$$\hat{\tau}_1 = \hat{\tau}_1^J + \hat{\tau}_1^B , \tag{91}$$

where

$$\hat{\tau}_1^{J,B} = \frac{2}{Q^2} \int_{Y_{J,B}}^{\infty} dY'_{J,B}\; q_{J,B}\cdot \widehat{P}(Y'_{J,B}) . \tag{92}$$

Here $\widehat{P}(Y'_{J,B})$ is a momentum flow operator that can be defined and explicitly constructed in terms of the energy-momentum tensor, which can be obtained for massless partons using [85–88] and for massive hadrons using [72]. It measures the momentum flow in the generalized rapidity direction $Y'_{J,B}$, which we define as we did below Eq. (51) by

$$e^{-2Y_J} = \frac{n_J\cdot p}{\bar{n}_J\cdot p} , \qquad e^{-2Y_B} = \frac{n_B\cdot p}{\bar{n}_B\cdot p} . \tag{93}$$

The lower limits $Y_{J,B}$ on the integral in Eq. (92) are given according to Eq. (50) by $Y_{J,B} = \frac{1}{2}\ln(1/R_{J,B})$. These values depend on the frame of reference and choice of 1-jettiness τ_1. For example, for the choice τ_1^c of Eq. (42) in the CM frame for y near 1, the beam and jet regions are hemispheres and $Y_{J,B} = 0$. For the choice τ_1^b of Eq. (32) in the CM frame, the jet region is given by the lower limit $Y_J = \frac{1}{2}\ln(y/x)$, and the beam region is given by the lower limit $Y_B = \frac{1}{2}\ln(x/y)$.

In the massless limit the generalized rapidities $\exp(-2Y_{J,B}) \to 1-\cos\theta_{J,B}/1-\cos\theta_{B,J} n_J\cdot n_B/2$ defining generalized "pseudorapidities". They depend only on angles $\theta_{J,B}$ from the $\mathbf{n}_{J,B}$ directions and $n_J\cdot n_B$, and so simply characterize angular directions in space over which we integrate in Eq. (92).

Using Eq. (92) the hadronic tensor Eq. (89) can be written

$$W^{\mu\nu}_{II'}(x,Q^2,\tau_1) = \int d^4x\, e^{iq\cdot x} \langle P| J_I^{\mu\dagger}(x) \delta(\tau_1 - \hat{\tau}_1) J^{\nu}_{I'}(0)|P\rangle , \tag{94}$$

recalling that q is given by Eq. (77). $\hat{\tau}_1$ can also be expressed in terms of momentum operators in the regions $\mathcal{H}_{J,B}$, using Eq. (48):

$$\hat{\tau}_1 = \frac{n_J\cdot\hat{p}_J}{Q_J} + \frac{n_B\cdot\hat{p}_B}{Q_B} , \tag{95}$$

where $\hat{p}_{J,B}$ measures the total 4-momentum in region $\mathcal{H}_{J,B}$.

V. FACTORIZATION IN SCET

Soft-collinear effective theory (SCET) [18–22] is a systematic expansion of QCD in a small parameter λ which characterizes the scale of collinear and soft radiation from energetic massless partons. Soft and collinear modes are defined by the scaling of their momenta in light-cone coordinates with respect to light-like vectors $n, \bar{n}$ (not necessarily back-to-back) satisfying $n^2 = \bar{n}^2 = 0$ and $n\cdot\bar{n} = 2$. We express the components of a vector p in $n, \bar{n}$ light-cone coordinates as $p = (\bar{n}\cdot p, n\cdot p, p_\perp)$, where

$$p = \bar{n}\cdot p \frac{n}{2} + n\cdot p \frac{\bar{n}}{2} + p_\perp , \tag{96}$$

with $p_\perp$ being orthogonal to $n, \bar{n}$, defined as

$$p_\perp^\mu = g_\perp^{\mu\nu} p_\nu , \quad g_\perp^{\mu\nu} = g^{\mu\nu} - \frac{n^\mu\bar{n}^\nu + n^\nu\bar{n}^\mu}{2} . \tag{97}$$

In these light-cone coordinates, n-collinear and soft momenta scale as:

$$\text{collinear:} \qquad p_n \sim Q(1, \lambda^2, \lambda) \tag{98a}$$

$$\text{soft:} \qquad p_s \sim Q(\lambda^2, \lambda^2, \lambda^2) . \tag{98b}$$

The parameter λ is determined by the virtuality of the modes $p_n^2 \sim Q^2\lambda^2$ that contribute to the observable in question. Collinear momenta will be expressed as the sum of a large "label" piece and a small "residual" piece: $p_n = \tilde{p}_n + k$, where $\tilde{p}_n = \bar{n}\cdot\tilde{p}\, n/2 + \tilde{p}_\perp$ contains the $\mathcal{O}(Q)$ longitudinal and $\mathcal{O}(Q\lambda)$ transverse pieces, and k is the residual $\mathcal{O}(Q\lambda^2)$ piece.

A. Matching onto SCET

Now we are ready to match the currents in Eq. (94) onto operators in SCET. The QCD current

$$J^\mu_{If}(x) = \bar{q}_f(x)\Gamma^\mu_I q_f(x) , \tag{99}$$

with $\Gamma^\mu_V = \gamma^\mu$ and $\Gamma^\mu_A = \gamma^\mu\gamma_5$, matches onto operators in SCET,

$$\begin{aligned} J^\mu_{If}(x) = \sum_{n_1 n_2} \int d^3\tilde{p}_1 d^3\tilde{p}_2 e^{i(\tilde{p}_1-\tilde{p}_2)\cdot x} \\ \times \Big[C^\mu_{If q\bar{q}\alpha\beta}(\tilde{p}_1,\tilde{p}_2) \mathcal{O}^{\alpha\beta}_{q\bar{q}}(\tilde{p}_1,\tilde{p}_2;x) \\ + C^\mu_{If gg\lambda\rho}(\tilde{p}_1,\tilde{p}_2) \mathcal{O}^{\lambda\rho}_{gg}(\tilde{p}_1,\tilde{p}_2;x) \Big] , \end{aligned} \tag{100}$$

neglecting power corrections of $\mathcal{O}(\lambda^2)$. The quark and gluon SCET operators are

$$\mathcal{O}^{\alpha\beta}_{q\bar{q}}(\tilde{p}_1,\tilde{p}_2;x) = \bar{\chi}^{\alpha j}_{n_1,\tilde{p}_1}(x) \chi^{\beta j}_{n_2,\tilde{p}_2}(x) \tag{101a}$$

$$\mathcal{O}^{\lambda\rho}_{gg}(\tilde{p}_1,\tilde{p}_2;x) = \sqrt{\omega_1\omega_2}\, \mathcal{B}^{\perp\lambda c}_{n_1,\tilde{p}_1}(x) \mathcal{B}^{\perp\rho c}_{n_2,-\tilde{p}_2}(x) \tag{101b}$$

where we sum over fundamental color indices j and adjoint color indices c, but fix the spin indices $\alpha\beta$ and $\lambda\rho$.

We leave implicit that $\chi \equiv \chi_q$ carries flavor q. Below we will also leave the flavor index f on the current J_I implicit. The collinear fields $\chi_{n_i,\tilde{p}_i}$ and $\mathcal{B}^{\perp}_{n_i,\tilde{p}_i}$ carry label momenta

$$\tilde{p}_i = \frac{\omega_i n_i}{2} + \tilde{p}_i^{\perp}\,, \tag{102}$$

where $i = 1, 2$. The momentum of each collinear field can be written in $n_i, \bar{n}_i$ light-cone coordinates as in Eq. (96), with the residual x dependence of the SCET fields being conjugate to momenta k of order $Q\lambda^2$. In Eq. (100), the integrals over $\tilde{p}_{1,2}$ are continuous versions of discrete sums over the label momenta, and the measures are given by $d^3\tilde{p}_i \equiv d\omega_i d^2\tilde{p}^i_{\perp}$.

The quark jet fields $\chi_{n_1,\tilde{p}}(x)$ are products of collinear quark fields with collinear Wilson lines,

$$\chi_{n,\tilde{p}} = \left[\delta(\omega - \bar{n}\cdot\mathcal{P})\delta^2(\tilde{p}_\perp - \mathcal{P}_\perp) W_n^\dagger \xi_n\right], \tag{103}$$

where $\mathcal{P}^\mu$ is a label momentum operator [20] which acts on collinear fields and conjugate fields as:

$$\mathcal{P}^\mu \phi_{n,p} = \tilde{p}^\mu \phi_{n,p}\,, \quad \mathcal{P}^\mu \phi^\dagger_{n,p} = -\tilde{p}^\mu \phi^\dagger_{n,p} \tag{104}$$

and W_n is the Wilson line

$$W_n(x) = \sum_{\text{perms}} \exp\left[-\frac{g}{\bar{n}\cdot\mathcal{P}}\bar{n}\cdot A_n(x)\right], \tag{105}$$

where $A^\mu_n(x) = \sum_{\tilde{p}} A^\mu_{n,\tilde{p}}(x)$ is a n-collinear gluon field. The gluon jet fields $\mathcal{B}^\perp_n$ are collinear gauge-invariant products of gluon fields and Wilson lines,

$$\mathcal{B}^\perp_{n,\tilde{p}} = \frac{1}{g}[\delta(\omega + \bar{n}\cdot\mathcal{P})\delta^2(\tilde{p}_\perp + \mathcal{P}_\perp) W_n^\dagger (\mathcal{P}_\perp + g A^\perp_n) W_n]\,. \tag{106}$$

The matching coefficients $C_{q\bar{q}}, C_{gg}$ in Eq. (100) are calculated order-by-order in α_s by requiring that matrix elements of both sides of Eq. (100) between collinear states in QCD and in SCET be equal.

Collinear fields are decoupled from soft fields by the field redefinitions [21]

$$\chi_n = Y_n \chi^{(0)}_n\,, \quad A^a_n T^a = \mathcal{Y}^{ab}_n A^{(0)\,b}_n T^a = Y_n A^{(0)b}_n T^b Y^\dagger_n\,, \tag{107}$$

where Y_n is a Wilson line of soft gluons in the fundamental representation. For $n = n_B$ we have

$$Y_{n_B}(x) = P\exp\left[ig\int_{-\infty}^{0} ds\, n_B\cdot A_s(n_B s + x)\right], \tag{108}$$

and $\mathcal{Y}_{n_B}$ is defined similarly but in the adjoint representation. Soft gluons carry momenta scaling as λ^2 in all components. Additional factors accompanying outgoing states turn the path in Eq. (108) into x to ∞ [89] for outgoing collinear particles, see also [90]. So for $n = n_J$ we have

$$Y^\dagger_{n_J}(x) = P\exp\left[ig\int_{0}^{+\infty} ds\, n_J\cdot A_s(n_J s + x)\right]. \tag{109}$$

After the field redefinition Eq. (107), the operators in Eq. (101) become

$$\begin{aligned}
\mathcal{O}^{\alpha\beta}_{q\bar{q}}(\tilde{p}_1,\tilde{p}_2;x) &= \bar{\chi}^{(0)\alpha j}_{n_1,\tilde{p}_1}(x) T[Y^\dagger_{n_1} Y_{n_2}]^{jk}(x) \chi^{(0)\beta k}_{n_2,\tilde{p}_2}(x)\,,\\
\mathcal{O}^{\lambda\rho}_{gg}(\tilde{p}_1,\tilde{p}_2;x) &= \sqrt{\omega_1\omega_2}\,\mathcal{B}^{(0)\perp\lambda c}_{n_1,\tilde{p}_1}(x)\\
&\quad\times T[\mathcal{Y}^\dagger_{n_1}\mathcal{Y}_{n_2}]^{cd}(x)\mathcal{B}^{(0)\perp\rho d}_{n_2,-\tilde{p}_2}(x)\,.
\end{aligned} \tag{110}$$

The directions n_1 and n_2 will each get set equal to either n_J or n_B later on, replacing Y_{n_i} with Y_{n_B} in Eq. (108) for $n_i = n_B$ or with $Y^\dagger_{n_J}$ in Eq. (109) for $n_i = n_J$. Henceforth we use only the decoupled collinear fields and drop the $^{(0)}$ superscripts.

The measurement operators in Eq. (95) also split up into collinear and soft pieces. Since $\hat{p}$ is linear in the energy-momentum tensor, which itself splits linearly into decoupled collinear and soft components after the field redefinition Eq. (107) [85], $\hat{p}$ splits up as

$$\hat{p} = \hat{p}^{n_1} + \hat{p}^{n_2} + \hat{p}^s \tag{111}$$

where $\hat{p}^{n_1,n_2,s}$ is built only out of the n_1-collinear, n_2-collinear, or soft energy-momentum tensor of SCET, respectively.

After matching the product of currents $J^\dagger_\mu J'_\nu$ in the hadronic tensor in Eq. (94) onto SCET, there will be products of the quark and gluon operators $(\mathcal{O}_{q\bar{q}} + \mathcal{O}_{gg})(\mathcal{O}'_{q\bar{q}} + \mathcal{O}'_{gg})$. The $\mathcal{O}_{q\bar{q}}\mathcal{O}'_{gg}$ and $\mathcal{O}_{gg}\mathcal{O}'_{q\bar{q}}$ cross terms will vanish inside the proton-proton matrix element by quark-number conservation (only one of the fields $\bar{\chi}_{n_1}$ or χ_{n_2} in $\mathcal{O}_{q\bar{q}}$ will create/annihilate a quark in the collinear proton). Thus only the $\mathcal{O}_{q\bar{q}}\mathcal{O}'_{q\bar{q}}$ and $\mathcal{O}_{gg}\mathcal{O}'_{gg}$ operator products can contribute.

In fact, for DIS, only the quark operator product contributes, just as in Drell-Yan (DY) [67]. Following the arguments in [67], we know that the matching coefficients $C^\mu_{Igg}(\tilde{p}_1,\tilde{p}_2)$ must be a linear combination of $\tilde{p}^\mu_1$ and $\tilde{p}^\mu_2$, and obey the symmetry

$$C^{\lambda\rho}_{Igg\mu}(\tilde{p}_1,\tilde{p}_2) = C^{\rho\lambda}_{Igg\mu}(-\tilde{p}_2,-\tilde{p}_1)\,, \tag{112}$$

due to the structure of the operator Eq. (101b). This requires C^μ_{Igg} to be proportional to $(\tilde{p}_2 - \tilde{p}_1)^\mu$, which the x integration in Eq. (94) will eventually set equal to q^μ. Vector current conservation in QCD requires $q_\mu C^\mu_{Vgg} = 0$, which requires that C^μ_{Vgg} be identically zero. The axial current matching coefficient C^μ_{Agg} can be nonzero, but still proportional to $\tilde{p}^\mu_2 - \tilde{p}^\mu_1 = q^\mu$, which gives zero contribution when contracted with the lepton tensor Eq. (84). Thus for DIS we need only consider the quark operator contribution as in DY.

B. Factorization of the Hadronic Tensor

The hadronic tensor Eq. (94) can now be written in SCET as

$$
\begin{aligned}
W_{\mu\nu}^{II'}(x,Q^2,\tau_1) = \int d^4x\, e^{iq\cdot x} \sum_{\substack{n_1 n_2\\ n_1' n_2'}} \int d^3\tilde{p}_1 d^3\tilde{p}_2 d^3\tilde{p}_1' d^3\tilde{p}_2'\, e^{i(\tilde{p}_2-\tilde{p}_1)\cdot x} \int d\tau_J d\tau_B d\tau_s \delta(\tau_1-\tau_J-\tau_B-\tau_s) \\
\times \langle P_{n_B}|\, \bar{C}^{\beta\alpha}_{I q\bar{q}\mu}(\tilde{p}_1,\tilde{p}_2) \bar{\chi}^{\beta k}_{n_2,\tilde{p}_2} \overline{T}[Y^\dagger_{n_2} Y_{n_1}]^{kj} \chi^{\alpha j}_{n_1,\tilde{p}_1}(x) \delta\Big(\tau_J - \frac{n_J\cdot\hat{p}^{n_J}}{Q_J}\Big)\delta\Big(\tau_B - \frac{n_B\cdot\hat{p}^{n_B}}{Q_B}\Big) \\
\times \delta\Big(\tau_s - \frac{n_J\cdot\hat{p}^s_J}{Q_J} - \frac{n_B\cdot\hat{p}^s_B}{Q_B}\Big) C^{\alpha'\beta'}_{I' q\bar{q}\nu}(\tilde{p}_1',\tilde{p}_2') \bar{\chi}^{\alpha' j'}_{n_1',\tilde{p}_1'} T[Y^\dagger_{n_1'} Y_{n_2'}]^{j'k'} \chi^{\beta' k'}_{n_2',\tilde{p}_2'}(0)\,|P_{n_B}\rangle\,. \qquad (113)
\end{aligned}
$$

We have explicitly specified that the proton is an n_B-collinear state. The conjugate quark matching coefficient is given by $\bar{C}^{\beta\alpha}_{I q\bar{q}\mu}(\tilde{p}_1,\tilde{p}_2) = [\gamma^0 C^\dagger_{I q\bar{q}}(\tilde{p}_1,\tilde{p}_2)\gamma^0]^{\beta\alpha}$. We have used that the measurement operator $\hat{\tau}_1$ can be written in the form Eq. (95), and that the momentum operators $\hat{p}_{J,B}$ split up linearly into purely n_J- and n_B-collinear and soft operators as in Eq. (111). We dropped the subscripts J, B on the collinear momentum operators restricting them to the jet or beam regions $\mathcal{H}_{J,B}$ determined by the definition of τ_1, since all n_B collinear particles are grouped in region B and all n_J-collinear particles are grouped in region J. In the soft sector, the restrictions of the operators $\hat{\tau}^s_{J,B}$ to the $\mathcal{H}_{J,B}$ regions remain.

Since the n_1-collinear, n_2-collinear and the soft sectors are all decoupled from one another, the proton matrix element in Eq. (113) can be factored,

$$
\begin{aligned}
W_{\mu\nu}^{II'}(x,Q^2,\tau_1) = \int d^4x \int d^3\tilde{p}_1 d^3\tilde{p}_2 e^{i(q+\tilde{p}_2-\tilde{p}_1)\cdot x} \int d\tau_J d\tau_B d\tau_s \delta(\tau_1-\tau_J-\tau_B-\tau_s) \bar{C}^{\beta\alpha}_{I q\bar{q}\mu}(\tilde{p}_1,\tilde{p}_2) C^{\alpha'\beta'}_{I' q\bar{q}\nu}(\tilde{p}_1,\tilde{p}_2) \\
\times \langle 0|\,[Y^\dagger_{n_B} Y_{n_J}]^{kj}(x) \delta\Big(\tau_s - \frac{n_J\cdot\hat{p}^s_J}{Q_J} - \frac{n_B\cdot\hat{p}^s_B}{Q_B}\Big) [Y^\dagger_{n_J} Y_{n_B}]^{j'k'}(0)\,|0\rangle \qquad (114) \\
\times \Big\{ \langle P_{n_B}|\, \bar{\chi}^{\beta k}_{n_B,\tilde{p}_2}(x) \delta\Big(\tau_B - \frac{n_B\cdot\hat{p}^{n_B}}{Q_B}\Big) \chi^{\beta' k'}_{n_B}(0)\,|P_{n_B}\rangle \langle 0|\, \chi^{\alpha j}_{n_J,\tilde{p}_1}(x) \delta\Big(\tau_J - \frac{n_J\cdot\hat{p}^{n_J}}{Q_J}\Big) \bar{\chi}^{\alpha' j'}_{n_J}(0)\,|0\rangle \\
+ \langle P_{n_B}|\, \chi^{\alpha j}_{n_B,\tilde{p}_1}(x) \delta\Big(\tau_B - \frac{n_B\cdot\hat{p}^{n_B}}{Q_B}\Big) \bar{\chi}^{\alpha' j'}_{n_B}(0)\,|P_{n_B}\rangle \langle 0|\, \bar{\chi}^{\beta k}_{n_J,\tilde{p}_2}(x) \delta\Big(\tau_J - \frac{n_J\cdot\hat{p}^{n_J}}{Q_J}\Big) \chi^{\beta' k'}_{n_J}(0)\,|0\rangle \Big\}.
\end{aligned}
$$

The last two lines account for the two ways to choose a pair of collinear fields in the proton matrix element. We have performed the sums over $n_{1,2}, n_{1,2}'$ sums using that the fields within each collinear matrix element must all be in the same collinear sector. We also require that the fields in the proton matrix element must be in the same collinear sector as the proton, and those in the vacuum matrix element with the direction n_J in the definition of τ_1. The integrals over $\tilde{p}_{1,2}'$ have been absorbed into the definition of the unlabeled fields $\chi_{n_{1,2}}$. In the soft matrix element we have used the fact that $T[Y^\dagger_{n_J} Y_{n_B}] = Y^\dagger_{n_J} Y_{n_B}$ and $\overline{T}[Y^\dagger_{n_B} Y_{n_J}] = Y^\dagger_{n_B} Y_{n_J}$ since the two Wilson lines are space-like separated and the time ordering is the same as the path ordering [91, 92]. For the soft Wilson line matrix element corresponding to antiquarks in the beam and jet functions, we have used charge conjugation to relate it to the matrix element shown in Eq. (114).

It is measuring τ_1 to be small that enforces that the direction n_J on the collinear fields in the vacuum matrix element be equal to the direction of the vector q_J in the definition of the 1-jettiness τ_1. We are free to choose any vector q_J to define the observable τ_1. Requiring that the final-state jet J be close to the direction of q_J may, in general, impose additional kinematic constraints on x, y, Q^2 to ensure this. We will find below that for $\tau_1^{a,b}$, q_J is already chosen to be close to the final-state jet and so imposes no additional constraints, while for τ_1^c requiring the jet be close to $q_J^c = k$ requires y to be near 1.

Next we wish to perform the x integral in Eq. (114) to enforce label momentum conservation. Before doing so, we consider the residual momentum dependence conjugate to the coordinate x in the SCET matrix elements. The collinear field $\chi_{n,\tilde{p}}(x)$ with a continuous label momentum $\tilde{p}$ depends only on single spatial component $\bar{n}\cdot x$ because the residual momenta (conjugate to the spatial components $n\cdot x, x_\perp$) are reabsorbed into $\tilde{p}$ when the discrete label is made continuous. Then, the matrix element of n-collinear fields are $\mathcal{M}_n = \mathcal{M}_n(\bar{n}\cdot x)$. For convenience the soft matrix element with $Y_n(x)$ and $Y_{\bar{n}}(x)$ will be defined as $\mathcal{M}_s(x)$. Their Fourier transforms take the form

$$
\mathcal{M}_n(\bar{n}\cdot x) = \int \frac{dn\cdot k}{2\pi} e^{in\cdot k\, \bar{n}\cdot x/2} \widetilde{\mathcal{M}}_n(n\cdot k)\,, \qquad \mathcal{M}_s(x) = \int \frac{d^4k_s}{(2\pi)^4} e^{ik_s\cdot x} \widetilde{\mathcal{M}}_s(k_s)\,, \qquad (115)
$$

where k, k_s is a residual or soft momentum of order $Q\lambda^2$. When combined with the exponentials containing q or label momenta $\tilde{p}_{1,2}$, we can expand the exponents using $q+\tilde{p}+k = (q+\tilde{p})[1+\mathcal{O}(\lambda^2)]$, and drop the terms of order λ^2.

Then the remaining integrals over $n\cdot k, k_s$ are simply the Fourier transforms of the position space matrix elements evaluated at $x=0$. So, we can set $x=0$ in the SCET matrix elements, and perform the x integral in Eq. (114) to enforce label momentum conservation.

In performing the x integration, we have a choice to write x and momenta in $n_B, \bar{n}_B$ coordinates or $n_J, \bar{n}_J$ coordinates. In fact, we have freedom to define the vectors $\bar{n}_{J,B}$ as long as we choose them such that $\bar{n}_B^2 = \bar{n}_J^2 = 0$ and $n_J\cdot\bar{n}_J = n_B\cdot\bar{n}_B = 2$. Since the measurement of τ_1 involves measurements of both $n_J\cdot p$ and $n_B\cdot p$ components of particles' momenta, it is convenient to choose $\bar{n}_B$ to be proportional to n_J and $\bar{n}_J$ to be proportional to n_B, as we did in Eq. (51), a choice we will continue to use in what follows.

For the first pair of collinear matrix elements in Eq. (114), the x integral and accompanying phase factor for label momentum conservation take the form

$$\begin{aligned}\int d^4x\, e^{i(q+\tilde{p}_2-\tilde{p}_1)\cdot x} &= \int \frac{dn_B\cdot x\, d\bar{n}_B\cdot x}{2} d^2x_\perp \exp\biggl\{(\bar{n}_B\cdot q+\omega_2)\frac{n_B\cdot x}{2} + n_B\cdot q\frac{\bar{n}_B\cdot x}{2} - \omega_1\frac{n_J\cdot x}{2} + (q_\perp+\tilde{p}_2^\perp-\tilde{p}_1^\perp)\cdot x_\perp\biggr\}\\ &= 2(2\pi)^4\delta(\bar{n}_B\cdot q+\omega_2)\delta\Bigl(n_B\cdot q - \frac{n_J\cdot n_B\,\omega_1}{2}\Bigr)\delta^2(q_\perp+\tilde{p}_2^\perp-\tilde{p}_1^\perp)\\ &= \frac{4}{n_J\cdot n_B}(2\pi)^4\delta(\bar{n}_B\cdot q+\omega_2)\delta(\bar{n}_J\cdot q-\omega_1)\delta^2(q_\perp+\tilde{p}_2^\perp-\tilde{p}_1^\perp)\,, \end{aligned} \tag{116}$$

where we used Eq. (51) to rewrite $n_J\cdot x$ in terms of $\bar{n}_B\cdot x$ in the first line and to rewrite $n_B\cdot q$ in terms of $\bar{n}_J\cdot q$ in the last line. Exchanging ω_2 and $-\omega_1$ in Eq. (116) gives us the label momentum-conserving delta functions for the second pair of collinear matrix elements in Eq. (114). Using these delta functions to perform the $\omega_{1,2}$ and $\tilde{p}_1^\perp$ integrals in Eq. (114), we obtain

$$\begin{aligned} W_{\mu\nu}^{II'}(x,Q^2,\tau_1) &= 2(2\pi)^4(Q_JQ_B)^2\int d^2\tilde{p}_\perp \frac{2}{n_J\cdot n_B}\int d\tau_J d\tau_B d\tau_s^J\, d\tau_s^B \delta(\tau_1-\tau_J-\tau_B-\tau_s^J-\tau_s^B)\\ &\quad\times\bigl[\bar{C}_{Iq\bar{q}\mu}^{\beta\alpha}C_{I'q\bar{q}\nu}^{\alpha'\beta'}\bigr]\Bigl(\bar{n}_J\cdot q\frac{n_J}{2}+q_\perp+\tilde{p}_\perp, -\bar{n}_B\cdot q\frac{n_B}{2}+\tilde{p}_\perp\Bigr)\\ &\quad\times\langle 0|\,[Y_{n_B}^\dagger Y_{n_J}]^{kj}(0)\delta(Q_J\tau_s^J-n_J\cdot\hat{p}_J^s)\delta(Q_B\tau_s^B-n_B\cdot\hat{p}_B^s)[Y_{n_J}^\dagger Y_{n_B}]^{j'k'}(0)\,|0\rangle\\ &\quad\times\biggl\{\langle P_{n_B}|\,\bar{\chi}_{n_B}^{\beta k}(0)\delta(Q_B\tau_B-n_B\cdot\hat{p}^{n_B})\Bigl[\delta(\bar{n}_B\cdot q+\bar{n}_B\cdot\mathcal{P})\delta^2(\tilde{p}_\perp-\mathcal{P}_\perp)\chi_{n_B}^{\beta'k'}(0)\Bigr]\,|P_{n_B}\rangle\\ &\qquad\times\langle 0|\,\chi_{n_J}^{\alpha j}(0)\delta(Q_J\tau_J-n_J\cdot\hat{p}^{n_J})\delta(\bar{n}_J\cdot q+\bar{n}_J\cdot\mathcal{P})\delta^2(q_\perp+\tilde{p}_\perp+\mathcal{P}_\perp)\bar{\chi}_{n_J}^{\alpha'j'}(0)\,|0\rangle\\ &\quad+\langle P_{n_B}|\,\chi_{n_B}^{\alpha j}(0)\delta(Q_B\tau_B-n_B\cdot\hat{p}^{n_B})\bigl[\delta(\bar{n}_B\cdot q+\bar{n}_B\cdot\mathcal{P})\delta^2(\tilde{p}_\perp-\mathcal{P}_\perp)\bar{\chi}_{n_B}^{\alpha'j'}(0)\bigr]\,|P_{n_B}\rangle\\ &\qquad\times\langle 0|\,\bar{\chi}_{n_J}^{\beta k}(0)\delta(Q_J\tau_J-n_J\cdot\hat{p}^{n_J})\delta(\bar{n}_J\cdot q+\bar{n}_J\cdot\mathcal{P})\delta^2(q_\perp+\tilde{p}_\perp+\mathcal{P}_\perp)\chi_{n_J}^{\alpha'j'}(0)\,|0\rangle\biggr\}, \end{aligned} \tag{117}$$

where we use the change of variables $\tilde{p}_2^\perp=\tilde{p}_\perp$ in 3rd and 4th lines and $\tilde{p}_2^\perp=-\tilde{p}_\perp-q_\perp$ in 5th and 6th lines. Recall that $\bar{n}_B$ and $\bar{n}_J$ are now fixed by Eq. (51). The collinear fields without labels implicitly contain a sum over all labels, with the delta functions then fixing the labels to a single value (it is important to recall that label operators $\mathcal{P}^\mu$ acting on fields $\bar{\chi}_{n,\tilde{p}}$ give minus the label momentum, $-\tilde{p}^\mu$ [20]). The vector n_J (may) implicitly depend on the integration variable $\tilde{p}_\perp$, at least for the case of the τ_1^a distribution, which we will deal with below. For τ_1^b and τ_1^c the vector n_J is independent of $\tilde{p}_\perp$. We have also indicated that the arguments of the matching coefficients $\bar{C}, C$ are both set equal to the label momenta of the fields in the collinear proton and vacuum matrix elements.

The result in Eq. (117) is organized in terms of factorized matrix elements that can now be related to known functions in SCET.

C. SCET Matrix Elements

1. Beam Functions

The proton matrix elements in Eq. (117) can be expressed in terms of *generalized beam functions* [93, 94] in SCET. In covariant gauges (for discussion of similar matrix elements in light-cone gauges see [95–97]) they are defined by

$$\mathcal{B}_q\Bigl(\omega k^+,\frac{\omega}{P^-},k_\perp^2,\mu\Bigr) = \frac{\theta(\omega)}{\omega}\int\frac{dy^-}{4\pi}e^{ik^+y^-/2}\bigl\langle P_n(P^-)\bigr|\,\bar{\chi}_n\Bigl(y^-\frac{n}{2}\Bigr)\frac{\bar{n}\!\!\!/}{2}\Bigl[\delta(\omega-\bar{n}\cdot\mathcal{P})\frac{1}{\pi}\delta(k_\perp^2-\mathcal{P}_\perp^2)\chi_n(0)\Bigr]\bigl|P_n(P^-)\bigr\rangle\,, \tag{118}$$

$$\mathcal{B}_{\bar{q}}\Bigl(\omega k^+,\frac{\omega}{P^-},k_\perp^2,\mu\Bigr) = \frac{\theta(\omega)}{\omega}\int\frac{dy^-}{4\pi}e^{ik^+y^-/2}\bigl\langle P_n(P^-)\bigr|\,\mathrm{tr}\,\frac{\bar{n}\!\!\!/}{2}\chi_n\Bigl(y^-\frac{n}{2}\Bigr)\Bigl[\delta(\omega-\bar{n}\cdot\mathcal{P})\frac{1}{\pi}\delta(k_\perp^2-\mathcal{P}_\perp^2)\bar{\chi}_n(0)\Bigr]\bigl|P_n(P^-)\bigr\rangle\,,$$

where the light-cone components of vectors are given by $V^+ \equiv n\cdot V$ and $V^- \equiv \bar n\cdot V$. Note the dependence of the beam functions on the transverse label momentum $k_\perp$ is only on the squared magnitude $k_\perp^2$. The matrix elements in Eqs. (118) and (119) are similar to those that define parton distribution functions, but the separation of the collinear fields in the n direction means there is energetic collinear radiation from the proton with virtuality $\sim \omega k^+ \gg \Lambda^2_{\rm QCD}$ (assuming we are measuring k^+ to be large enough), which must be integrated out to match Eq. (118) onto nonperturbative PDFs (where the separation of $\bar\chi_n, \chi_n$ fields is zero). The generalized beam functions Eq. (118) are related to the ordinary beam functions originally defined in [67] by integrating over all $\mathbf{k}_\perp$:

$$B_{q,\bar q}\Big(\omega k^+, \frac{\omega}{P^-}, \mu\Big) = \int d^2\mathbf{k}_\perp \mathcal{B}_{q,\bar q}\Big(\omega k^+, \frac{\omega}{P^-}, k_\perp^2, \mu\Big)\,. \tag{119}$$

This relationship would be subtle for PDFs, where it is true for the bare matrix elements, but where after renormalization the two objects may no longer be simply related. In the beam function case both sides have the same anomalous dimension which is independent of $k_\perp$ and there is no such subtelty.

The proton matrix elements in Eq. (117) can now be expressed as

$$\begin{aligned}
&\langle P_{n_B}|\,\bar\chi^{\beta k}_{n_B}(0)\delta(Q_B\tau_B - n_B\cdot\hat p^{n_B})\big[\delta(\bar n_B\cdot q + \bar n_B\cdot\mathcal{P})\delta^2(\tilde p_\perp - \mathcal{P}_\perp)\chi^{\beta' k'}_{n_B}(0)\big]\,|P_{n_B}\rangle \\
&\qquad = -\bar n_B\cdot q\,\frac{\not n^{\beta'\beta}_B}{4}\frac{\delta^{kk'}}{N_C}\mathcal{B}_q\Big(s_B\tau_B, -\frac{\bar n_B\cdot q}{\bar n_B\cdot P}, \tilde p_\perp^2, \mu\Big), \\
&\langle P_{n_B}|\,\chi^{\alpha j}_{n_B}(0)\delta(Q_B\tau_B - n_B\cdot\hat p^{\bar n})\big[\delta(\bar n_B\cdot q + \bar n_B\cdot\mathcal{P})\delta^2(\tilde p_\perp - \mathcal{P}_\perp)\bar\chi^{\alpha' j'}_{n_B}(0)\big]\,|P_{n_B}\rangle \\
&\qquad = -\bar n_B\cdot q\,\frac{\not n^{\alpha\alpha'}_B}{4}\frac{\delta^{jj'}}{N_C}\mathcal{B}_{\bar q}\Big(s_B\tau_B, -\frac{\bar n_B\cdot q}{\bar n_B\cdot P}, \tilde p_\perp^2, \mu\Big)\,,
\end{aligned} \tag{120}$$

where s_B is defined in Eq. (58). Now, to simplify the second argument of the beam functions, we note that

$$x = -\frac{q^2}{2q\cdot P} = -\frac{\bar n_B\cdot q\, n_B\cdot q + q_\perp^2}{n_B\cdot q\,\bar n_B\cdot P} = -\frac{\bar n_B\cdot q}{\bar n_B\cdot P} + \mathcal{O}(\lambda^2)\,, \tag{121}$$

where in the second equality we used that the proton momentum P is exactly along the n_B direction, and in the last step used that $q_\perp$ is no bigger than $\mathcal{O}(Q\lambda^2)$. (The directions n_J and n_B will always be chosen so that this is true, according to Eqs. (116) and (B1a). In other words, for events with small 1-jettiness, all the large momentum q transferred into the final state is collimated along n_J and n_B with no $\mathcal{O}(Q)$ momentum going in a third direction.) Thus to leading order in λ the second argument of the beam functions in Eq. (120) is always just x.

2. Jet Functions

The vacuum collinear matrix elements in Eq. (117) can be written in terms of jet functions in SCET [21], defined with transverse displacement of the jet in [67] by

$$\begin{aligned}
J_q(\omega k^+ + \omega_\perp^2, \mu) &= \frac{(2\pi)^2}{N_C}\int\frac{dy^-}{2\,|\omega|}e^{ik^+y^-/2}\,\mathrm{tr}\,\Big\langle 0\Big|\frac{\bar{\not n}}{2}\chi_n\Big(y^-\frac{n}{2}\Big)\delta(\omega + \bar n\cdot\mathcal{P})\delta^2(\omega_\perp + \mathcal{P}_\perp)\bar\chi_n(0)\Big|0\Big\rangle, \\
J_{\bar q}(\omega k^+ + \omega_\perp^2, \mu) &= \frac{(2\pi)^2}{N_C}\int\frac{dy^-}{2\,|\omega|}e^{ik^+y^-/2}\Big\langle 0\Big|\bar\chi_n\Big(y^-\frac{n}{2}\Big)\delta(\omega + \bar n\cdot\mathcal{P})\delta^2(\omega_\perp + \mathcal{P}_\perp)\frac{\bar{\not n}}{2}\chi_n(0)\Big|0\Big\rangle\,.
\end{aligned} \tag{122}$$

Thus the vacuum collinear matrix elements in Eq. (117) can be expressed

$$\begin{aligned}
&\langle 0|\,\chi^{\alpha j}_{n_J}(0)\delta(Q_J\tau_J - n_J\cdot\hat p_n)\delta(\bar n_J\cdot q + \bar n_J\cdot\mathcal{P})\delta^2(q_\perp + \tilde p_\perp + \mathcal{P}_\perp)\bar\chi^{\alpha' j'}_{n_J}(0)\,|0\rangle \\
&\qquad = \frac{\bar n_J\cdot q}{(2\pi)^3}\frac{\not n_J^{\alpha\alpha'}}{4}\delta^{jj'}J_q(s_J\tau_J + (q_\perp + \tilde p_\perp)^2, \mu)\,, \\
&\langle 0|\,\bar\chi^{\beta k}_{n_J}(0)\delta(Q_J\tau_J - n_J\cdot\hat p_n)\delta(\bar n_J\cdot q + \bar n_J\cdot\mathcal{P})\delta^2(q_\perp + \tilde p_\perp + \mathcal{P}_\perp)\chi^{\beta' k'}_{n_J}(0)\,|0\rangle \\
&\qquad = \frac{\bar n_J\cdot q}{(2\pi)^3}\frac{\not n_J^{\beta'\beta}}{4}\delta^{kk'}J_{\bar q}(s_J\tau_J + (q_\perp + \tilde p_\perp)^2, \mu)\,,
\end{aligned} \tag{123}$$

where s_J is defined in Eq. (58) and $(q_\perp + \tilde p_\perp)^2 = -(\mathbf{q}_\perp + \tilde{\mathbf{p}}_\perp)^2$.

3. Hard and Soft Functions

Using the above definitions of beam and jet functions, the hadronic tensor in Eq. (117) can be written as

$$\begin{aligned} W_{\mu\nu}^{II'}(x,Q^2,\tau_1) = -2(2\pi)\bar{n}_B\cdot q\,\bar{n}_J\cdot q (Q_J Q_B)^2 \int d^2\tilde{p}_\perp \frac{2}{n_J\cdot n_B}\int d\tau_J d\tau_B d\tau_s^J\, d\tau_s^B \delta(\tau_1-\tau_J-\tau_B-\tau_s^J-\tau_s^B) \\ \times S(Q_J\tau_s^J, Q_B\tau_s^B, n_J\cdot n_B,\mu) J_q(s_J\tau_J + (q_\perp+\tilde{p}_\perp)^2,\mu) \\ \times \Big[H_{q\bar{q}\mu\nu}^{II'}(q^2,n_J,n_B)\mathcal{B}_q(s_B\tau_B,x,\tilde{p}_\perp^2,\mu) + H_{q\bar{q}\mu\nu}^{II'}(q^2,n_B,n_J)\mathcal{B}_{\bar{q}}(s_B\tau_B,x,\tilde{p}_\perp^2,\mu)\Big]. \end{aligned} \tag{124}$$

where the hard function is defined

$$H_{q\bar{q}\mu\nu}^{II'}((\tilde{p}_1-\tilde{p}_2)^2,n_a,n_b) = \mathrm{Tr}\Big[\bar{C}_{Iq\bar{q}\mu}(\tilde{p}_1,\tilde{p}_2)\frac{\not{n}_a}{4} C_{I'q\bar{q}\nu}(\tilde{p}_1,\tilde{p}_2)\frac{\not{n}_b}{4}\Big], \tag{125}$$

and the soft function is defined

$$S(k_J,k_B,q_J,q_B,\mu) = \frac{1}{N_C}\,\mathrm{tr}\,\langle 0|\,[Y_{n_B}^\dagger Y_{n_J}](0)\delta(k_J-n_J\cdot\hat{p}_J^s)\delta(k_B-n_B\cdot\hat{p}_B^s)[Y_{n_J}^\dagger Y_{n_B}](0)\,|0\rangle\,. \tag{126}$$

To write Eq. (124) we used the equality of the quark and antiquark jet functions $J_{q,\bar{q}}$ in QCD.

a. Structure of the hard functions In Eq. (125), the matching coefficients $C, \bar{C}$ in the hard function Eq. (125) for the vector and axial currents $I = V, A$ take the form

$$C_{Vf\,q\bar{q}}^\mu(\tilde{p}_1,\tilde{p}_2) = C_{Vfq}((\tilde{p}_1-\tilde{p}_2)^2)\gamma_\perp^\mu\,, \quad C_{Af\,q\bar{q}^\mu}(\tilde{p}_1,\tilde{p}_2) = C_{Afq}((\tilde{p}_1-\tilde{p}_2)^2)\gamma_\perp^\mu\gamma_5\,, \tag{127}$$

where $\gamma_\perp^\mu$ is transverse to the directions $n_{1,2}$ of the label momenta $\tilde{p}_{1,2}$. We have shown the index f for the quark flavor in the current explicitly. In Eq. (124) these directions are $n_{J,B}$. The scalar coefficients $C_{Vf\,q\bar{q}}, C_{Af\,q\bar{q}}$ depend only on the symmetric Lorentz-invariant combination $(\tilde{p}_1-\tilde{p}_2)^2$. Using the momentum-conserving delta function in Eq. (117), this combination takes the value $(\tilde{p}_1-\tilde{p}_2)^2 = q^2$. Inserting Eq. (127) into Eq. (125) we obtain

$$H_{q\bar{q}\mu\nu}^{II'}(q^2,n_J,n_B,\mu) = C_{Ifq}(q^2,\mu)C_{I'f'q}(q^2,\mu)\,\mathrm{Tr}\Big(\Gamma_\mu^I\frac{\not{n}_J}{4}\Gamma_\nu^{I'}\frac{\not{n}_B}{4}\Big), \tag{128}$$

where $\Gamma_\mu^V = \gamma_\perp^\mu$ and $\Gamma_\mu^A = \gamma_\perp^\mu\gamma_5$. Thus, there are two distinct traces to take in Eq. (128):

$$\begin{aligned} H_{q\bar{q}\mu\nu}^{VV,AA}(q^2,n_J,n_B,\mu) &= -\frac{n_J\cdot n_B}{4}C_{V,A\,fq}(q^2,\mu)C_{V,A\,f'q}(q^2,\mu)g_\perp^{\mu\nu}\,, \\ H_{q\bar{q}\mu\nu}^{VA,AV}(q^2,n_J,n_B,\mu) &= -i\frac{n_J\cdot n_B}{4}C_{V,A\,fq}(q^2,\mu)C_{A,V\,f'q}(q^2,\mu)\epsilon_\perp^{\mu\nu}\,, \end{aligned} \tag{129}$$

where $g_\perp^{\mu\nu}$ and $\epsilon_\perp^{\mu\nu}$ are symmetric and antisymmetric tensors orthogonal to n_J and n_B given in Eq. (B1). Hence, $H^{VV,AA}$ and $H^{VA,AV}$ are symmetric and antisymmetric, respectively, under exchanging n_J and n_B.

b. Structure of the soft function The soft function Eq. (126) depends on the momenta $k_{B,J}$ projected onto the $n_{B,J}$ directions in the regions $\mathcal{H}_{B,J}$, respectively. The shape of these regions in turn depends on the vectors $q_{B,J} = \omega_{B,J}n_{B,J}/2$ in the definition of the 1-jettiness τ_1 in Eq. (24). Indicating this dependence explicitly, we express the soft function Eq. (126) as

$$\begin{aligned} S(k_J,k_B,q_J,q_B,\mu) = \frac{1}{N_C}\,\mathrm{tr}\sum_{X_s}\big|\langle X_s|\,[Y_{n_J}^\dagger Y_{n_B}](0)\,|0\rangle\big|^2\;\delta\Big(k_J-\sum_{i\in X_s}\theta(q_B\cdot k_i - q_J\cdot k_i)n_J\cdot k_i\Big) \\ \times\,\delta\Big(k_B-\sum_{i\in X_s}\theta(q_J\cdot k_i - q_B\cdot k_i)n_B\cdot k_i\Big)\,. \end{aligned} \tag{130}$$

Note that the soft function for DIS involves the square of one incoming and one outgoing Wilson line, and hence differs from that for $e^+e^-\to$ dijets that has two outgoing lines, and for $pp\to L+0-$jets which has two incoming lines. We can relate Eq. (130) to the usual hemisphere soft function for DIS by generalizing an argument given in [98]. Note that the Wilson lines Y_n are invariant under rescaling of n (boost invariance):

$$Y_{\beta n_B} = P\exp\left[ig\int_{-\infty}^0 ds\,\beta n_B\cdot A_s(\beta n_B s)\right] = P\exp\left[ig\int_{-\infty}^0 ds\,n_B\cdot A_s(n_B s)\right] = Y_{n_B}\,, \tag{131}$$

and similarly for the lines extending from 0 to $+\infty$, $Y_{\beta n_J} = Y_{n_J}$. Recall from Eq. (50) that

$$R_J = \sqrt{\frac{\omega_B n_B \cdot n_J}{2\omega_J}}\,, \qquad R_B = \sqrt{\frac{\omega_J n_J \cdot n_B}{2\omega_B}}\,, \tag{132}$$

so defining $n'_J = n_J/R_J$ and $n'_B = n_B/R_B$ we have $(q_B - q_J)\cdot k_i = \frac{1}{2}\omega_B R_B\,(n'_B - n'_J)\cdot k_i$ since $\omega_J R_J = \omega_B R_B$. This implies that the same partitioning defined in Eq. (130) can be expressed with $\theta(n'_B\cdot k_i - n'_J\cdot k_i)$ and $\theta(n'_J\cdot k_i - n'_B\cdot k_i)$. Furthermore $n'_B\cdot n'_J = 2$. Thus expressing Eq. (130) in terms of the rescaled vectors, n'_J and n'_B, we obtain

$$\begin{aligned} S(k_J,k_B,q_J,q_B,\mu) &= \frac{1}{N_C R_J R_B}\,\mathrm{tr}\sum_{X_s}\Big|\langle X_s|\,[Y^\dagger_{n'_J}Y_{n'_B}](0)\,|0\rangle\Big|^2\,\delta\Big(\frac{k_J}{R_J} - \sum_{i\in X_s}\theta(n'_B\cdot k_i - n'_J\cdot k_i)n'_J\cdot k_i\Big) \\ &\quad\times\delta\Big(\frac{k_B}{R_B} - \sum_{i\in X_s}\theta(n'_J\cdot k_i - n'_B\cdot k_i)n'_B\cdot k_i\Big) \\ &= \frac{1}{R_J R_B}\,S_{\rm hemi}\Big(\frac{k_J}{R_J},\frac{k_B}{R_B},\mu\Big)\,. \end{aligned} \tag{133}$$

In the last equality we have expressed the fact that the expression in Eq. (133) is the same as the hemisphere soft function (up to the overall $1/(R_J R_B)$ in front), with momentum arguments rescaled by $R_{J,B}$ as indicated. Therefore from here on we will write all the τ_1 factorization theorems in terms of the DIS hemiphere soft function. Note that the vectors $n'_{J,B}$ have been rescaled from $n_{J,B}$ such that they no longer have timelike components equal to 1 nor spacelike magnitudes equal to each other, and therefore do not partition the final states X_s into hemispheres as viewed in the original $n_{J,B}$ frame of reference. However, the soft function in Eq. (133) depends on $n'_{J,B}$ exactly like the hemisphere soft function depends on $n_{J,B}$ and depends on the dot product $n'_J\cdot n'_B$, which is 2, making it equal to the hemisphere soft function. Physically, there exists a frame where n'_J and n'_B are back-to-back with equal time-like components, so that the partitioning in this frame gives hemispheres.

In the 1-jettiness cross sections below, the soft function Eq. (133) will always be projected symmetrically onto a function of a single variable k_S, following from Eq. (124):

$$S_{\rm hemi}(k_S,\mu) = \int dk_S^J\,dk_S^B\,\delta(k_S - k_S^J - k_S^B)S_{\rm hemi}(k_S^J,k_S^B,\mu)\,, \tag{134}$$

We will use the same name $S_{\rm hemi}$ for the hemisphere soft function of two variables in Eq. (133) and its one-variable projection Eq. (134), distinguishing them by the number of arguments we write.

4. *Final Form of Factorization Theorem for Hadronic Tensor*

Changing variables in the arguments of the beam, jet, and soft functions in Eq. (124) gives

$$\begin{aligned} W^{II'}_{\mu\nu}(x,Q^2,\tau_1) &= \int d^2p_\perp\frac{8\pi}{n_J\cdot n_B}\int dt_J dt_B dk_s^J\,dk_s^B\,\delta\left(\tau_1 - \frac{t_J}{s_J} - \frac{t_B}{s_B} - \frac{k_s^J + k_s^B}{Q_R}\right)J_q\big(t_J - (\mathbf{q}_\perp + \mathbf{p}_\perp)^2,\mu\big) \\ &\quad\times S_{\rm hemi}\big(k_s^J,k_s^B,\mu\big)\Big[H^{II'}_{q\bar q\mu\nu}(q^2,n_J,n_B,\mu)\mathcal{B}_q(t_B,x,\mathbf{p}_\perp^2,\mu) + H^{II'}_{q\bar q\mu\nu}(q^2,n_B,n_J,\mu)\mathcal{B}_{\bar q}(t_B,x,\mathbf{p}_\perp^2,\mu)\Big]\,. \end{aligned} \tag{135}$$

We have written the arguments of the jet and beam function in terms of dimension 2 variables $t_{J,B}$, the arguments of the soft function in terms of the total light-cone momentum $k_s^J \equiv n_J\cdot k_s^J$ in region J and $k_s^B \equiv n_B\cdot k_s^B$ in region B, and have rewritten the transverse momentum arguments of the jet and beam functions in terms of two-vectors $\mathbf{q}_\perp, \mathbf{p}_\perp$ instead of the the four-vectors $q_\perp, \tilde p_\perp$. The constant Q_R is defined in Eq. (54) and $s_{J,B}$ are defined in Eq. (58), and their special values for $\tau_1^{a,b,c}$ are given in Table II.

5. *Factorization Theorem for Cross Section*

In the cross section Eq. (88), the hard function Eq. (128) gets contracted with the leptonic tensor $L_{\mu\nu}$ in Eq. (84). The contraction of the leptonic tensor and the hard function can be performed using the tensor contractions in

Eqs. (B2) and (B3), and can be expressed in terms of Born-level cross section and scalar hard coefficients as

$$\sum_{II'} L^{II'}_{\mu\nu ff'}(x,Q^2)\frac{8\pi}{n_J\cdot n_B} H^{II'}_{q\bar{q}\mu\nu}(q^2,n_J,n_B,\mu) = \frac{d\sigma_0}{dx\,dQ^2} H_q(q_J,q_B,Q^2,\mu)\,, \tag{136a}$$

$$\sum_{II'} L^{II'}_{\mu\nu ff'}(x,Q^2)\frac{8\pi}{n_J\cdot n_B} H^{II'}_{q\bar{q}\mu\nu}(q^2,n_B,n_J,\mu) = \frac{d\sigma_0}{dx\,dQ^2} H_{\bar{q}}(q_J,q_B,Q^2,\mu)\,, \tag{136b}$$

where the Born-level cross section is given by

$$\frac{d\sigma_0}{dx\,dQ^2} = \frac{4\pi\alpha_{em}^2}{x^2 s^2 Q^2}\frac{q_J\cdot k'\, q_B\cdot k + q_J\cdot k\, q_B\cdot k'}{q_J\cdot q_B}\,. \tag{137}$$

The hard coefficients of the quark and antiquark beam functions are

$$H_{q\,,\bar{q}}(q_J,q_B,Q^2,\mu) = \sum_{ff'}\left[\left(C^*_{Vfq}C_{Vf'q}L^{VV}_{gff'} + C^*_{Afq}C_{Af'q}L^{AA}_{gff'}\right) \mp r(q_J,q_B)\left(C^*_{Vfq}C_{Af'q}L^{VA}_{\epsilon ff'} + C^*_{Afq}C_{Vf'q}L^{AV}_{\epsilon ff'}\right)\right], \tag{138}$$

where the relative minus signs for $H_{\bar{q}}$ come from the interchange of $n_{J,B}$ in Eq. (136). The coefficients $C_{V,A} \equiv C_{V,A}(q^2,\mu)$ are functions of q^2 and μ and the leptonic coefficients $L_{g,\epsilon} \equiv L_{g,\epsilon}(Q^2)$ given in Eq. (86). The coefficient $r(q_J,q_B)$ is given by

$$r(q_J,q_B) = \frac{q_J\cdot k'\, q_B\cdot k - q_J\cdot k\, q_B\cdot k'}{q_J\cdot k'\, q_B\cdot k + q_J\cdot k\, q_B\cdot k'}\,. \tag{139}$$

Because the coefficient r is a function of scalar products of $q_{B,J}$ and k and k' it becomes a function of y and Q^2 once $q_{B,J}$ are specified as in Sec. III A. So, the hard coefficient $H_{q\,\bar{q}}$ also is a function of y and Q^2 through the coefficient r.

Contracting Eq. (84) with Eq. (135) then gives for the cross section Eq. (88),

$$\begin{aligned}\frac{d\sigma}{dx\,dQ^2\,d\tau_1} = \int d^2\mathbf{p}_\perp \frac{d\sigma_0}{dx\,dQ^2}\int dt_J dt_B dk_S \delta\left(\tau_1 - \frac{t_J}{s_J} - \frac{t_B}{s_B} - \frac{k_S}{Q_R}\right) J_q(t_J - (\mathbf{q}_\perp+\mathbf{p}_\perp)^2,\mu)\, S_{\rm hemi}(k_S,\mu) \\ \times\left[H_q(q_J,q_B,Q^2,\mu)\mathcal{B}_q(t_B,x,\mathbf{p}_\perp^2,\mu) + H_{\bar{q}}(q_J,q_B,Q^2,\mu)\mathcal{B}_{\bar{q}}(t_B,x,\mathbf{p}_\perp^2,\mu)\right],\end{aligned} \tag{140}$$

where we used the projection Eq. (134) of the soft function onto a single variable.

D. Results for three versions of 1-jettiness $\tau_1^a, \tau_1^b, \tau_1^c$

Now we will specialize the generic factorization theorem for 1-jettiness in Eq. (140) to the specific cases $\tau_1^{a,b,c}$. The discussion will be most efficient if we begin with τ_1^b.

1. 1-jettiness τ_1^b

The reference vectors $q_B^b = xP$ and $q_J^b = q + xP$ in Eq. (32) are used to define the 1-jettiness τ_1^b. In any frame q can be written as $q = q_J^b - q_B^b$, so with respect to the directions n_B^b, n_J^b, the transverse component $q_\perp = 0$ so that the argument of the jet function in Eq. (140) is $(\mathbf{q}_\perp + \mathbf{p}_\perp)^2 = \mathbf{p}_\perp^2$. Meanwhile, the coefficient $r(q_J,q_B)$ in Eq. (139) is given by

$$r(q+xP,xP) = \frac{y(2-y)}{1+(1-y)^2}\,. \tag{141}$$

Note that r is a function only of y. So, the hard coefficients $H_{q\,\bar{q}}$ in Eq. (138) depend on y and Q^2, and we define the hard coefficients for τ_1^b by $H^b_{q\,,\bar{q}}(y,Q^2,\mu) \equiv H_{q\,,\bar{q}}(q+xP,P,Q^2,\mu)$. Therefore, using Eq. (140) the final factorization theorem for τ_1^b is given by

$$\begin{aligned}\frac{d\sigma}{dx\,dQ^2\,d\tau_1^b} = \frac{d\sigma_0^b}{dx\,dQ^2}\int dt_J dt_B dk_S\,\delta\left(\tau_1^b - \frac{t_J}{Q^2} - \frac{t_B}{Q^2} - \frac{k_S}{Q}\right) S_{\rm hemi}\,(k_S,\mu) \\ \times\int d^2\mathbf{p}_\perp J_q(t_J - \mathbf{p}_\perp^2,\mu)\Big[H_q^b(y,Q^2,\mu)\mathcal{B}_q(t_B,x,\mathbf{p}_\perp^2,\mu) + H_{\bar{q}}^b(y,Q^2,\mu)\mathcal{B}_{\bar{q}}(t_B,x,\mathbf{p}_\perp^2,\mu)\Big]\,,\end{aligned} \tag{142}$$

where we used Table II to substitute for $s_{J,B}, Q_R$ in Eq. (140), and where the Born-level cross section is given by

$$\frac{d\sigma_0^b}{dx\,dQ^2} = \frac{2\pi\alpha_{em}^2}{Q^4}\left[(1-y)^2+1\right]\,. \tag{143}$$

2. 1-jettiness τ_1^a

For the 1-jettiness τ_1^a defined in Eq. (29), the minimization inside the sum over final state particles i groups particles with the reference vector to which they are closest. The reference vector q_J^a with which the jet particles are grouped is aligned with the jet momentum p_J, so that the jet has zero transverse label momentum with respect to n_J^a. This direction n_J^a is the one which would minimize τ_1^a (to leading $\mathcal{O}(\lambda^2)$)with respect to variations of q_J^a. A jet with momentum $p_J = \omega_J n_J/2 + \tilde{p}_{J\perp} + k$, where k is residual, has a mass $m^2 = \omega_J n_J\cdot k + \tilde{p}_{J\perp}^2$, so $n_J\cdot k = (m^2 - \tilde{p}_{J\perp}^2)/\omega_J$. The choice of n_J which makes $\tilde{p}_{J\perp}^2 = 0$ minimizes $n_J\cdot k$ (note that $\tilde{p}_\perp^2 \le 0$).

The cross section for the τ_1^a distribution is given by Eq. (140), with $q_B = q_B^a \equiv xP$ and $q_J = q_J^a$, where q_J^a is the vector q_J in Eq. (29) that minimizes τ_1^a. We will write q_J^a in terms of the vector $q_J^b = q + xP$ that was used to define the 1-jettiness τ_1^b. Now, the vector q_J^b has a direction n_J^b and magnitude ω_J^b, given by

$$q_J^b = \omega_J^b \frac{n_J^b}{2} = P_T e^Y \frac{n_z}{2} + P_T e^{-Y}\frac{\bar{n}_z}{2} + P_T \hat{n}_T^J\,, \tag{144}$$

expressed in the CM frame, where p_T, Y are given by Eq. (36). With respect to n_J^b and n_P, the collinear fields in the jet function matrix elements still have nonzero transverse labels. Now, for each $\tilde{p}_J^\perp$, we rotate n_J^b to a vector n_J^a so that the transverse label with respect to n_J^a is zero. This requires that the total label momenta in the two coordinate systems be equal:

$$\omega_J^b \frac{n_J^b}{2} + \tilde{p}_J^\perp = \omega_J^a \frac{n_J^a}{2}\,, \tag{145}$$

so n_J^a differs from n_J^b at most by a quantity of $\mathcal{O}(\lambda)$. Now we express q in n_J^a, n_P coordinates. In Eq. (140), the transverse label on the collinear fields in the jet function is $q_\perp + p_\perp$. The n_J^a, n_P coordinate system is defined as that which makes this quantity is zero, so $q_\perp = -p_\perp$. By using $q^2 = -xys$ and $n_P\cdot q = y\sqrt{s}$, q is expressed as

$$q = y\sqrt{s}\frac{n_J^a}{n_J^a\cdot n_P} - \left(x\sqrt{s} + \frac{p_\perp^2}{y\sqrt{s}}\right)\frac{n_P}{2} - p_\perp\,. \tag{146}$$

Then Eq. (140) takes the form

$$\begin{aligned}\frac{d\sigma}{dx\,dQ^2\,d\tau_1^a} = \int d^2\mathbf{p}_\perp \frac{d\sigma_0^a}{dx\,dQ^2}\int dt_J dt_B dk_S\,\delta\left(\tau_1^a - \frac{t_J}{Q^2} - \frac{t_B}{Q^2} - \frac{k_S}{Q}\right) J_q(t_J,\mu) S_{\rm hemi}(k_S,\mu) \\ \times\left[H_q(q_J^a, q_B^a, Q^2,\mu)\mathcal{B}_q(t_B,x,\mathbf{p}_\perp^2,\mu) + H_{\bar{q}}(q_J^a,q_B^a,Q^2,\mu)\mathcal{B}_{\bar{q}}(t_B,x,\mathbf{p}_\perp^2,\mu)\right],\end{aligned} \tag{147}$$

where we used Table II to substitute for $s_{J,B}$ and Q_R.

The generalized beam functions appearing here explicitly depend on $p_\perp$. The vector n_J^a appearing in q_J^a implicitly depends on $p_\perp$. Now, n_J^a differs from n_J^b (which is independent of $p_\perp$) by a quantity of order λ. Here we can expand the hard and soft functions and the Born cross section around $n_J^a = n_J^b + \mathcal{O}(\lambda)$ and drop the power corrections in λ. This makes everything in Eq. (147) independent of $p_\perp$ except for the generalized beam function. The integral over $p_\perp$ then turns the generalized beam function into the ordinary beam function Eq. (119). Thus the final factorization theorem for the τ_1^a cross section is

$$\begin{aligned}\frac{d\sigma}{dx\,dQ^2\,d\tau_1^a} = \frac{d\sigma_0^b}{dx\,dQ^2}\int dt_J dt_B dk_S\,\delta\left(\tau_1^a - \frac{t_J}{Q^2} - \frac{t_B}{Q^2} - \frac{k_S}{Q}\right) J_q(t_J,\mu) S_{\rm hemi}(k_S,\mu) \\ \times\left[H_q^b(y,Q^2,\mu)B_q(t_B,x,\mu) + H_{\bar{q}}^b(y,Q^2,\mu)B_{\bar{q}}(t_B,x,\mu)\right],\end{aligned} \tag{148}$$

where the Born cross section is given by Eq. (143) and $H_{q,\bar{q}}^b(y,Q^2)$ is given by Eq. (138) with r in Eq. (141). The hard and soft functions in Eq. (148) are the same as those in Eq. (142) for τ_1^b.

Eq. (148) differs from Eq. (142) in that the jet and beam functions are no longer convolved together in the transverse momentum $p_\perp$. The 1-jettiness τ_1^a is proportional to the invariant mass of the jet, while τ_1^b measures the projection $q_J^b\cdot p_J$ onto the fixed axis $q_J^b = q + xP$. The emission of ISR with transverse momentum $p_\perp$, causing a shift in the jet momentum by the same amount due to momentum conservation, will not change the mass of the jet, but it will change the projection of the jet momentum onto the q_J^b axis. Thus τ_1^a involves no convolution over $p_\perp$, while τ_1^b does.

3. 1-jettiness τ_1^c

For the 1-jettiness τ_1^c, the directions n_J and n_B are along the electron and proton directions, respectively:

$$n_J = n_e\,, \quad n_B = n_P\,, \tag{149}$$

where $n_{e,P}$ are the light-cone directions of $q_J = k = \omega_e n_e/2$ and $q_B = P = \omega_P n_P/2$. In the CM frame, $n_{e,P}$ are back-to-back, $n_e = n_z$ and $n_P = \bar{n}_z$. In this frame, q is given by

$$q = y\sqrt{s}\frac{n_z}{2} - xy\sqrt{s}\frac{\bar{n}_z}{2} + q_\perp\,, \tag{150}$$

where $q_\perp = Q\sqrt{1-y}\,\hat{n}_\perp$. Let us consider for a moment the power counting of the argument of the jet function in Eq. (140) with τ_1^c. The requirement that $q_\perp \sim Q\lambda$ requires that $1-y \sim \lambda^2$. This is ensured by measuring τ_1^c to be $\mathcal{O}(\lambda^2)$. The argument of the jet function (call it m_J^2) in the factorization theorem Eq. (140) for τ_1^c is

$$m_J^2 = t_J - (1-y)Q^2 - 2Q\sqrt{1-y}\,\hat{\mathbf{n}}_\perp\cdot\mathbf{p}_\perp - \mathbf{p}_\perp^2\,. \tag{151}$$

Now, the jet function will be proportional to a theta function $\theta(m_J^2)$, requiring $m_J^2 > 0$. Measuring τ_1^c to be of order λ^2 and therefore forcing t_J to be of order $Q^2\lambda^2$ then enforces that $1-y \sim \lambda^2$. Then, we can set $y = 1$ to leading order everywhere in Eq. (140) except in the argument of the jet function. In terms of x, using the relation $xys = Q^2$, requiring $y \lesssim 1$ is equivalent to requiring $x \gtrsim Q^2/s$, which sets a lower bound on x.

The normalization constants $s_{J,B}, Q_R$ in Eq. (140) are given for τ_1^c in Table II. The Born-level cross section and the coefficient $r(q_J, q_B)$ in the hard coefficients reduce to

$$\frac{d\sigma_0^c}{dx\,dQ^2} = \frac{2\pi\alpha_{em}^2}{Q^4}\,, \qquad r(k,P) = 1\,, \tag{152}$$

where we see the Born cross section is now Eq. (143) in the limit $y \to 1$. This happens because the expression Eq. (137) is evaluated with $q_J = k$, which is the actual jet direction only near $y \to 1$. The hard coefficient is now independent of x, y and depends only on Q^2: $H^c_{q,\bar{q}}(Q^2,\mu) = H_{q,\bar{q}}(k,P,Q^2,\mu)$. From Eq. (140) the final factorization theorem for the cross section in with τ_1^c is then given by

$$\begin{aligned}\frac{d\sigma}{dx\,dQ^2\,d\tau_1^c} = \frac{d\sigma_0^c}{dx\,dQ^2}\int d^2\mathbf{p}_\perp \int dt_J dt_B dk_S\, \delta\left(\tau_1 - \frac{t_J}{Q^2} - \frac{t_B}{xQ^2} - \frac{k_S}{\sqrt{x}\,Q}\right) J_q(t_J - (\mathbf{q}_\perp + \mathbf{p}_\perp)^2,\mu)\, S_{\rm hemi}(k_S,\mu) \\ \times \Big[H_q^c(Q^2,\mu)\mathcal{B}_q(t_B,x,\mathbf{p}_\perp^2,\mu) + H_{\bar{q}}^c(Q^2,\mu)\mathcal{B}_{\bar{q}}(t_B,x,\mathbf{p}_\perp^2,\mu)\Big]\,.\end{aligned} \tag{153}$$

This is like the τ_1^b cross section Eq. (142) in that the jet and beam functions are convolved in the transverse momentum $\mathbf{p}_\perp$ of ISR, but in this case the momentum transfer q itself has a nonzero transverse momentum with respect to the light-cone directions $n_{e,P}$. This will make the evaluation of the $\mathbf{p}_\perp$ integral considerably more involved than in the τ_1^b cross section Eq. (142).

VI. FIXED-ORDER PREDICTIONS AT $\mathcal{O}(\alpha_s)$

In this Section we evaluate to $\mathcal{O}(\alpha_s)$ the predictions of the factorization theorems for the cross sections differential in the different versions of 1-jettiness in Eq. (142) for τ_1^b, and Eq. (148) for τ_1^a and Eq. (153) for τ_1^c. These formulas correctly predict the singular terms at small τ_1 in the fixed-order differential cross section, although they have to be resummed to all orders in α_s to accurately predict the behavior at small τ_1. We will do this in the next Section. Also, for the predictions to be correct for large τ_1, they would have to be matched onto $\mathcal{O}(\alpha_s)$ and $\mathcal{O}(\alpha_s^2)$ fixed-order full QCD calculations, an analysis we defer to future work. Nevertheless we can estimate the size of these matching corrections by comparing our predictions integrated up to large τ_1 to the known total QCD cross section $\sigma(x,Q^2)$ at $\mathcal{O}(\alpha_s)$, which we will do in Sec. VIII.

A. Hard Function

At $\mathcal{O}(\alpha_s)$, the matching coefficients C_{Vfq}, C_{Afq} for the vector and axial currents Eq. (99) that appear in the hard coefficient in Eq. (138) are equal and diagonal in flavor, and were calculated in [36, 91]:

$$C_{Vfq}(q^2) = C_{Afq}(q^2) = \delta_{fq}C(q^2)\,, \tag{154}$$

$$C(q^2) = 1 + \frac{\alpha_s(\mu)C_F}{4\pi}\left(-\ln^2\frac{\mu^2}{-q^2} - 3\ln\frac{\mu^2}{-q^2} - 8 + \frac{\pi^2}{6}\right).$$

For DIS recall $q^2 = -Q^2$. Then, the hard coefficients $H_{q,\bar{q}}$ in the cross section Eq. (140) are given to $\mathcal{O}(\alpha_s)$ by

$$H_{q,\bar{q}}(q_J, q_B, Q^2, \mu) = H(Q^2, \mu) L_{q,\bar{q}}(q_J, q_B, Q^2)\,, \quad (155)$$

where we have defined the universal SCET 2-quark hard coefficient,

$$\begin{aligned} H(Q^2,\mu) &\equiv \left|C(q^2,\mu)\right|^2 \quad (156)\\ &= 1 + \frac{\alpha_s(\mu) C_F}{2\pi}\left(-\ln^2\frac{\mu^2}{Q^2} - 3\ln\frac{\mu^2}{Q^2} - 8 + \frac{\pi^2}{6}\right), \end{aligned}$$

and the factor containing the components of the leptonic tensor Eq. (84),

$$L_{q,\bar{q}}(q_J, q_B, Q^2) = L^{VV}_{gqq} + L^{AA}_{gqq} \mp r(q_J, q_B)(L^{VA}_{\epsilon qq} + L^{AV}_{\epsilon qq})\,, \quad (157)$$

where $r(q_J, q_B)$ was defined in Eq. (139).

1. $\tau_1^{a,b}$ cross sections

For the $\tau_1^{a,b}$ cross sections Eqs. (142) and (148), $q_B = xP$ and $q_J = q + xP$, so that $r(q_J, q_B)$ is given by Eq. (141). Then the leptonic factor $L_{q,\bar{q}}$ in Eq. (157) becomes

$$\begin{aligned} &L^a_{q,\bar{q}}(q_J, q_B, Q^2) \quad (158)\\ &= L^{VV}_{gqq} + L^{AA}_{gqq} \mp \frac{y(2-y)}{(1-y)^2+1}(L^{VA}_{\epsilon qq} + L^{AV}_{\epsilon qq})\\ &= Q_q^2 - \frac{2Q_q v_q v_e}{1 + m_Z^2/Q^2} + \frac{(v_q^2 + a_q^2)(v_e^2 + a_e^2)}{(1 + m_Z^2/Q^2)^2}\\ &\quad \mp \frac{2y(2-y)}{(1-y)^2+1}\frac{a_q a_e [Q_q(1 + m_Z^2/Q^2) - 2 v_q v_e]}{(1 + m_Z^2/Q^2)^2}\,. \end{aligned}$$

2. τ_1^c cross section

For the τ_1^c cross section Eq. (153), $q_J = k$ and $q_B = P$, the electron and proton momenta, respectively. Then $r(k, P) = 1$ in Eq. (139), and the leptonic factor $L_{q,\bar{q}}$ in Eq. (157) becomes

$$\begin{aligned} L^c_{q,\bar{q}}(k, P, Q^2) &= L^{VV}_{gqq} + L^{AA}_{gqq} \mp (L^{VA}_{\epsilon qq} + L^{AV}_{\epsilon qq}) \quad (159)\\ &= Q_q^2 - \frac{2Q_q(v_q v_e \pm a_q a_e)}{1 + m_Z^2/Q^2}\\ &\quad + \frac{(v_q^2 + a_q^2)(v_e^2 + a_e^2) \pm 4 v_q a_q v_e a_e}{(1 + m_Z^2/Q^2)^2}\,. \end{aligned}$$

B. Soft Function

The soft function $S_{\rm hemi}(k_S, \mu)$ that appears in the cross sections Eqs. (142), (148), and (153) is given by Eqs. (133) and (134). For $e^+e^- \to$ dijets, $S^{\rm dijet}_{\rm hemi}$ is known at $\mathcal{O}(\alpha_s)$ [99] and $\mathcal{O}(\alpha_s^2)$ [60, 61, 100]. At 1-loop order the dijet soft function is the same for DIS. Beginning at 2-loop order, the finite part of the soft function for DIS could possibly differ due to switching incoming and outgoing Wilson lines, but the anomalous dimensions and thus the logs are the same.

To $\mathcal{O}(\alpha_s)$, the soft function Eq. (133) takes the form:

$$\begin{aligned} &S_{\rm hemi}(k_s^J, k_s^B, \mu) = \delta(k_s^J)\delta(k_s^B)\\ &+ S^{(1)}(k_s^J, \mu)\delta(k_s^B) + \delta(k_s^J) S^{(1)}(k_s^B, \mu)\,, \end{aligned} \quad (160)$$

where

$$S^{(1)}(k_s, \mu) = \frac{\alpha_s C_F}{4\pi}\left\{\frac{\pi^2}{6}\delta(k_s) - \frac{8}{\mu}\left[\frac{\theta(k_s)\ln(k_s/\mu)}{k_s/\mu}\right]_+\right\}, \quad (161)$$

and the projection Eq. (134) is then given to $\mathcal{O}(\alpha_s)$ by

$$S_{\rm hemi}(k_S, \mu) = \delta(k_S) + 2S^{(1)}(k_S, \mu)\,. \quad (162)$$

It has previously been observed that the sizes $R_{J,B}$ of the regions $\mathcal{H}_{J,B}$ to which soft radiation is confined enter the arguments of the logs in the soft function [81, 101, 102], which is due to changing the effective scale at which the soft modes live [103].

C. Jet Function

The jet function Eq. (122) is given to $\mathcal{O}(\alpha_s)$ by [104, 105]

$$J_{q,\bar{q}}(t, \mu) = \delta(t) + \frac{\alpha_s(\mu) C_F}{4\pi}\left\{(7 - \pi^2)\delta(t) - \frac{3}{\mu^2}\left[\frac{\theta(t)}{t/\mu^2}\right]_+ + \frac{4}{\mu^2}\left[\frac{\theta(t)\ln(t/\mu^2)}{t/\mu^2}\right]_+\right\}. \quad (163)$$

It is in fact known to two-loop order [105] and its anomalous dimension to three loops [38].

D. Beam Functions

1. Generalized Beam Functions

The generalized beam functions in Eq. (118) can be matched onto ordinary PDFs, defined in SCET as [22]:

$$f_q(\omega'/P^-,\mu) = \theta(\omega')\,\langle P_n(P^-)|\,\bar\chi_n(0)\frac{\bar{n}\!\!\!/}{2}[\delta(\omega'-\bar n\cdot\mathcal{P})\chi_n(0)]\,|P_n(P^-)\rangle\,, \tag{164a}$$

$$f_{\bar q}(\omega'/P^-,\mu) = \theta(\omega')\,\langle P_n(P^-)|\,\mathrm{tr}\,\frac{\bar{n}\!\!\!/}{2}\chi_n(0)[\delta(\omega'-\bar n\cdot\mathcal{P})\bar\chi_n(0)]\,|P_n(P^-)\rangle\,. \tag{164b}$$

The matching result is [68, 94]:

$$\mathcal{B}_i(t,x,\mathbf{k}_\perp^2,\mu) = \sum_j\int_x^1\frac{d\xi}{\xi}\mathcal{I}_{ij}\Big(t,\frac{x}{\xi},\mathbf{k}_\perp^2,\mu\Big)f_j(\xi,\mu)\Big[1+\mathcal{O}\Big(\frac{\Lambda^2_{\rm QCD}}{t},\frac{\Lambda^2_{\rm QCD}}{\mathbf{k}_\perp^2}\Big)\Big]\,, \tag{165}$$

where $i,j = q,\bar q,g$. This expansion is valid for perturbative beam radiation satisfying $t,\mathbf{k}_\perp^2 \gg \Lambda^2_{\rm QCD}$. At tree level, $\mathcal{I}_{ij}^{(0)}(t,z,\mathbf{k}_\perp^2,\mu) = (1/\pi)\delta_{ij}\delta(t)\delta(1-z)\delta(\mathbf{k}_\perp^2)$, leading to $\mathcal{B}_i^{(0)}(t,x,\mathbf{k}_\perp^2,\mu) = (1/\pi)\delta(t)\delta(\mathbf{k}_\perp^2)f_i(x,\mu)$.

To $\mathcal{O}(\alpha_s)$, the nonzero matching coefficients in the generalized quark beam function were computed in [68, 94], and we use the results from [94]:

$$\begin{aligned}\mathcal{I}_{qq}(t,z,\mathbf{k}_\perp^2,\mu) = {}& \frac{1}{\pi}\delta(t)\delta(1-z)\delta(\mathbf{k}_\perp^2) + \frac{\alpha_s(\mu)C_F}{2\pi^2}\theta(z)\bigg\{\frac{2}{\mu^2}\bigg[\frac{\theta(t)\ln(t/\mu^2)}{t/\mu^2}\bigg]_+\delta(1-z)\delta(\mathbf{k}_\perp^2) \\ &+\frac{1}{\mu^2}\bigg[\frac{\theta(t)}{t/\mu^2}\bigg]_+\bigg[P_{qq}(z)-\frac{3}{2}\delta(1-z)\bigg]\delta\Big(\mathbf{k}_\perp^2-\frac{(1-z)t}{z}\Big) \\ &+\delta(t)\delta(\mathbf{k}_\perp^2)\bigg[\bigg[\frac{\theta(1-z)\ln(1-z)}{1-z}\bigg]_+(1+z^2)-\frac{\pi^2}{6}\delta(1-z)+\theta(1-z)\Big(1-z-\frac{1+z^2}{1-z}\ln z\Big)\bigg]\bigg\}\,,\end{aligned} \tag{166a}$$

$$\mathcal{I}_{qg}(t,z,\mathbf{k}_\perp^2,\mu) = \frac{\alpha_s(\mu)T_F}{2\pi^2}\theta(z)\bigg\{\frac{1}{\mu^2}\bigg[\frac{\theta(t)}{t/\mu^2}\bigg]_+P_{qg}(z)\delta\Big(\mathbf{k}_\perp^2-\frac{(1-z)t}{z}\Big)+\delta(t)\delta(\mathbf{k}_\perp^2)\bigg[P_{qg}(z)\ln\frac{1-z}{z}+2\theta(1-z)z(1-z)\bigg]\bigg\}\,, \tag{166b}$$

where $P_{qq,qg}$ are the $q\to qg$ and $g\to q\bar q$ splitting functions,

$$P_{qq}(z) = \bigg[\frac{\theta(1-z)}{1-z}\bigg]_+(1+z^2)+\frac{3}{2}\delta(1-z) = \bigg[\theta(1-z)\frac{1+z^2}{1-z}\bigg]_+\,, \tag{167a}$$

$$P_{qg}(z) = \theta(1-z)[(1-z)^2+z^2]\,. \tag{167b}$$

They appear in the anomalous dimensions of the PDFs, which to all orders obey

$$\mu\frac{d}{d\mu}f_i(\xi,\mu) = \sum_j\int\frac{d\xi'}{\xi'}\gamma_{ij}^f\Big(\frac{\xi}{\xi'},\mu\Big)f_j(\xi',\mu)\,. \tag{168}$$

At $\mathcal{O}(\alpha_s)$ the anomalous dimensions for the quark PDF are

$$\gamma_{qq}^f(z,\mu) = \frac{\alpha_s(\mu)C_F}{\pi}\theta(z)P_{qq}(z)\,,\qquad \gamma_{qg}^f(z,\mu)\frac{\alpha_s(\mu)T_F}{\pi}\theta(z)P_{qg}(z)\,. \tag{169}$$

2. Ordinary Beam Functions

The ordinary beam functions Eq. (119) satisfy the matching condition [67, 106, 107]:

$$B_i(t,x,\mu) = \sum_j\int_x^1\frac{d\xi}{\xi}\mathcal{I}_{ij}\Big(t,\frac{x}{\xi},\mu\Big)f_j(\xi,\mu)\Big[1+\mathcal{O}\Big(\frac{\Lambda^2_{\rm QCD}}{t}\Big)\Big]\,, \tag{170}$$

where at tree level $\mathcal{I}_{ij}^{(0)}(t,z,\mu) = \delta_{ij}\delta(t)\delta(1-z)$, leading to $B_i^{(0)}(t,x,\mu) = \delta(t) f_i(x,\mu)$. To $\mathcal{O}(\alpha_s)$, the matching coefficients in the quark beam function are given by integrating Eq. (166) over $\mathbf{k}_\perp$ [67, 107]:

$$\mathcal{I}_{qq}(t,z,\mu) = \delta(t)\delta(1-z) + \frac{\alpha_s(\mu)C_F}{2\pi}\theta(z)\biggl\{\frac{2}{\mu^2}\biggl[\frac{\theta(t)\ln(t/\mu^2)}{t/\mu^2}\biggr]_+\delta(1-z) + \frac{1}{\mu^2}\biggl[\frac{\theta(t)}{t/\mu^2}\biggr]_+\biggl[P_{qq}(z) - \frac{3}{2}\delta(1-z)\biggr] + \delta(t)\biggl[\biggl[\frac{\theta(1-z)\ln(1-z)}{1-z}\biggr]_+(1+z^2) - \frac{\pi^2}{6}\delta(1-z) + \theta(1-z)\Bigl(1-z-\frac{1+z^2}{1-z}\ln z\Bigr)\biggr]\biggr\}, \tag{171a}$$

$$\mathcal{I}_{qg}(t,z,\mu) = \frac{\alpha_s(\mu)T_F}{2\pi}\theta(z)\biggl\{\frac{1}{\mu^2}\biggl[\frac{\theta(t)}{t/\mu^2}\biggr]_+P_{qg}(z) + \delta(t)\biggl[P_{qg}(z)\ln\frac{1-z}{z} + 2\theta(1-z)z(1-z)\biggr]\biggr\}. \tag{171b}$$

E. Dijet Cross Section

We can now form the SCET predictions for the τ_1 cross section Eq. (140) to $\mathcal{O}(\alpha_s)$ by plugging in the $\mathcal{O}(\alpha_s)$ expressions for the hard function given by Eqs. (155), (156), and (157), the soft function given by Eqs. (160) and (161), the jet function given by Eq. (163), and the generalized beam function given by Eqs. (165) and (166). It is convenient to express the result in terms of the *cumulant* τ_1 distribution, defined by

$$\sigma_{\rm c}(x,Q^2,\tau_1) = \frac{1}{\sigma_0}\int_0^{\tau_1} d\tau_1' \frac{d\sigma}{dx\,dQ^2\,d\tau_1'}\,, \tag{172}$$

where σ_0 is the Born cross section defined in Eq. (137). We will give here the results for the $\tau_1^{a,b}$ cumulants at $\mathcal{O}(\alpha_s)$. The more complicated results for the τ_1^c and generic τ_1 cumulants are given in App. G.

1. τ_1^a cross section

Plugging in the $\mathcal{O}(\alpha_s)$ results for the hard function given by Eqs. (155), (156), and (158), the soft function given by Eqs. (160) and (161) with $s_{J,B}$ and Q_R given in Table II, the jet function given by Eq. (163), and the ordinary beam function given by Eq. (170) into the τ_1^a cross section Eq. (148), we obtain for the τ_1^a cumulant given by Eq. (172) in the CM frame:

$$\begin{aligned}\sigma_{\rm c}(x,Q^2,\tau_1^a) = \theta(\tau_1^a)\int_x^1\frac{dz}{z}\bigl[L_q^a(x,Q^2)f_q(x/z,\mu) + L_{\bar q}^a(x,Q^2)f_{\bar q}(x/z,\mu)\bigr] \\ \times\biggl\{\delta(1-z)\biggl[1 - \frac{\alpha_s C_F}{4\pi}\Bigl(9 + \frac{2\pi^2}{3} + 6\ln\tau_1^a + 4\ln^2\tau_1^a\Bigr)\biggr] \\ + \frac{\alpha_s C_F}{2\pi}\biggl[\mathcal{L}_1(1-z)(1+z^2) + \theta(1-z)\Bigl(1-z-\frac{1+z^2}{1-z}\ln z\Bigr) + \ln\Bigl(\frac{Q^2\tau_1^a}{\mu^2}\Bigr)P_{qq}(z)\biggr]\biggr\} \\ + \frac{\alpha_s T_F}{2\pi}\theta(\tau_1^a)\bigl[L_q^a(x,Q^2) + L_{\bar q}^a(x,Q^2)\bigr]\int_x^1\frac{dz}{z}f_g(x/z,\mu)\biggl\{\ln\Bigl(\frac{Q^2\tau_1^a}{\mu^2}\frac{1-z}{z}\Bigr)P_{qg}(z) + 2\theta(1-z)z(1-z)\biggr\}.\end{aligned} \tag{173}$$

The factorization scale μ still appears on the right-hand side of the equation, though the cross section is in fact independent of μ. The μ-dependence in the PDFs on the first line is cancelled by the μ-dependence in the logs multiplying the splitting functions on the third and final lines to $\mathcal{O}(\alpha_s)$. The residual μ-dependence is $\mathcal{O}(\alpha_s^2)$ and would be cancelled by the higher-order corrections.

2. τ_1^b cross section

The τ_1^b cross section is nearly identical to the τ_1^a cross section except for the presence of the $\mathbf{p}_\perp$-dependent generalized beam function in Eq. (142) instead of the ordinary beam function. The effect of the nontrivial $\mathbf{p}_\perp$-dependent terms in the generalized beam function Eq. (165) is simply to multiply the arguments of the μ-dependent logs in Eq. (173)

by z, giving the simple relation

$$\sigma_{\rm c}(x,Q^2,\tau_1^b) = \sigma_{\rm c}(x,Q^2,\tau_1^a)\Big|_{\tau_1^a\to\tau_1^b} + \theta(\tau_1^b)\frac{\alpha_s}{2\pi}\int_x^1\frac{dz}{z}\ln z\Big\{C_F\big[L_q^a(Q^2)f_q(x/z,\mu)+L_{\bar q}^a(Q^2)f_{\bar q}(x/z,\mu)\big]P_{qq}(z) \\ +T_F\big[L_q^a(Q^2)+L_{\bar q}^a(Q^2)\big]P_{qg}(z)f_g(x/z,\mu)\Big\}, \tag{174}$$

In the Appendix we give the $\mathcal{O}(\alpha_s)$ τ_1^c cross section. In the next section we resum the large logarithms of $\tau_1^{a,b,c}$ that appear in these fixed-order expansions to all orders in α_s to NNLL accuracy.

VII. RESUMMED PREDICTIONS FOR τ_1 CROSS SECTIONS

The fixed-order predictions for the τ_1 cross sections presented in the previous Section contain logarithms of τ_1 which grow large in the limit $\tau_1 \to 0$ and must be resummed to all orders in α_s to yield accurate predictions for small τ_1. In this Section we use the factorization theorem Eq. (140) for the τ_1 1-jettiness cross section and its specialized cases Eqs. (142), (148), and (153) for $\tau_1^b, \tau_1^a, \tau_1^c$ to predict the cross sections differential in these variables to next-to-next-to-leading logarithmic (NNLL) accuracy, estimate the perturbative uncertainty by appropriate scale variations, and discuss power corrections due to hadronization, including their universality and impact in the tail and peak regions.

A. Perturbative Resummation to NNLL

The hard, jet, beam, and soft functions in Eq. (140) obey renormalization group (RG) evolution equations whose solutions allow us to resum large logarithms of ratios of the separated hard, jet, beam, and soft scales. These solutions allow us to express any of these functions $G = \{H, J, B, S\}$ at one scale μ which contains logs of μ over some scale Q_G in terms of the function evaluated at a different scale $\mu_G \sim Q_G$ where the logs are small.

The hard function $H(Q^2,\mu)$ obeys the RG equation

$$\mu\frac{d}{d\mu}H(Q^2,\mu) = \gamma_H(\mu)H(Q^2,\mu)\,, \tag{175}$$

where the anomalous dimension γ_H has the form

$$\gamma_H(\mu) = \Gamma_H[\alpha_s(\mu)]\ln\frac{Q^2}{\mu^2} + \gamma_H[\alpha_s(\mu)]\,, \tag{176}$$

with a *cusp* piece $\Gamma_H[\alpha_s] = 2\Gamma^q_{\rm cusp}$ and a *non-cusp* piece $\gamma_H[\alpha_s]$ (which is conventionally denoted by the same symbol as the total anomalous dimension). Their expansions in α_s are given below in Eq. (182) and Eqs. (D28) and (D29). Similarly the jet and beam functions which are both functions of a dimension-2 variable t obey RG equations of the form

$$\mu\frac{d}{d\mu}G(t,\mu) = \int dt'\gamma_G(t-t',\mu)G(t',\mu)\,, \tag{177}$$

where the anomalous dimension γ_G takes the form

$$\gamma_G(t,\mu) = \Gamma_G[\alpha_s(\mu)]\frac{1}{\mu^2}\left[\frac{\theta(t/\mu^2)}{t/\mu^2}\right]_+ + \gamma_G[\alpha_s(\mu)]\delta(t)\,, \tag{178}$$

where here $G = \{J, B\}$, and the plus distribution is defined in App. C. The cusp pieces $\Gamma_{J,B} = -2\Gamma^q_{\rm cusp}$ and non-cusp pieces $\gamma_{J,B}$ of the jet and beam anomalous dimensions are given in Eqs. (D28) and (D30). The beam function also depends on x and the generalized beam function also depends on $\mathbf{p}_\perp^2$, but they do not change the structure of the RG equation Eq. (177).

Finally, the soft function in Eq. (133) obeys the RG equation

$$\mu\frac{d}{d\mu}S_{\rm hemi}(k_J,k_B,\mu) = \int dk_J' dk_B' \\ \times\gamma_S(k_J-k_J',k_B-k_B',\mu)S_{\rm hemi}(k_J',k_B',\mu)\,, \tag{179}$$

where the anomalous dimension factorizes into the form

$$\gamma_S(k_J,k_B,\mu) = \gamma_S(k_J,\mu)\delta(k_B) + \gamma_S(k_B,\mu)\delta(k_J), \tag{180}$$

which is required by μ-independence of the total cross section Eq. (140) [108]. Each piece $\gamma_S(k,\mu)$ takes the form

$$\gamma_S(k,\mu) = 2\Gamma_S[\alpha_s(\mu)]\frac{1}{\mu}\left[\frac{\theta(k/\mu)}{k/\mu}\right]_+ + \gamma_S[\alpha_s(\mu)]\delta(k)\,, \tag{181}$$

where $\Gamma_S = \Gamma_{\rm cusp}$, and the non-cusp piece is given by $\gamma_S = -\gamma_H/2 - \gamma_J$.

The cusp and non-cusp pieces of the anomalous dimensions of all the functions above all have perturbative expansions in α_s:

$$\Gamma_G[\alpha_s] = \sum_{n=0}^\infty\Gamma_G^n\Big(\frac{\alpha_s}{4\pi}\Big)^{n+1},\ \gamma_G[\alpha_s] = \sum_{n=0}^\infty\gamma_G^n\Big(\frac{\alpha_s}{4\pi}\Big)^{n+1}, \tag{182}$$

which defines the coefficients Γ_G^n, γ_G^n. Furthermore, the cusp pieces of the anomalous dimension are proportional to the same *cusp anomalous dimension* $\Gamma^q_{\rm cusp}[\alpha_s]$, whose perturbative expansion along with the non-cusp anomalous dimensions are given in App. D. The explicit solutions to the RG equations for the hard, jet, beam, and soft functions individually are given in App. D.

The solutions of the RG equations Eqs. (175), (177), and (179) allow us to express the hard, jet, beam, and

soft functions at any scale μ in terms of their values at different scales $\mu_{H,J,B,S}$ where logarithms of μ_G/Q_G in their perturbative expansions are small. There are a different conventional ways in the literature to express the resummed cross section in terms of the solutions for hard, jet, beam, and soft functions to the RG equations. One method [14, 76] performs the exact inverse transform back from Fourier space, and carries out analytically the convolution of all the evolution factors and the fixed-order functions for the τ_1 factorization theorem Eq. (140) in momentum space. In this section we use this method and formalism, relegating some of the required formulas to App. E. We give an alternative equivalent form of the resummed cross sections in App. F, using a method [38, 80] that first Laplace transforms the cross section and writes certain corrections as derivative operators before transforming back to momentum space. This avoids taking explicit convolutions of the evolution factors and the fixed-order functions. If one carries out these derivatives analytically then the final results from the two formalisms are identical.

In this section we give just the final results for the RG improved cross sections for the 1-jettinesses $\tau_1^{a,b,c}$ using the formalism of [14, 76]. We will express the results in terms of the *cumulant* $\tau_1^{a,b,c}$ distributions:

$$\sigma_{\rm c}(x,Q^2,\tau_1) = \frac{1}{\sigma_0}\int_0^{\tau_1} d\tau_1' \frac{d\sigma}{dx\,dQ^2\,d\tau_1'}\,, \tag{183}$$

where we note that $\sigma_{\rm c}$ is dimensionless due to the division by σ_0. The differential cross section can be obtained by taking the derivative of $\sigma_{\rm c}(x,Q^2,\tau_1)$ with respect to τ_1. Care must be exercised in this procedure because $\sigma_{\rm c}$ also depends on τ_1 dependent jet/beam and soft scales in the factorization theorem Eq. (140), $\sigma_{\rm c}(x,Q^2,\tau_1,\mu_i(\tilde\tau_1))$. The appropriate procedure is to use, for $\epsilon\to 0$,

$$\frac{d\hat\sigma}{d\tau_1} = \frac{\sigma_c(x,Q^2,\tau_1+\epsilon,\mu_i(\tau_1)) - \sigma_c(x,Q^2,\tau_1-\epsilon,\mu_i(\tau_1))}{2\epsilon}, \tag{184}$$

where $d\hat\sigma/d\tau_1 = (1/\sigma_0)d\sigma/d\tau_1$. See Ref. [14] for further discussion of this point.

1. $\tau_1^{a,b}$ cross sections

The cross section in Eq. (140) is expressed as a convolution of jet, beam, and soft functions in momentum space. To resum the large logs, each function is RG evolved from a scale where the logs are small, an operation which is in the form of a convolution of an RG evolution kernel and the fixed order function as in Eqs. (D5) and (D14). The evolution kernels $U_{J,B,S}$ in Eqs. (D5) and (D15) are plus distributions, and each fixed order function can also be written as a sum of plus distributions as in App. E 1. Thus, the resummed cross section contains numerous convolutions of plus distributions $\mathcal{L}^\eta$, $\mathcal{L}_n$, which we can compute by repeatedly applying the plus distribution convolution identity in Eq. (E8). The cross section then gets written as a resummation factor times sums of products of coefficients called V in App. E 2 and J_n, $I_n^{qq,qg}$, and S_n in App. E 1.

The resummed τ_1^a and τ_1^b cross sections in Eqs. (142) and (148), obtained from RG evolution of the hard, jet, beam, and soft functions, are given by:

$$\begin{aligned}\sigma_{\rm c}(x,Q^2,\tau) = {}& \frac{e^{\mathcal{K}-\gamma_E\Omega}}{\Gamma(1+\Omega)}\left(\frac{Q}{\mu_H}\right)^{\eta_H(\mu_H,\mu)}\left(\frac{\tau\,Q^2}{\mu_B^2}\right)^{\eta_B(\mu_B,\mu)}\left(\frac{\tau\,Q^2}{\mu_J^2}\right)^{\eta_J(\mu_J,\mu)}\left(\frac{\tau\,Q}{\mu_S}\right)^{2\eta_S(\mu_S,\mu)}\\ &\times\left[\sum_j L_q^a(x,Q^2)\int_x^1\frac{dz}{z}\,f_j(x/z,\mu_B)\,[W_{qj}(z,\tau)+\Delta W_{qj}(z)] + (q\leftrightarrow\bar q)\right],\end{aligned} \tag{185a}$$

$$\begin{aligned}W_{qj}(z,\tau) = {}& H(Q^2,\mu_H)\sum_{\substack{n_1,n_2,\\ n_3=-1}}^{1} J_{n_1}\Big[\alpha_s(\mu_J),\frac{\tau Q^2}{\mu_J^2}\Big]\,I_{n_2}^{qj}\Big[\alpha_s(\mu_B),z,\frac{\tau Q^2}{\mu_B^2}\Big]\,S_{n_3}\Big[\alpha_s(\mu_S),\frac{\tau Q}{\mu_S}\Big]\\ &\times\sum_{\ell_1=-1}^{n_1+n_2+1}\sum_{\ell_2=-1}^{\ell_1+n_3+1} V_{\ell_1}^{n_1 n_2}V_{\ell_2}^{\ell_1 n_3}\,V_{-1}^{\ell_2}(\Omega)\,,\end{aligned} \tag{185b}$$

$$\Delta W_{qj}(z) = \begin{cases} 0 & \text{for}\quad \tau_1^a \\ \frac{\alpha_s(\mu_B)}{2\pi}\left[\delta_{jq}C_F P_{qq}(z)+\delta_{jg}T_F P_{qg}(z)\right]\ln z & \text{for}\quad \tau_1^b\end{cases} \tag{185c}$$

Here j sums over quark flavors and gluons, and the $+(q\leftrightarrow\bar q)$ includes the term where the virtual gauge boson couples to an antiquark. In Eq. (185a) the exponent is a resummation factor that resums the large logs and the terms W_{qj}

and ΔW_{qj} are fixed-order factors which do not contain large logs. The evolution kernels $\mathcal{K}$ and Ω are given by

$$\mathcal{K} \equiv \mathcal{K}(\mu_H, \mu_J, \mu_B, \mu_S, \mu) = K_H(\mu_H, \mu) + K_J(\mu_J, \mu) + K_B(\mu_B, \mu) + 2K_S(\mu_S, \mu) \tag{186a}$$

$$\Omega \equiv \Omega(\mu_J, \mu_B, \mu_S, \mu) = \eta_J(\mu_J, \mu) + \eta_B(\mu_B, \mu) + 2\eta_S(\mu_S, \mu)\,, \tag{186b}$$

where the individual evolution kernels K_H, $K_J = K_B$, K_S, $\eta_J = \eta_B$, and η_S are given below in Eqs. (D3), (D5), and (D15). Note that $\mathcal{K}$ and Ω are indpendent of μ because the μ dependence cancels between the various K_i and η_i factors in the sums. Their expressions to NNLL accuracy are given in Eq. (D26) App. D. The coefficients J_n, I_n^{qq}, I_n^{qg}, S_n in Eq. (185b) are given in Eq. (E7). The constants V_k^{mn} and $V_k^n(\Omega)$ are given in App. E 2.

Note that in the resummed cross section Eq. (185) the coefficients J_n, I_n^{qj}, and S_n are functions of logarithms of their last argument as shown in Eq. (E7) and the hard function also depends on the logarithm $\ln(Q^2/\mu_H^2)$. The logs in these fixed-order factors can be minimized by choosing the canonical scales

$$\mu_H = Q\,, \quad \mu_J = \mu_B = Q\sqrt{\tau_1^{a,b}}\,, \quad \mu_S = Q\tau_1^{a,b}\,. \tag{187}$$

Large logs of ratios of these scales to the arbitrary factorization scale μ are then resummed to all orders in α_s in the evolution kernels $\mathcal{K}$ and Ω. The choices in Eq. (187) are appropriate in the tail region of the distribution where τ_1 is not too close to zero and not too large so that the logs of τ_1 are still large enough to dominate non-log terms and need to be resummed. Near $\tau_1 \sim 0$ and $\tau_1 \sim 1$, we will need to make more sophisticated choices for the scales, which we will discuss in Sec. VII C.

2. τ_1^c cross section

The resummed τ_1^c cross section obtained from RG evolution of the hard, jet, beam, and soft functions in Eq. (153) is given by

$$\begin{aligned}\sigma_{\rm c}^c(x, Q^2, \tau) = {}& \frac{e^{K-\gamma_E\Omega}}{\Gamma(1+\Omega)}\left(\frac{Q}{\mu_B}\right)^{\eta_H(\mu_H,\mu)}\left(\frac{(\tau-1+y)\,xQ^2}{\mu_B^2}\right)^{\eta_B(\mu_H,\mu)}\left(\frac{(\tau-1+y)\,Q^2}{\mu_J^2}\right)^{\eta_J(\mu_H,\mu)}\left(\frac{(\tau-1+y)\,\sqrt{x}Q}{\mu_S}\right)^{2\eta_S(\mu_H,\mu)} \\ & \times L_q^c(x, Q^2)\int_x^1 \frac{dz}{z} f_j(x/z)\,\left[W_{qj}^c(z, \tau-1+y) + \Delta W_{qj}^c(z, \tau-1+y)\right] + (q \leftrightarrow \bar{q})\,,\end{aligned} \tag{188}$$

where W_{qj}^c and ΔW_{qj}^c are the fixed-order terms from jet, beam, and soft functions:

$$\begin{aligned}W_{qj}^c(z,\tau) = {}& H(Q^2,\mu_H)\sum_{\substack{n_1,n_2,\\ n_3=-1}}^{1} J_{n_1}\left[\alpha_s(\mu_J), \frac{\tau Q^2}{\mu_J^2}\right] I_{n_2}^{qj}\left[\alpha_s(\mu_B), z, \frac{\tau x Q^2}{\mu_B^2}\right]\; S_{n_3}\left[\alpha_s(\mu_S), \frac{\tau\sqrt{x}Q}{\mu_S}\right] \\ & \times \sum_{\ell_1=-1}^{n_1+n_2+1}\sum_{\ell_2=-1}^{\ell_1+n_3+1} V_{\ell_1}^{n_1 n_2} V_{\ell_2}^{\ell_1 n_3}\, V_{-1}^{\ell_2}(\Omega)\,,\end{aligned} \tag{189a}$$

$$\begin{aligned}\Delta W_{qj}^c(z,\tau) = {}& \frac{\alpha_s(\mu_B)}{2\pi}\left[\delta_{jq}C_F P_{qq}(z) + \delta_{jg}T_F P_{qg}(z)\right]\Bigg[\theta(\tau)\,\left\{\ln\left[\frac{\tau(1-X)}{(1-y)X}\right] - H(-1-\Omega)\right\} \\ & + \theta\left(\frac{\tau}{(1-y)X}+1\right)\left\{\frac{1}{\Omega}\left(\frac{|\tau|}{(1-y)X}\right)^{-\Omega}{}_2F_1\left[-\Omega,-\Omega;1-\Omega;-\frac{\tau}{(1-y)X}\right] - \theta(-\tau)\,\frac{\pi}{\sin(\pi\Omega)}\right\}\Bigg]\,,\end{aligned} \tag{189b}$$

where $X \equiv x(1-z)/(x+z-xz)$. Note that the τ in $W_{qj}^c(z,\tau)$ and $\Delta W_{qj}^c(z,\tau)$ gets shifted by $1-y$ in Eq. (188). $H(n)$ is the harmonic number and ${}_2F_1(a,b;c;z)$ is the hypergeometric function. The additional more complicated terms in ΔW_{qj}^c are due to the nontrivial $\mathbf{p}_\perp$ integral in Eq. (153) which convolves the terms in the generalized beam function with nontrivial $\mathbf{p}_\perp^2$ dependence with the dependence of the jet function on $(\mathbf{q}_\perp + \mathbf{p}_\perp)^2$, with $\mathbf{q}_\perp \neq 0$ when $y < 1$. Note that the term on the last line of Eq. (189b) contributes below $\tau_1^c = 1-y$ when plugged into Eq. (188), but that the size of the correction in this region is very small.

The second arguments of J_n, I_n^{qj}, and S_n in Eq. (189a) show that the canonical scales should be chosen to minimize the logs of the agruments, which are the fixed-order terms in the hard, jet, beam, and soft functions.

$$\mu_H = Q\,, \quad \mu_J = Q\sqrt{\tau_1^c - 1 + y}\,, \quad \mu_B = Q\sqrt{x(\tau_1^c - 1 + y)}\,, \quad \mu_S = \sqrt{x}Q(\tau_1^c - 1 + y)\,. \tag{190}$$

	$\Gamma[\alpha_s]$	$\gamma[\alpha_s]$	$\beta[\alpha_s]$	$\{H,J,B,S\}[\alpha_s]$
LL	α_s	1	α_s	1
NLL	α_s^2	α_s	α_s^2	1
NNLL	α_s^3	α_s^2	α_s^3	α_s

	$\Gamma[\alpha_s]$	$\gamma[\alpha_s]$	$\beta[\alpha_s]$	$\{H,J,B,S\}[\alpha_s]$
LL	α_s	1	α_s	1
NLL′	α_s^2	α_s	α_s^2	α_s
NNLL′	α_s^3	α_s^2	α_s^3	α_s^2

TABLE III: Orders of logarithmic accuracy and required order of cusp (Γ) and non-cusp (γ) anomalous dimensions, beta function β, and fixed-order hard, jet, beam, and soft matching coefficients H, J, B, S. The "primed" counting includes the fixed-order coefficients to one higher order in α_s.

Here the whole cross section is shifted to the right by an amount $1-y$ due to the nonzero $\mathbf{q}_\perp$ and choice of axes for τ_1^c. Unlike $\tau_1^{a,b}$, the jet and beam scales are separated by a factor $\sqrt{x}$ due to the different normalization of the q_B reference vector in the definition of τ_1^c. For τ_1^c, $q_B^c = P$ while for $\tau_1^{a,b}$, $q_B^{a,b} = xP$. The soft scale is also rescaled by $\sqrt{x}$. We will discuss below a more sophisticated choice of scales than Eq. (190) that give rise to proper behavior in the limits $\tau_1^c \to 1-y$ and $\tau_1^c \sim 1$.

3. Logarithms included in our LL, NLL, and NNLL results

It is worth briefly discussing the logarithmic accuracy of our resummed results. Although this discussion is standard in the literature, sometimes the same notation is used for different levels of resummed precision, so it is worth being specific about our notation. The order in α_s to which the anomalous dimensions, running coupling, and fixed-order hard, jet, beam, and soft functions are known determines the accuracy to which the logarithms of τ in cross section are resummed. It is most straightforward to count the number of logs thus resummed in the Laplace transform of the cross section (equivalently we could consider the Fourier transform to position space),

$$\tilde{\sigma}(x,Q^2,\nu) = \int_0^\infty d\tau\, e^{-\nu\tau} \frac{d\sigma}{dx\, dQ^2\, d\tau}\,. \tag{191}$$

The fixed-order expansion of $\tilde{\sigma}(x,Q^2,\nu)$ takes the form,

$$\begin{aligned}\tilde{\sigma}(x,Q^2,\nu) = \; & 1 \; + \; \frac{\alpha_s}{4\pi}(c_{12}L^2 + c_{11}L + c_{10} + \tilde{d}_1(\nu)) \\ & + \left(\frac{\alpha_s}{4\pi}\right)^2 (c_{24}L^4 + c_{23}L^3 + c_{22}L^2 + c_{21}L + c_{20} + \tilde{d}_2(\nu)) \\ & + \left(\frac{\alpha_s}{4\pi}\right)^3 (c_{36}L^6 + c_{35}L^5 + c_{34}L^4 + c_{33}L^3 + c_{32}L^2 + c_{31}L + c_{30} + \tilde{d}_3(\nu)) + \cdots\,,\end{aligned} \tag{192}$$

where $L \equiv \log\nu$. The largest log at each order in α_s is $\alpha_s^n L^{2n}$. Our results in Eqs. (185) and (188), once Laplace transformed, reorganize and resum the logarithms into the form:

$$\begin{aligned}\tilde{\sigma}(x,Q^2,\nu) = \; & \exp\Bigg[\, \frac{\alpha_s}{4\pi}(C_{12}L^2 + C_{11}L + C_{10}) \\ & + \left(\frac{\alpha_s}{4\pi}\right)^2 (C_{23}L^3 + C_{22}L^2 + C_{21}L + C_{20}) \\ & + \left(\frac{\alpha_s}{4\pi}\right)^3 (C_{34}L^4 + C_{33}L^3 + C_{32}L^2 + C_{31}L + C_{30}) + \cdots \Bigg] + \tilde{d}(x,Q^2,\nu)\,,\end{aligned} \tag{193}$$

where the largest log at each order in the exponent is $\alpha_s^n L^n$. The coefficients c_{nm}, C_{nm}, and $d_n(\nu)$ are functions of x and Q^2. The function $\tilde{d}(x,Q^2,\nu)$ contains terms $\tilde{d}_n(\nu)$ and is a non-singular function of ν that vanishes as $\nu \to \infty$ ($\tau \to 0$). Transforming Eqs. (192) and (193) back to momentum space using

$$\frac{d\sigma}{dx\, dQ^2\, d\tau} = \int_{\gamma-i\infty}^{\gamma+i\infty} \frac{d\nu}{2\pi i} e^{\nu\tau}\tilde{\sigma}(x,Q^2,\nu)\,, \tag{194}$$

where γ lies to the right of all singularities of the integrand in the complex plane, defines the accuracy to which

logs of τ in the cross section and its cumulant $\sigma_c(x, Q^2, \tau)$ are resummed.

Our main results in Eqs. (185) and (188) resum singular logarithmic terms $\alpha_s^n \ln^m \tau$, but not the terms in the non-singular $d(x, Q^2, \tau)$ (inverse transform of $\tilde{d}$). The $d(x, Q^2, \tau)$ must either be calculated by comparing a full QCD perturbation theory calculation with the resummed result and determining the difference order by order in α_s, or by determining the next-to-singular infinite towers of logarithmic terms in $d(x, Q^2, \tau)$ by carrying out a factorization and resummation analysis in SCET at subleading power.

Fixed-order perturbation theory sums the series in Eq. (192) row-by-row, order-by-order in α_s. When the logs are large this expansion is not well behaved. Resummed perturbation theory instead sums the exponent in Eq. (193) column-by-column, in a modified power expansion that counts $\ln\tau \sim 1/\alpha_s$ when the logs are large. Everything in the first column of Eq. (193) is $\mathcal{O}(1/\alpha_s)$ [leading log (LL)], the second $\mathcal{O}(1)$ [next-to-leading-log (NLL)], the third $\mathcal{O}(\alpha_s)$ (NNLL), etc. in this counting. Each order of logarithmic accuracy is achieved by calculating the cusp and non-cusp anomalous dimensions, running coupling, and fixed-order hard, jet, beam, and soft functions to the orders given in Table III. Another common counting used in the literature (eg. [14, 76, 99]) is the primed counting which accounts for the fixed-order matching coefficients H, J, B, S at one higher order than in the unprimed counting. This primed counting is particularly useful when one also requires predictions for transition regions where the size of the logarithmic and non-logarthmic $d_n(\tau)$ terms are comparable. Since in this paper we have not considered the nonsingular terms we adopt the unprimed counting (LL, NLL, NNLL) throughout.

B. Comparison to NLL DIS Thrust τ_Q

As discussed above in Sec. III B there are several versions of DIS thrust discussed in the literature. Here we consider the version of thrust called τ_Q in [15], to which we can directly compare our results for τ_1^b, since as shown above in Eq. (63) of Sec. III D they are one and the same. We will see that at NLL accuracy the result in [15] for τ_Q is equivalent to our result in Eq. (185) for τ_1^b for the particular scale choices Eq. (187) in the SCET cross section. The NLL resummed cross section given in [15] in the $\overline{\text{MS}}$ scheme is, in our notation,

$$\begin{aligned}\sigma_c(\tau_Q) = \theta(\tau_Q)\Bigg\{\sum_q e_q^2\Big[f_q(x,\sqrt{\tau}Q) \\ + \frac{\alpha_s(Q)}{2\pi}\int_x^1 \frac{dz}{z} C_{1q}(z) f_q(x/z,Q)\Big] \\ + \Big(\sum_q e_q^2\Big)\frac{\alpha_s(Q)}{2\pi}\int_x^1 \frac{dz}{z} C_{1g}(z) f_g(x/z,Q)\Bigg\} e^{-g_1 \ln\tau + g_2}\,,\end{aligned} \tag{195}$$

where

$$\begin{aligned}C_{1q}(z) &= C_F\Big[2\mathcal{L}_1(1-z) - (1+z)\ln(1-z) \\ &\qquad + 1 - z - \Big(\frac{\pi^2}{3} + \frac{9}{2}\Big)\delta(1-z)\Big]\,, \\ C_{1g}(z) &= T_F[P_{qg}(z)\ln(1-z) + 2z(1-z)]\,,\end{aligned} \tag{196}$$

and complete expressions for the resummation constants $g_{1,2}$ can be found in Ref. [15]. They have fixed-order expansions in $\alpha_s = \alpha_s(Q)$ given by

$$\begin{aligned}g_1 \ln\tau &= G_{12}\frac{\alpha_s}{2\pi}\ln^2\tau - G_{23}\Big(\frac{\alpha_s}{2\pi}\Big)^2 \ln^3\tau + \cdots \\ g_2 &= -G_{11}\frac{\alpha_s}{2\pi}\ln\tau + G_{22}\Big(\frac{\alpha_s}{2\pi}\Big)^2\ln^2\tau + \cdots\,,\end{aligned} \tag{197}$$

with the coefficients

$$\begin{aligned}&G_{12} = -2C_F\,, \quad G_{11} = 3C_F\,, \quad G_{23} = 2\pi\beta_0 G_{12}\,, \\ &G_{22} = -\frac{4}{3}\pi^2 C_F^2 + \Big(\frac{\pi^2}{3} - \frac{169}{36}\Big)C_A C_F + \frac{11}{18}C_F n_f\,.\end{aligned} \tag{198}$$

Note that the cross section Eq. (195) includes only the photon contribution for the intermediate gauge boson mediating the scattering, so for the comparison we specialize our results to this case.

By comparing to the resummed cross section in Eq. (185), we find that the result of [15] given in Eq. (195) is equivalent to the SCET photon induced cross section at NLL order with the following fixed choices for the scales in the evolution factors:

$$\mu_H = Q\,, \quad \mu = \mu_J = \mu_B = Q\sqrt{\tau_1}\,, \quad \mu_S = Q\tau_1\,. \tag{199}$$

Thus the two results agree at NLL order.

We note that in the fixed-order coefficient in Eq. (195), the choice $\mu = Q\sqrt{\tau}$ has been made in the tree level term, but the $\mathcal{O}(\alpha_s)$ terms have been evaluated at $\mu = Q$. In the SCET result Eq. (185) (or Eq. (F7)) pieces of the $\alpha_s(\mu)$ terms are evaluated at $\mu = Q$, $\mu = Q\sqrt{\tau}$, or $\mu = Q\tau$ according to whether they come from the hard, beam/jet, or soft functions, while the PDFs are evaluated at $\mu = Q\sqrt{\tau}$. The difference between the SCET result and Eq. (185) is NNLL, since the error is $\sim \alpha_s^2 \ln\tau$ in the fixed-order coefficient. In our counting taking the correct scales for $\alpha_s(\mu)$ is required for NLL′ accuracy, since this provides the appropriate boundary conditions for the full NNLL result. Thus the result in Eq. (195) with $\alpha_s(Q)$ is at an intermediate level of accuracy between NLL and NLL′.

Note that the SCET expression Eq. (185) still shows the full dependence on the individual scales $\mu_{H,B,J,S}$ instead of the single scale μ, and the dependence on each of these scales cancels out to the order in resummed perturbation theory that we are working. The remaining scale dependence thus provides a useful way to estimate the theoretical uncertainty due to the truncation of higher order terms in resummed perturbation theory.

C. Scale Profile Functions

In general there are three relevant regions with different power counting

$$\begin{aligned} &\text{peak region:} && \tau_1 \sim 2\Lambda_{\rm QCD}/Q_R \ll 1\,, \\ &\text{tail region:} && 2\Lambda_{\rm QCD}/Q_R \ll \tau_1 \ll 1\,, \\ &\text{far-tail region:} && \tau_1 \sim 1\,. \end{aligned} \tag{200}$$

For the peak and tail regions of the distribution we have $\tau_1 \ll 1$ and we must sum the large logarithms. In the tail region the results in Eqs. (187) and (190) above are the canonical scales for $\mu_{H,J,B,S}$ for which the logs in the fixed-order hard, jet, beam, and soft functions are minimized. Evolution from these scales to another scale μ resums the logs of the ratios $\mu/\mu_{H,J,B,S}$ to all orders in α_s. In the peak region for small τ_1, the scale $\mu_S \sim Q\tau_1$ goes towards the nonperturbative region. The validity of our resummation analysis relies on there being a perturbative expansion for the soft function anomalous dimensions at the scale μ_S, $\Gamma_S[\alpha_s(\mu_S)]$ and $\gamma_S[\alpha_s(\mu_S)]$. Therefore in the SCET approach it is mandatory that we stop the renormalization group evolution at a scale $\mu_S \sim 1\,\text{GeV}$ that can still be considered perturbative. This requires the scales to deviate from the canonical form. Finally, for larger values of τ_1 the logs are no longer large, and the nonsingular terms in the fixed-order expansion become equally important. In this large τ_1 region we should turn off the resummation, which will revert the results to a fixed-order expansion in α_s. Again this forces the scales to deviate from the canonical ones.

To achieve these properties we use *profile functions* to describe the functional dependence of the scale $\mu_{S,B,J}$ on τ_1. First we will consider the profile functions for the $\tau_1^{a,b}$ cross sections and then for τ_1^c.

1. $\tau_1^{a,b}$ profile functions

For the $\tau_1^{a,b}$ cross sections, the canonical scales are given in Eq. (187), $\mu_S \sim \tau_1$, $\mu_{B,J} \sim \sqrt{\tau_1}Q$, $\mu_H \sim Q$. The perturbative resummation of large logs of ratios of these scales is valid when $\Lambda_{\rm QCD} \ll \mu_S \ll \mu_{B,J} \ll \mu_H$, which is the tail region. We will define boundaries , $t_1 < \tau_1 < t_2$ for the region of τ_1 where this condition is satisfied, and use scales that are within a factor of 2 of the canonical ones. Beyond this region, when $\tau_1 > t_2$, τ_1 is of $\mathcal{O}(1)$, and the logs are the same order as the nonsingular terms in the fixed-order expansion. In this region, the scales must be taken to be of the same order, $\mu_S \simeq \mu_{B,J} \simeq \mu_H \sim Q$, which turns off the resummation in Eq. (185). Finally for $\tau_1 < t_1$, the soft scale approaches $\Lambda_{\rm QCD}$ and nonperturbative corrections become important. In this region we freeze the soft scale μ_S used in the perturabtive cross section to a value above $\Lambda_{\rm QCD}$: $\mu_S \sim 1$–2 GeV. The hard scale is $\mu_H \sim Q$ and beam and jet scale are determined by hard and soft scales as $\sqrt{\mu_H \mu_S} \sim \mu_{J,B}$.

Profile functions for scales that satisfy the above criteria have been used for other cross sections in [14, 28, 76]. Here, we adopt the profile functions in [28]. The hard, beam, jet, and soft scales we use are given by

$$\begin{aligned} \mu_H &= \mu\,, \\ \mu_{B,J}(\tau_1) &= \biggl[1 + e_{B,J}\theta(t_3-\tau_1)\Bigl(1-\frac{\tau_1}{t_3}\Bigr)^2\biggr]\sqrt{\mu\,\mu_{\rm run}(\tau_1\,,\mu)}\,, \\ \mu_S(\tau_1) &= \biggl[1 + e_S\theta(t_3-\tau_1)\Bigl(1-\frac{\tau_1}{t_3}\Bigr)^2\biggr]\mu_{\rm run}(\tau_1\,,\mu)\,, \end{aligned} \tag{201}$$

where $e_{B,J,S}$ are parameters used to vary the jet, beam, and soft scales to estimate theoretical uncertainty of the perturbative predictions. t_3 is the point above which all scales are set equal, $\mu_H = \mu_{B,J} = \mu_S = \mu$. The common function $\mu_{\rm run}(\tau_1, \mu)$ is given by

$$\begin{aligned} \mu_{\rm run}(\tau_1,\mu) &= \begin{cases} \mu_0 + a\tau_1^2/t_1 & \tau_1 \le t_1\,, \\ 2a\,\tau_1 + b & t_1 \le \tau_1 \le t_2\,, \\ \mu - a(\tau_1 - t_3)^2/(t_3 - t_2) & t_2 \le \tau_1 \le t_3\,, \\ \mu & \tau_1 > t_3\,, \end{cases} \\ a &= \frac{\mu_0 - \mu}{t_1 - t_2 - t_3}\,, \qquad b = \frac{\mu t_1 - \mu_0(t_2 + t_3)}{t_1 - t_2 - t_3}\,, \end{aligned} \tag{202}$$

The function $\mu_{\rm run}(\tau_1, \mu)$ quadratically approaches μ_0 below t_1 and μ above t_2, and it is linearly increasing from t_1 to t_2. The continuity of $\mu_{\rm run}(\tau_1, \mu)$ and its derivative at t_1 and t_2 determines a and b.

The default values of parameters we will use for what we will consider the "central values" of the $\tau_1^{a,b}$ cross sections are:

$$\begin{aligned} &\mu = Q\,, \quad e_{B,J} = e_S = 0\,, \quad \mu_0 = 2\ \text{GeV}\,, \\ &t_1 = \frac{3\ \text{GeV}}{Q}\,, \quad t_2 = 0.4\,, \quad t_3 = 0.6\,. \end{aligned} \tag{203}$$

To estimate theoretical uncertainty due to missing higher order terms in fixed-order and resummed perturbation theory, we vary the parameters μ, $e_{B,J}$, and e_S from their default values by $\mathcal{O}(1)$ factors in order to vary corresponding scales μ_H, $\mu_{B,J}$, and μ_S by $\mathcal{O}(1)$ factors, respectively. We separately vary the parameters one by one and keep the others at their default values. The total number of variations we perform around the central values are as follows:

$$1)\quad \mu = 2^{\pm1}Q\,, \quad e_{B,J} = 0\,, \quad e_S = 0 \tag{204a}$$

$$2)\quad \mu = Q\,, \quad e_{B,J} = \pm\frac{1}{3}, \pm\frac{1}{6}\,, \quad e_S = 0 \tag{204b}$$

$$3)\quad \mu = Q\,, \quad e_{B,J} = 0\,, \quad e_S = \pm\frac{1}{3}, \pm\frac{1}{6}\,. \tag{204c}$$

Variation 1 moves all the scales in Fig. 4 together up and down by factors of 2, and corresponds to the scale variation used to estimate the fixed order theoretical uncertainty in perturbation theory. Variations 2 and 3 are additional variations we are able to perform because of

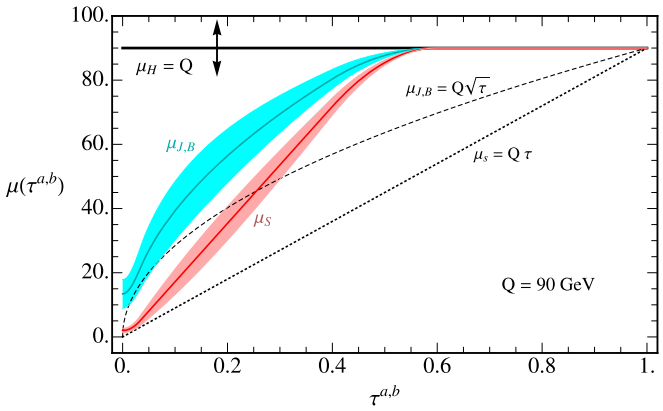

FIG. 4: $\tau_1^{a,b}$ profile functions for the scales μ_H, $\mu_{B,J}(\tau_1)$, $\mu_S(\tau_1)$ with $Q = 90$ GeV used in the resummed factorized cross section Eq. (185). The double arrow and the colored bands illustrate the scale variations in Eq. (204) used to obtain theoretical uncertainty estimates.

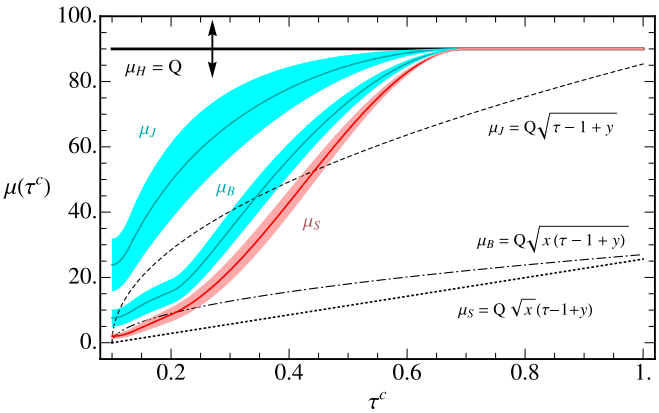

FIG. 5: τ_1^c profile functions for the scales μ_H^c, $\mu_{B,J}^c(\tau_1)$, $\mu_S^c(\tau_1)$ with $x = 0.1$, $y = 0.9$, and $Q = 90$ GeV, along with the simple canonical scales Eq. (190). The double arrow and colored bands illustrate the scale variations in Eq. (204).

having independent $\mu_{J,B}$ and μ_S scales in the resummed cross section Eq. (185) and give an estimate of the uncertainty at each order in logarithmic accuracy in resummed perturbation theory that can not be achieved by varying the single scale μ. Variation 1 alone underestimates the total uncertainty.

The size of the cross section at a given value of τ_1 may not vary monotonically with $e_{J,B}, e_S$, and ideally we would vary them continuously within some finite band to find the maximum uncertainty. The four values we test for $e_{J,B}, e_S$ in Eq. (204) are a discrete approximation to such a procedure that remains computationally tractable. We take the largest and smallest values of the cross section among these points and use them to define the width of the uncertainty band from $e_{J,B}$ or e_S variation.

To make a conservative estimate of the total uncertainty, we sum in quadrature the uncertainties we get from variations 1, 2, and 3 individually. We find that the total size of the bands provided by Eq. (204) are reasonable estimates of the theoretical uncertainty when we compare the cross sections at different orders of logarithmic accuracy.

Fig. 4 shows profile functions for μ_H, $\mu_{B,J}(\tau_1)$, $\mu_S(\tau_1)$ with $Q = 90$ GeV. The solid lines are the central values of the scales with default values in Eq. (203), the double-headed arrow implies variation 1 and the bands represent variations 2 and 3 in Eq. (204). The dashed and dotted lines are the canonical scales in Eq. (187).

2. τ_1^c profile functions

For τ_1^c, the canonical scales in Eq. (190) are

$$\mu_H \sim Q\,, \qquad \mu_S \sim Q\sqrt{x}(\tau_1 - 1 + y)\,,$$
$$\mu_B \sim Q\sqrt{x(\tau_1 - 1 + y)}\,, \quad \mu_J \sim Q\sqrt{\tau_1 - 1 + y}\,, \tag{205}$$

where they satisfy the relation $\mu_{B,J}^2 = x^{\pm 1/2}\mu_H\mu_S$ Compared to the canonical scales for $\tau_1^{a,b}$ in Eq. (187), there are two differences in the canonical scales for τ_1^c. First, τ_1 is replaced by $\tau_1 - (1-y)$ because the transverse momentum of jet is nonzero, which is $(1-y)Q^2$ at tree level and the projection onto q_J^c differs from the projection onto jet axis by $(1-y)Q^2$. This requires that canonical scales in Eq. (187) and profile in Eq. (201) are shifted by $1-y$. Second, the soft scale and beam scale are multiplied by $\sqrt{x}$ because of rescaling of the beam axis from xP for $\tau_1^{a,b}$ to P for τ_1^c.

In this paper we consider the case $\sqrt{x} \sim \mathcal{O}(1)$ and this factor changes the scales by $\mathcal{O}(1)$, which is the size of perturbative uncertainties from varying μ, $e_{B,J}$ and e_S. This means that multiplying μ_B and μ_S by $\sqrt{x}$ in Eq. (201) should not make a difference within the perturbative uncertainty. So, we could use the profile in Eq. (201) but shifted by $1-y$. On the other hand, by modifying the profile the canonical relations among the scales $\mu_{H,J,B,S}$ for τ_1^c Eq. (190) can be maintained and we can account for the extra factors of $\sqrt{x}$. Therefore, for these profiles we define $\mu_{H,J,B,S}^c$ as

$$\mu_H^c = \mu\,, \quad \mu_{B,J,S}^c(\tau_1) = \mu_{B,J,S}(x, \tau_1 - 1 + y)\,, \tag{206}$$

$$\mu_J(x,\tau_1) = \Big[1 + e_J\theta(t_3-\tau_1)\Big(1-\frac{\tau_1}{t_3}\Big)^2\Big]\sqrt{\mu\,\mu_{\rm run}^c(x,\tau_1,\mu,0)},$$
$$\mu_B(x,\tau_1) = \Big[1 + e_B\theta(t_3-\tau_1)\Big(1-\frac{\tau_1}{t_3}\Big)^2\Big]\sqrt{\mu\,\mu_{\rm run}^c(x,\tau_1,\mu,1)},$$
$$\mu_S(x,\tau_1) = \Big[1 + e_S\theta(t_3-\tau_1)\Big(1-\frac{\tau_1}{t_3}\Big)^2\Big]\mu_{\rm run}^c(x,\tau_1,\mu,1/2).$$

The $\mu_{\rm run}^c$ used here depend on x and index $0, 1, 2$ that is different for μ_J, μ_B, μ_S. We want $\mu_{\rm run}^c(x\,,\tau_1\,,\mu\,,n) \sim x^n\tau_1\mu$ with $n = 0, 1/2, 1$ so that the canonical scaling for $\mu_{J,S,B}$ in Eq. (190) is respected in the small τ_1 region. In the large τ_1 limit, $\mu_{\rm run}^c(x\,,\tau_1\,,\mu\,,n)$ should go to μ, so that μ_S and $\mu_{B,J}$ both go to μ.

As in Eq. (202) $\mu_{\rm run}^c$ should run linearly between t_1

and t_2. However, the slope of $\mu^c_{\rm run}$ in Eq. (206) should be different for the three cases $n = 0, 1/2, 1$. Therefore, we cannot use Eq. (202) to define $\mu^c_{\rm run}$ because all parameters in $\mu_{\rm run}$ are fixed by matching boundary conditions and the slope is fixed. Instead, by replacing the quadratic polynomial in Eq. (202) by a cubic polynomial one can introduce a free parameter and this parameter can be chosen such that $\mu^c_{\rm run}(x\,,\tau_1\,,\mu\,,n) \sim x^n\tau_1\mu$ between t_1 and t_2. We define $\mu^c_{\rm run}$ as

$$\mu^c_{\rm run}(x\,,\tau_1\,,\mu\,,n) = \begin{cases} x^{n-\frac{1}{2}}\mu_0 + a(n)\,\tau_1^2/t_1 & \tau_1 \le t_1\,, \\ 2a(n)\,\tau_1 + b(n) & t_1 \le \tau_1 \le t_2\,, \\ \mu_{\rm cubic}(x\,,\tau_1\,,\mu\,,n) & t_2 \le \tau_1 \le t_3\,, \\ \mu & \tau_1 > t_3\,, \end{cases}$$

$$\mu_{\rm cubic}(x\,,\tau_1\,,\mu\,,n) = \mu - c(n)\left(\frac{\tau_1-t_3}{t_3-t_2}\right)^2 - d(n)\left(\frac{\tau_1-t_3}{t_3-t_2}\right)^3$$

$$b(n) = x^{n-1/2}\mu_0 - a(n)t_1\,,$$

$$c(n) = 3(\mu - x^{n-1/2}\mu_0) - a(n)(2t_3 + 4t_2 - 3t_1)\,,$$

$$d(n) = 2(\mu - x^{n-1/2}\mu_0) - 2a(n)(t_3 + t_2 - t_1)\,. \qquad (207)$$

Here the parameters $b(n)$, $c(n)$, $d(n)$ are determined by continuity of $\mu_{\rm run}$ and its derivative at t_1, t_2, t_3. The slope $a(n)$ is a free parameter which is chosen to satisfy $a(n) \sim x^n\mu$ to achieve canonical scaling of jet, beam, and soft scales:

$$a(n) = x^n\,\frac{\mu - x^{-1/2}\mu_0}{t_3 + t_2 - t_1}. \qquad (208)$$

Note that in $x \to 1$ limit, Eq. (207) reduces to Eq. (202) and profiles for τ_1^c in Eq. (206) reduce to the profiles in Eq. (201) for τ_1^a and τ_1^b.

We choose the same default parameters and scale variations as for $\tau_1^{a,b}$ in Eqs. (203) and (204) except for t_2:

$$t_2 = 0.1\,. \qquad (209)$$

Because of the different definition of the profiles for τ_1^c this value of t_2 must be smaller than the value for the $\tau_1^{a,b}$ profiles. This occurs because $\mu_{\rm run}$ in Eq. (207) changes faster than that the $\mu_{\rm run}$ in Eq. (202) between t_2 and t_3. As can be seen from Fig. 5 the final profiles for μ_S have similar shapes.

Fig. 5 shows τ_1^c profile functions for μ_H^c, $\mu_{B,J}^c(\tau_1)$, $\mu_S^c(\tau_1)$ defined in Eq. (206) with $x = 0.1$, $y = 0.9$, and $Q = 90$ GeV. The solid lines are the central values of the scales with default values in Eq. (209) for t_2 and in Eq. (203) for all other parameters. The double-headed arrow represents variation 1 and the uncertainty bands are variations 2 and 3 in Eq. (204). The dashed, dotted, and dotted-dashed are the canonical scales in Eq. (190).

D. Nonperturbative Soft Function

The hemisphere soft function defined in Eq. (134) describes soft radiation between jets at the nonperturbative scale $\Lambda_{\rm QCD}$ as well as at perturbative scales above $\Lambda_{\rm QCD}$. The results given in Eqs. (160) and (D14) are valid in the perturbative region. In the $\overline{\rm MS}$ scheme the soft function valid at both scales is given by a convolution between a purely perturbative function $S^{\rm pert}_{\rm hemi}$ and a nonperturbative model function F [108]:

$$S_{\rm hemi}(k,\mu) = \int dk'\, S^{\rm pert}_{\rm hemi}(k-k',\mu)\, F(k')\,. \qquad (210)$$

The function $F(k)$ contains information about physics at the nonperturbative scale and has support for $k \sim \Lambda_{\rm QCD}$, falling off exponentially outside this region. Inserting Eq. (210) into the factorization formula in Eq. (140) one obtains the convolved form for the cross section:

$$\frac{d\sigma(\tau_1)}{d\tau_1} = \int dk\, \frac{d\sigma^{\rm pert}}{d\tau_1}\left(\tau_1 - \frac{k}{Q_R}\right) F(k)\,, \qquad (211)$$

where $d\sigma^{\rm pert}/d\tau_1$ is the cross section calculated by using only the perturbative soft function and Q_R is given by Eq. (54). Eq. (211) correctly describes both the peak region $Q_R\tau_1 \sim \Lambda_{\rm QCD}$ where the entire function $F(k)$ is required, as well as the tail region $Q_R\tau_1 \gg \Lambda_{\rm QCD}$ where only its first moment is required since we can expand in $\Lambda_{\rm QCD}/(Q_R\tau_1)$.

For the peak region, various ways to parametrize models for $F(k)$ have been proposed [76, 108, 109]. We will adopt one proposed in [76] that expands F systematically in an infinite set of basis functions:

$$F(k) = \frac{1}{\lambda}\left[\sum_{n=0}^{N} c_n f_n\left(\frac{k}{\lambda}\right)\right]^2\,, \qquad (212)$$

where in principle we can choose any complete basis of functions f_n. We adopt the same basis that has already been used in [14, 76], and exhibits fast convergence of the expansion. The normalization condition $\int dk\, F(k) = 1$ gives the constraint $\sum_i c_i^2 = 1$. The characteristic scale λ of size $\mathcal{O}(\Lambda_{\rm QCD})$ is an additional parameter if the sum is truncated at finite N, as we will do in practice.

In the tail region where $Q_R\tau_1 \gg \Lambda_{\rm QCD}$, Eq. (211) is consistent with the power correction from an operator product expansion,

$$\frac{d\sigma(\tau_1)}{d\tau_1} = \left\{\frac{d\sigma^{\rm pert}(\tau_1)}{d\tau_1} - \frac{2\Omega_1^{a,b,c}}{Q_R}\,\frac{d^2\sigma^{\rm pert}(\tau_1)}{d\tau_1^2}\right\} \qquad (213)$$
$$\times\left[1 + \mathcal{O}\left(\frac{\alpha_s\Lambda_{\rm QCD}}{Q\tau_1}\right) + \mathcal{O}\left(\frac{\Lambda^2_{\rm QCD}}{Q^2\tau_1^2}\right) + \cdots\right].$$

To lowest order in $\Lambda_{\rm QCD}/(Q\tau_1)$ this result agrees with a simple shift $\tau_1 \to \tau_1 - 2\Omega_1/Q_R$. Here the coefficient of the power correction $2\Omega_1^{a,b,c}$ is a nonperturbative matrix element and it corresponds to the first moment of the nonperturbative function $\int dk\, k\, F(k)$ which could in principle differ for each of $\tau_1^{a,b,c}$. The first set of power corrections indicated on the second line of Eq. (213) comes from perturbative corrections to the leading power correction

[72], and the second set involves purely nonperturbative corrections at subleading order. In the next section we will consider the question of universality of the Ω_1^a, Ω_1^b, Ω_1^c parameters for the observables τ_1^a, τ_1^b, τ_1^c.

In the peak region the parameters c_i and λ should be determined by fitting to experimental data. Since data is not yet available, our only purpose here will be to get an idea of the impact of the nonperturbative shape function. We take the simplest function $F(k)$ with $N = 0$. Then, $c_0 = 1$ by normalization and λ is the only parameter. To get the right first moment, we require $\lambda = 2\,\Omega_1$. We use $\Omega_1 = 0.35$ GeV, which is determined from measurements of $e^+e^- \to$ dijets [14]. However, Ω_1 in DIS is not necessarily the same as in e^+e^- collisions, and we merely consider this to be an illustrative but reasonable value.

E. Universality Classes for Ω_1 Parameters Defined with Different Directions

The various versions of 1-jettiness $\tau_1^{a,b,c}$ or the generic version Eq. (24) depend on different choices of the axes $q_J = \omega_J n_J/2$ and $q_B = \omega_B n_B/2$. In this section we will show that the 1-jettiness power correction parameter is universal under changes to the axes used in its definition, by exploiting properties of operators [70, 71] and including hadron mass effects [69, 72].

If we use different axes for the decomposition of four-momenta then they can all be written in a form similar to the event shapes given in [72]:

$$\tau_1 = \frac{1}{2Q_R}\sum_i m_i^\perp f(r_i, \mathcal{Y}_{JB}^i)\,, \tag{214}$$

where Q_R is defined in Eq. (54), i sums over hadrons, and $m_i^\perp, r_i, \mathcal{Y}_{JB}^i$ are defined with respect to the vector $q_{J,B}$ by:

$$m^\perp \equiv \sqrt{\mathbf{p}_\perp^2 + m^2}\,,\; r_i \equiv \frac{p_\perp}{m^\perp}\,, \quad \mathcal{Y}_{JB} \equiv \frac{1}{2}\ln\frac{q_B\cdot p}{q_J\cdot p}\,, \tag{215}$$

where m is the mass of the hadron whose momentum is p^μ. For the 1-jettinesses τ_1 given in Eq. (24) we have

$$f(r, \mathcal{Y}) = e^{-|\mathcal{Y}|}\,. \tag{216}$$

For each different τ_1, i.e. each choice of $q_{J,B}$, the definition of $m^\perp$ and $\mathcal{Y}_{JB}$ change since they are computed with different coordinates. The Q_R also depends on $q_J \cdot q_B$, as given in Eq. (54).

Following the logic in [72] for massive hadrons and [70, 71] for massless particles, the leading power correction in the expansion Eq. (213) of distributions in event shapes of the form Eq. (214) is always described by the nonperturbative matrix element

$$\begin{aligned} 2\Omega_1^{a,b,c} = &\int_0^1 dr \int_0^\infty d\mathcal{Y}_{JB} f(r, \mathcal{Y}_{JB}) \\ &\times \langle 0|\, Y_{n_B}^\dagger Y_{n_J} \hat{\mathcal{E}}_T^{a,b,c}(r, \mathcal{Y}_{JB}) Y_{n_J}^\dagger Y_{n_B}\, |0\rangle\,. \end{aligned} \tag{217}$$

Here $\mathcal{E}_T$ is a "transverse velocity operator" defined as in [72], but now using the axes given by q_J and q_B,

$$\hat{\mathcal{E}}_T(r, \mathcal{Y}_{JB})\,|X\rangle = \sum_{i\in X} m_i^\perp \delta(r - r_i)\delta(\mathcal{Y}_{JB} - \mathcal{Y}_{JB}^i)\,|X\rangle\,. \tag{218}$$

It measures the total transverse mass of particles flowing in a slice of velocity and rapidity around r and $\mathcal{Y}_{JB}$. Now consider making an RPI-III transformation [84] in the matrix element in Eq. (217) which takes $n_J \to n_J/\zeta$ and $n_B \to \zeta n_B$. This transformation leaves the vacuum and the Wilson lines Y_{n_J} and Y_{n_B} invariant, but shifts $\mathcal{E}_T(r, \mathcal{Y}_{JB})$ to $\mathcal{E}_T(r, \mathcal{Y}_{JB} + \mathcal{Y}')$ where $\mathcal{Y}' = \ln\zeta$. This is the analog of the boost argument for back-to-back n_J and n_B in Ref. [70, 71]. Thus, the matrix element inside the integral in Eq. (217) is independent of $\mathcal{Y}_{JB}$, and we can integrate over $\mathcal{Y}_{JB}$ to obtain the power correction $\Omega_1^{a,b,c}$ for $\tau_1^{a,b,c}$, using the f given in Eq. (216):

$$\left[\int_{-\infty}^\infty d\mathcal{Y}_{JB}\, f(r, \mathcal{Y}_{JB})\right]\Omega_1^{JB}(r,\mu) = 2\,\Omega_1^{JB}(r,\mu)\,, \tag{219}$$

where the renormalized matrix element is

$$\Omega_1^{JB}(r,\mu) = \langle 0|\, Y_{n_B}^\dagger Y_{n_J} \hat{\mathcal{E}}_T(r,0) Y_{n_J}^\dagger Y_{n_B}\,|0\rangle\,. \tag{220}$$

This matrix element still depends on the choices of axes through $n_{B,J}$. By rescaling n_J and n_B as in Eq. (133) we find it is independent of $n_J \cdot n_B$. It still depends on these axes through the parameter r, since the transverse momenta $p_\perp$ inside r depends on the choice of these axes.

However, in the tail region the $\Omega_1^{JB}(r)$ always appears inside an integral. At LL order we have the resummed coefficient $C_1^{\rm LL}(k, r, \mu)$ from [72] for any τ_1 and the shape function OPE is

$$\begin{aligned} F(k) &= \delta(k) + \int_0^1 dr\, C_1^{\rm LL}(k, r, \mu) 2\Omega_1^{JB}(r,\mu) + \mathcal{O}\Big(\frac{\Lambda_{\rm QCD}^2}{k^3}\Big) \\ &= \delta(k) + \int_0^1 dr\, C_1^{\rm LL}(k, r, \mu) 2\Omega_1(r,\mu) + \mathcal{O}\Big(\frac{\Lambda_{\rm QCD}^2}{k^3}\Big)\,, \end{aligned} \tag{221}$$

where in the second line we removed the ^{JB} superscript on Ω_1 by using the fact that the only axis dependence occurs through the parameter r which is now just a dummy variable. It would be interesting to consider the universality beyond LL order for this Wilson coefficient.

Thus we see that at least to LL order there is a universal power correction $\Omega_1(r)$ for all three versions of 1-jettiness, $\tau_1^{a,b,c}$. Taking the tree level result $C_1^{\rm LL}(k, r, \mu) \to -\delta'(k)$ yields Eq. (213) and leads to the identification

$$\Omega_1^{a,b,c} = \int_0^1 dr\; \Omega_1(r)\,. \tag{222}$$

Eq. (221) also implies universality of the shift parameter appearing in Eq. (213) for $\tau_1^{a,b,c}$:

$$\Omega_1^a = \Omega_1^b = \Omega_1^c\,. \tag{223}$$

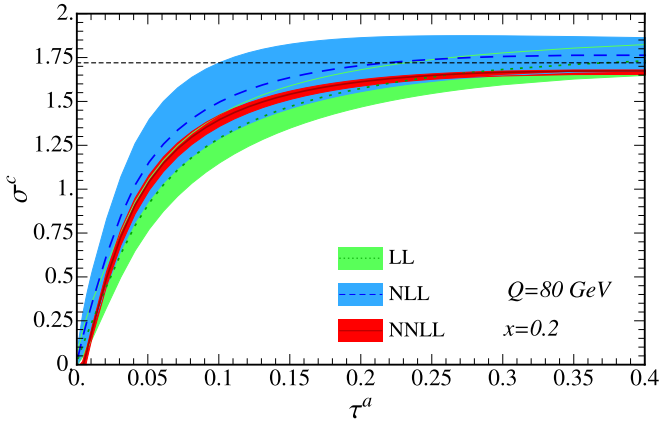

FIG. 6: Cumulant cross section in τ_1^a at $Q = 80$ GeV and $x = 0.2$. Colored bands show theoretical uncertainties around central values (lines) to LL (dotted line, green band), NLL (dashed line, blue band), and NNLL (solid line, red band) accuracy and the horizontal dashed line is the total cross section at fixed x, Q^2.

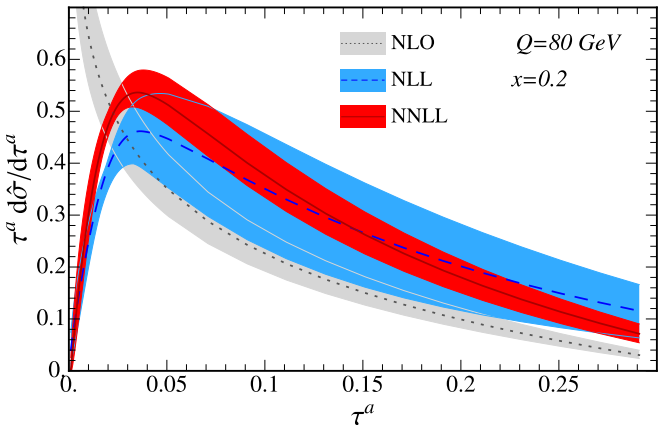

FIG. 7: Weighted differential cross section in τ_1^a at $Q = 80$ GeV and $x = 0.2$. Colored bands show theoretical uncertainties around central values (lines) at fixed order α_s (dotted line, gray band) and resummed to NLL (dashed line, blue band) and NNLL (solid line, red band) accuracy.

VIII. RESULTS

In this section we present our numerical results for the three versions of DIS 1-jettiness: τ_1^a, τ_1^b, and τ_1^c. We plot the cross sections accurate for small τ_1 resummed from LL to NNLL accuracy, and also the singular terms at fixed order $\mathcal{O}(\alpha_s)$ (NLO) for comparison. (We estimate the size of the small missing non-singular terms by comparing to the known $\mathcal{O}(\alpha_s)$ cross section integrated over all τ_1.) We start by describing the τ_1^a spectrum in detail, and then compare the features of the τ_1^b and τ_1^c cross sections relative to the results for τ_1^a. We choose $s = (300\ \text{GeV})^2$ as in the H1 and ZEUS experiments. For the PDFs, we use the MSTW2008 [110] set at NLO and include five quark and antiquark flavors excluding top. To be consistent with the α_s used in the NLO PDFs we use the 2-loop beta function for running α_s and $\alpha_s(m_Z) = 0.1202$.

We present results for the cumulant cross section $\sigma_c(\tau_1)$ defined in Eq. (183) and the dimensionless distribution

$$\frac{d\hat{\sigma}}{d\tau_1} = \frac{1}{\sigma_0}\frac{d\sigma}{d\tau_1} = \frac{d}{d\tau_1}\sigma_c(\tau_1)\,. \tag{224}$$

Note that both the cumulant $\sigma_c(\tau_1)$ and the differential distribution $d\hat{\sigma}/d\tau_1$ are differential in x and Q^2. However, for notational simplicity we made their x and Q^2 dependences implicit in this section.

A. τ_1^a cross section

In this subsection, we present results for the cumulant cross section $\sigma_c(\tau_1)$ and differential cross section $d\hat{\sigma}/d\tau_1$ for the "aligned" 1-jettiness $\tau_1 = \tau_1^a$.

Fig. 6 shows the τ_1^a cumulant cross section, defined by Eq. (183), at $Q = 80$ GeV and $x = 0.2$. In order to illustrate perturbative convergence the results resummed to LL, NLL, and NNLL accuracy are shown. The bands indicate perturbative uncertainties by varying the scales $\mu_{H,B,J,S}$ given by "profile functions" as described in Sec. VII C 1, and there is excellent order-by-order convergence, and beautiful precision at NNLL order. The cumulant cross section increases monotonically from the small τ_1^a region and begins to saturate near for large τ_1^a where the integral defining this cumulant becomes that for the total cross section. There is a small gap between the total cross section at $\mathcal{O}(\alpha_s)$ (dashed horizontal line) and our NNLL cumulant at large τ_1^a, reflecting the small size of nonsingular terms not taken into account in this paper. Note however that these terms are important at the level of precision of our cumulant cross section, and hence they will be considered in the future.

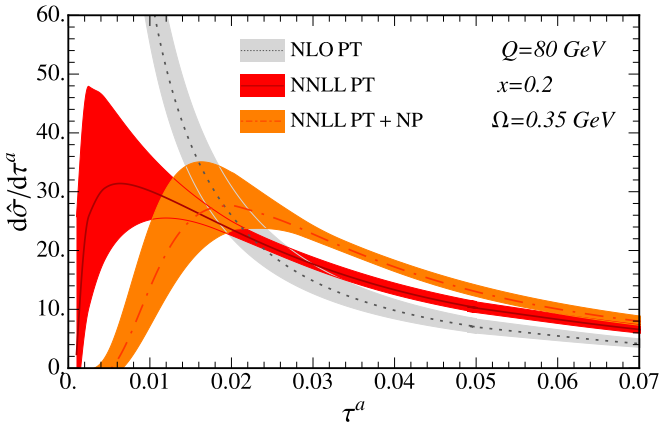

FIG. 8: Differential cross section in τ_1^a at $Q = 80$ GeV and $x = 0.2$ in the peak region, NNLL with nonperturbative shape function taken into account (NNLL PT+NP, dashed, orange), and without NP shape function at fixed-order α_s (NLO PT, dotted, gray) and resummed (NNLL PT, solid, red).

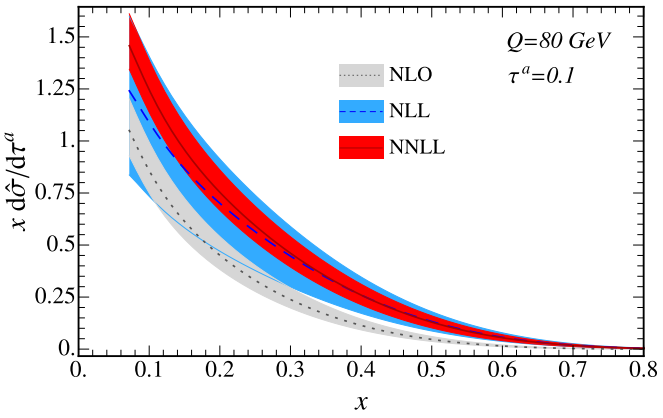

FIG. 9: x dependence of τ_1^a differential cross section at $Q = 80$ GeV and $\tau_1^a = 0.1$. Colored bands show theoretical uncertainties around central values at fixed-order α_s (dotted, gray) and resummed to NLL (dashed, blue) and NNLL accuracy (solid, red).

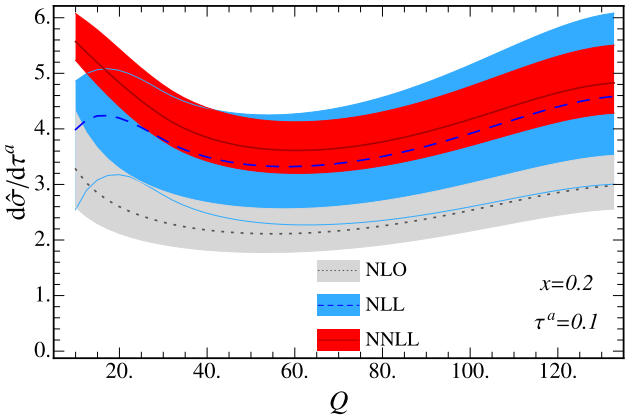

FIG. 10: Q dependence of τ_1^a differential cross section at $x = 0.2$ and $\tau_1^a = 0.1$, with theoretical uncertainties at fixed-order α_s (dotted, gray) and resummed to NLL (dashed, blue) and NNLL accuracy (solid, red)

We can characterize the $d\hat{\sigma}/d\tau_1^a$ cross section by three distinct physical regions: the peak region ($\tau_1^a \sim 2\Lambda_{\rm QCD}/Q$), the tail region ($2\Lambda_{\rm QCD}/Q \ll \tau_1^a \ll 1$), and the far-tail region ($\tau_1^a \sim \mathcal{O}(1)$). We will do this with four plots. We first show the purely perturbative cross section to study convergence and the impact of resummation compared to fixed order results. Next we show the impact of nonperturbative effects, which in the tail region produce a simple shift in the distribution, and have a significant impact on the shape of the spectrum in the peak region. We also illustrate the dependence of the cross section on x and Q^2 at fixed τ_1^a.

Fig. 7 shows the weighted differential cross section $\tau_1^a\, d\sigma/d\tau_1^a$ at $Q = 80$ GeV and $x = 0.2$. The results are weighted by τ_1^a for better visibility because the differential cross section falls very rapidly with τ_1^a. In the tail region, the overlap in resummed results shows a good perturbative convergence from NLL to NNLL. The large deviation between NLO and NNLL shows the large effect of resummation and the underestimated uncertainty of a pure fixed-order result. In the peak region, NLO result blows up as $(\ln \tau_1)/\tau_1$, while the NLL and NNLL results converge into a peak due to resummation of the large logs to all orders in α_s. Again the uncertainty bands overlap fairly well. In the far-tail region for larger τ_1, the resummation effect becomes small and the size of the deviation is reduced. Near the far-tail region ($\tau_1 \sim 0.3$), the NNLL curve begins to depart from the NLL band. In this region the nonlogarithmic α_s^2 term and nonsingular terms neglected in our NNLL result may begin to be significant.

Fig. 8 shows the differential cross section $d\sigma/d\tau_1$ at $Q = 80$ GeV and $x = 0.2$ in the peak region at fixed order and NNLL resummed accuracy. Note that it is not scaled by τ_1 as in Fig. 7. In this plot, the NNLL result convolved with a nonperturbative shape function (NNLL PT + NP) is shown in comparison with purely perturbative fixed-order NLO and resummed NNLL results (NLO PT and NNLL PT). As discussed in Sec. VII D we use the simplest shape function with one basis function $N = 0$ in Eq. (212) with a reasonable choice $\Omega_1 = 0.35$ GeV for the value of the first moment just to illustrate the impact of the nonperturbative effects. For practical analysis, a shape function with more basis functions should be used and the parameters c_i, λ in the model function Eq. (212) should be determined from experimental data. In the endpoint region, there is significant change from NLO and NNLL due to the resummation of large perturbative logs, and there is another large change from perturbative NNLL to the result convolved with the shape function due to nonperturbative effects. As we move into the tail region, the size of nonperturbative correction reduces to $\mathcal{O}(\Lambda_{\rm QCD}/\tau_1 Q)$ and the correction simplifies to the power correction in Eq. (213).

Fig. 9 shows the weighted differential cross section $x\, d\sigma/(dx\, dQ^2\, d\tau_1)$ as a function of x at $Q = 80$ GeV and $\tau_1^a = 0.1$. Note that the lower bound $x \geq Q^2/s$ is set by the relation $xys = Q^2$ in Eq. (9) and the constraint $y \leq 1$. The x dependence comes from the quark and anti-quark beam functions and the decreasing curves with increasing x are characteristic patterns of PDFs contained in the beam function. With decreasing x, NLO and NNLL curves rise faster than NLL curve because they contain the gluon PDF, which rises faster than the quark PDF, and whereas the NLL result only contains the tree-level beam function which is just the quark PDF.

Fig. 10 shows the Q dependence of the differential cross section at $x = 0.2$ and $\tau_1^a = 0.1$. Overall, Q dependence is mild. In the naive parton model the cross section is insensitive to Q because of the approximate scaling law in the Björken limit where $Q, s \to \infty$ with x fixed. This scaling is broken by logarithms of Q in QCD. It is also broken by the Z boson mass with the factors $1/(1 + m_Z^2/Q^2)$ in Eq. (158). As shown in the plot, well below $m_Z = 91.2$ GeV the curves vary gently in Q and near and above m_Z they increase due to the factor $Q^2/(Q^2 + m_Z^2)$.

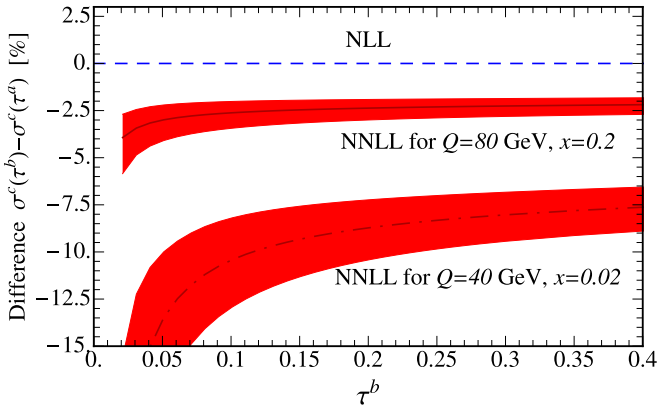

FIG. 11: Difference between τ_1^b and τ_1^a cumulant cross sections at $Q = 80$ GeV and $x = 0.2$ and at $Q = 40$ GeV and $x = 0.02$. The difference at NLL is zero for both parameter sets.

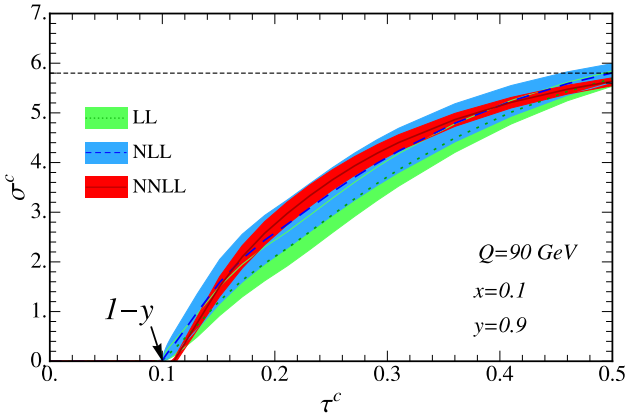

FIG. 12: τ_1^c cumulant cross section at $Q = 90$ GeV and $x = 0.1$, giving $y = 0.9$. Colored bands show theoretical uncertainties around central values for resummed results to LL (dotted, green), NLL (dashed, blue), and NNLL (solid, red) accuracy. The horizontal line is the total cross section. The arrow at $1 - y$ indicates the threshold in τ_1^c spectrum.

B. τ_1^b cross section

The τ_1^b cumulant cross section is different from τ_1^a by a single term at NLO in Eq. (185). The term contains $\ln z$ where z is integrated over from x to 1, and so the term becomes larger for smaller x. Fig. 11 shows their percent difference at NLL and NNLL for two sets of (Q, x): $(80, 0.2)$ and $(40, 0.02)$. The difference at NLL is zero because at LO fixed order τ_1^a and τ_1^b cross section are identical and the NLL logs are the same. At NNLL for $x = 0.2$ the size of difference is small, a few percent. The difference at the value $x = 0.02$ is larger than that for $x = 0.2$, becoming now a 10-15% effect. This difference is roughly constant in Q because of the mild Q dependence in Fig. 10.

C. τ_1^c cross section

The 1-jettiness τ_1^c is designed to measure a jet close to the z axis (incoming electron direction), and the factorization theorem for τ_1^c in Eq. (153) is valid for a jet with small transverse momentum $q_\perp^2 = (1-y)Q^2$. So, the parameters Q and x should be chosen such that $1 - y \ll 1$ in other words, $Q^2/(xs) \approx 1$. The parameters in Fig. 6 cannot be used because $y \approx 0.36$ for $Q = 80$ GeV and $x = 0.2$. For τ_1^c in Figs. 12 and 13 we choose $Q = 90$ GeV and $x = 0.1$ for which $y = 0.9$. Note that the profile functions for τ_1^c given in Eq. (206) are also different from those for $\tau_1^{a,b}$.

Fig. 12 shows the cumulant τ_1^c cross section resummed to LL, NLL, and NNLL accuracy. The most notable feature in the τ_1^c spectrum is the threshold $\theta(\tau_1^c - 1 + y)$ indicated by an arrow in the plot. The threshold is exactly respected in LL and NLL results and is effectively true at NNLL because, although Eq. (189b) contains terms violating this threshold at $\mathcal{O}(\alpha_s)$, their size is numerically small ($\sim 0.1\%$). In the region near this threshold nonperturbative corrections are quite important, and the purely perturbative cross section actually has a small negative dip (almost invisible in the plot).

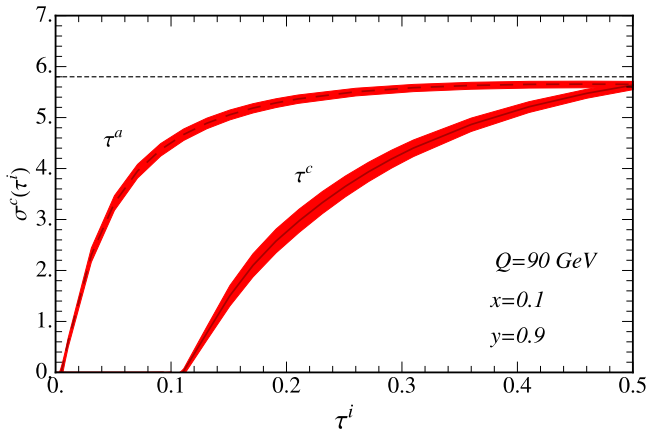

FIG. 13: Difference between τ_1^c cumulant cross sections in comparison to τ_1^a results at $Q = 90$ GeV and $x = 0.1$ which gives $y = 0.9$. The horizontal dashed line is the total cross section at this x, Q^2.

Fig. 13 shows τ_1^c in comparison with the τ_1^a cumulant cross section at NNLL. In addition to the threshold discussed in Fig. 12, the τ_1^c curve increases more slowly than the τ_1^a curve does. This is because the normalization of the τ_1^c axes in Eq. (42) are different from those for τ_1^a. The beam axis q_B for τ_1^c is larger than for τ_1^a by a factor of $1/x$ while the jet axis q_J is approximately the same in the limit $y \to 1$. This increases the projection of the particle momentum $q_B \cdot p_i$ by the factor of $1/x$ in 1-jettiness Eq. (24), but τ_1^c is not increased by quite the same factor because fewer particles are grouped into the $\mathcal{H}_B$ region due to the minimum in Eq. (24). Still, in Fig. 13 for the same value of the cross section the departure of τ_1^c from its threshold is larger than that of τ_1^a due to this factor.

IX. CONCLUSIONS

We have predicted 1-jettiness (τ_1) cross sections in DIS to NNLL accuracy in resummed perturbation theory, accurate for small τ_1 where hadrons produced in the final state are collimated into two jets, including one from ISR. We used three different versions of 1-jettiness, $\tau_1^{a,b,c}$, which group final-state hadrons into "beam" and "jet" regions differently and also have different sensitivity to the transverse momentum of ISR relative to the proton direction.

Each τ_1 is similar to thrust, measuring how closely final-state hadrons are collimated along "beam" and "jet" reference axes, but with important variations. τ_1^a measures the small light-cone momentum along two axes aligned with the proton direction and the actual jet direction, and averages over the transverse momentum of ISR in the calculation of the cross section. τ_1^b projects onto fixed axes such that the beam and jet regions are back-to-back hemispheres in the Breit frame. The fixed jet axis is not quite equal to the physical jet axis in the final state, causing τ_1^b to be sensitive to the transverse momentum $p_\perp$ of ISR and requiring a convolution over $p_\perp$ in the jet and beam functions in the τ_1^b factorization theorem. Finally τ_1^c groups final-state hadrons into back-to-back hemispheres in the CM frame, projecting momenta onto the initial proton and electron directions, and also requires a convolution over the transverse momenta of the ISR and final-state jets. Furthermore, the case of small τ_1^c also requires the DIS variable y to be near 1.

We proved factorization theorems for all three versions of τ_1 using the tools of SCET, carefully accounting for the differing dependences on the transverse momentum of ISR. These differences lead to the appearance of the ordinary beam function in the τ_1^a factorization theorem and the generalized $k_\perp$-dependent beam function in the τ_1^b and τ_1^c factorization theorems. We were able to relate the soft function appearing in any of these factorization theorems in any reference frame to the ordinary DIS hemisphere soft function by suitable rescaling of the arguments, using boost invariance.

The hard, jet, beam, and soft functions appearing in all the factorization theorems and their anomalous dimensions are known to sufficiently high order to allow us to immediately achieve NNLL resummed accuracy in our predictions for the $\tau_1^{a,b,c}$ cross sections. We gave predictions for the differential and cumulant τ_1 cross sections, illustrating the differences among $\tau_1^{a,b,c}$ due to the different dependences on the transverse momentum of ISR. We presented numerical predictions at x and Q^2 values explored at the HERA collider, but our analytical predictions can easily be applied to a much wider range of kinematics relevant at other experiments, such as at JLab [77] and the future EIC [78] and LHeC [79].

The resummed predictions we presented are accurate for small values of τ_1 where final-state hadrons are well collimated into two jets. For large τ_1 our predictions have to be matched onto fixed-order predictions of nonsingular terms in τ_1 from full QCD. We leave the performance of this matching at $\mathcal{O}(\alpha_s)$ and beyond to future work. However, we compared our cumulant τ_1 cross sections for large τ_1 to the known total cross section at fixed x and Q^2, and found that the cumulative effect of the matching corrections on the whole cross section is roughly at the several percent level for the kinematics we considered.

We showed how to incorporate nonperturbative hadronization corrections into our predictions by inclusion of a shape function that is convolved together with the perturbative soft function. The first moment of the shape function gives the parameter Ω_1 which describes the shift to the distribution in the tail region. We demonstrated that this parameter is universal for our three event shapes $\tau_1^{a,b,c}$ and for any values of x, Q^2, and so it can be extracted from one set of data to predict others. We also made a simple illustration of the effects of a shape function numerically on the cross section. We leave a more extensive study of nonperturbative effects and extractions of the model parameters from data to future work.

The extension of our results to N-jettiness τ_N in DIS with $N > 1$ is straightforward, at least if we define τ_N similarly to the 1-jettiness τ_1^a that we defined in Eq. (29). That is,

$$\tau_N^a = \frac{2}{Q^2} \sum_{i \in X} \min\{q_B^a \cdot p_i, q_1^a \cdot p_i, \ldots, q_N^a \cdot p_i\}\,, \qquad (225)$$

where $q_B^a = xP$ and q_i^a is the jet axis of the ith non-ISR jet in the final state as given by a jet algorithm or by minimization of the sum Eq. (225) over the directions of $q_1^a, \ldots, q_N^a$. As long as these jet reference axes are aligned with the physical jet axes, the transverse momentum $k_\perp$ of ISR will not affect the value of τ_N^a at leading order in λ. The factorization theorem will then look like Eq. (148), with suitable generalizations of the hard and soft functions and additional jet functions (cf. [27]):

$$\begin{aligned}\frac{d\sigma}{dx\,dQ^2\,d\tau_N^a} &= \frac{d\sigma_0}{dx\,dQ^2} \int dt_J^1 \cdots dt_J^N\, dt_B\, dk_S \qquad (226)\\ &\quad\times \delta\Big(\tau_N^a - \frac{t_B + t_J^1 + \cdots + t_J^N}{Q^2} - \frac{k_S}{Q}\Big)\\ &\quad\times \sum_{i,\kappa} B_i(t_B, x, \mu) J_{\kappa_1}(t_J^1, \mu) \cdots J_{\kappa_N}(t_J^N, \mu)\\ &\quad\times \mathrm{tr}\, \widehat{H}_{i\to\kappa}(\{q_m\}, L, \mu) \widehat{S}_N^{i\to\kappa}(k_S, \{q_m\}, \mu)\,,\end{aligned}$$

where $\widehat{H}_{i\to\kappa}(\{q_m\}, L, \mu)$ contains the underlying hard interaction $i(q_B)e(k) \to e(k')\kappa_1(q_1)\cdots\kappa_N(q_N)$, where i, κ_j denote parton types, L denotes the dependence on the leptonic states $e(k), e(k')$ and the exchanged virtual boson, and the sum over i, κ is over all relevant partonic channels. The hard and soft functions $\widehat{H}, \widehat{S}$ are matrices in color space, and the trace is over these colors. B_i is the ordinary beam function for the initial-state parton

of flavor i. Since Eq. (225) uses reference axes q_j^a that are aligned with the physical jet axes, the arguments t_J^j of the jet functions are the invariant masses of the jets and are not shifted by any transverse momentum $k_\perp$ of ISR. Thus only the ordinary beam function B_i appears in Eq. (226), $k_\perp$ having been averaged over. We leave the explicit evaluation of Eq. (226) for N-jettiness cross sections in DIS with $N > 1$ to future work.

Our results bring to the arena of DIS the power of SCET that has already vastly improved the precision of theoretical predictions of event shapes in e^+e^- collisions and pp collisions. The factorization theorems derived here point the way to methods to improve the precision of parton distributions, hadron structure, and the strong coupling α_s that we can extract from existing and future experiments. With further advances in our calculations to greater perturbative accuracy and improved modeling of the nonperturbative effects, the frontiers of the study of the strong interaction using jets in DIS can be pushed to higher precision.

Note Added: While this paper was being finalized, Ref. [111] appeared which also considers the event shape we call τ_1^a at NNLL order. A complete derivation of the factorization theorem was not presented there, where the focus is instead the use of 1-jettiness to probe nuclear PDFs and power corrections from dynamical effects in the nuclear medium.

Acknowledgments

CL is grateful to the MIT Center for Theoretical Physics for hospitality during the course of this work. The work of DK and IS is supported by the Office of Nuclear Physics of the U.S. Department of Energy under Contract DE-FG02-94ER40818, and the work of CL by DOE Contract DE-AC52-06NA25396 and by the LDRD office at Los Alamos.

Appendix A: Generalized Rapidity Gap ΔY

The 1-jettiness τ_1 in Eq. (48) is just one possible combination of jet and beam momenta that we can choose to measure in DIS. It is quite straightforward to keep $n_J\cdot p_J, n_B\cdot p_B$ as independent observables in the factorization theorem Eq. (135), and then to form other observables by taking different combinations of $n_J\cdot p_J, n_B\cdot p_B$. In this Appendix we consider one of these possibilities—the *generalized rapidity gap* ΔY between the beam jet and the other final-state jet.

The rapidity of a particle with momentum p with respect to the z-axis is given by

$$Y_{n_z\bar n_z}(p) = \frac{1}{2}\ln\frac{\bar n_z\cdot p}{n_z\cdot p}. \tag{A1}$$

If p is n_z-collinear, the rapidity $Y_{n_z\,\bar n_z}$ is large and positive, while it is large and negative if p is $\bar n_z$-collinear. Two jets produced in DIS are not, in general, back-to back, and the reference vectors that measure jets are not always aligned along one (z) axis, as Fig. 3 illustrates. The rapidity in Eq. (A1) can be generalized by replacing $n_{z,\bar z}$ with n_B and n_J as follows:

$$Y_{n_Jn_B}(p) = \frac{1}{2}\ln\frac{n_B\cdot p}{n_J\cdot p}, \tag{A2}$$

where $Y_{n_Jn_B}$ is large and positive for the n_J-collinear jet and is large and negative for the n_B-collinear jet. The generalized rapidity difference between two jets of momenta p_J and p_B is given by

$$\Delta Y \equiv Y_{n_Jn_B}(p_J) - Y_{n_Jn_B}(p_B) = \frac{1}{2}\ln\frac{n_B\cdot p_J}{n_J\cdot p_J}\frac{n_J\cdot p_B}{n_B\cdot p_B}. \tag{A3}$$

The $n_{B,J}$ in Eq. (A3) can be replaced by $q_{B,J}$ because the energy factors $\omega_{J,B}/2$ in the numerator and denominator cancel. By using Eq. (27) $q_{B,J}\cdot p_{B,J}$ can be expressed in terms of $\tau_{B,J}$. So, Eq. (A3) can be rewritten as

$$\Delta Y = \frac{1}{2}\ln\frac{4\,q_J\cdot p_B\,q_B\cdot p_J}{\tau_J\,\tau_B Q^4}\,, \tag{A4}$$

where the products $2\,q_J\cdot p_B$ and $2\,q_B\cdot p_J$ are $\mathcal{O}(Q^2)$ and ΔY is $\mathcal{O}\left[\ln(1/\sqrt{\tau_J\tau_B})\right] \sim \mathcal{O}\left[\ln(1/\lambda^2)\right]$. Eq. (A4) can be specified for DIS by using $q_J\cdot p_B \approx q_J\cdot(P+q)$ and $q_B\cdot p_J \approx q_B\cdot q$ where we use momentum conservation $P+q = p_B+p_J$ and suppress p_B^2 and p_J^2. As we have three versions of τ_1, there are three versions of ΔY:

$$\Delta Y^{a,b} = \frac{1}{2}\ln\frac{1-x}{x\tau_J\tau_B}\,,\quad \Delta Y^c = \frac{1}{2}\ln\frac{1-x}{x^2\tau_J\tau_B}\,. \tag{A5}$$

Appendix B: Tensors and contractions

The symmetric and asymmetric tensors transverse to both n_B and n_J are defined by

$$\begin{aligned} g_\perp^{\mu\nu} &= g^{\mu\nu} - \frac{n_J^\mu n_B^\nu + n_J^\nu n_B^\mu}{n_J\cdot n_B}\,, \qquad\qquad (\text{B1a})\\ &= g^{\mu\nu} - \frac{n_J^\mu \bar n_J^\nu + n_J^\nu \bar n_J^\mu}{2} = g^{\mu\nu} - \frac{n_B^\mu \bar n_B^\nu + n_B^\nu \bar n_B^\mu}{2}\,,\\ \epsilon_{\mu\nu}^\perp &= \frac{1}{n_J\cdot n_B}\epsilon_{\mu\nu\alpha\beta}n_J^\alpha n_B^\beta\,, \qquad\qquad (\text{B1b})\\ &= \frac{1}{2}\epsilon_{\mu\nu\alpha\beta}n_J^\alpha \bar n_J^\beta = \frac{1}{2}\epsilon_{\mu\nu\alpha\beta}\bar n_B^\alpha n_B^\beta\,, \end{aligned}$$

where $\bar n_B$ and $\bar n_J$ are conjugate to n_B and n_J as defined in Eq. (51) .

In order to calculate the contraction of the lepton tensor $L^{\mu\nu}$ with the hard function $H_{q\bar q\,\mu\nu}^{II'}$ as in Eq. (136), we must compute two tensor contractions: $g_{\mu\nu}^T g_\perp^{\mu\nu}$ and $\epsilon_{\mu\nu}^T\epsilon_\perp^{\mu\nu}$, where g^T, ϵ^T are defined in Eq. (85) and $g_\perp, \epsilon_\perp$ in Eq. (B1). These contractions are given by

$$\begin{aligned} g_{\mu\nu}^T g_\perp^{\mu\nu} &= \Big(g^{\mu\nu} - 2\frac{k^\mu k'^\nu + k^\nu k'^\mu}{Q^2}\Big)\Big(g^{\mu\nu} - \frac{n_J^\mu n_B^\nu + n_B^\nu n_J^\mu}{n_J\cdot n_B}\Big)\,,\\ &= \frac{4}{n_J\cdot n_B\,Q^2}(n_J\cdot k n_B\cdot k' + n_J\cdot k' n_B\cdot k). \qquad (\text{B2}) \end{aligned}$$

and

$$\epsilon_{\mu\nu}^T \epsilon_\perp^{\mu\nu} = \frac{2}{n_J\cdot n_B\, Q^2}\epsilon_{\alpha\beta\mu\nu}\epsilon_{\gamma\delta}^{\mu\nu} k^\alpha k'^\beta n_J^\gamma n_B^\delta\,, \\ = \frac{4}{n_J\cdot n_B\, Q^2}(n_J\cdot k'\, n_B\cdot k - n_J\cdot k\, n_B\cdot k')\,. \quad \text{(B3)}$$

The ratio Eq. (B2) over Eq. (B3) is the coefficient $r(q_J, q_B)$ defined in Eq. (139).

Appendix C: Plus distribution

The standard plus distribution for some function $q(x)$ is given by

$$\big[q(x)\big]_+ = \lim_{\epsilon\to 0}\frac{\mathrm{d}}{\mathrm{d}x}\big[\theta(x-\epsilon)\,Q(x)\big]\,, \\ = \lim_{\epsilon\to 0}\big[\theta(x-\epsilon)\,q(x) + \delta(x-\epsilon)\,Q(x)\big]\,, \quad \text{(C1)}$$

where

$$Q(x) = \int_1^x dx' q(x')\,. \quad \text{(C2)}$$

Integrating against a test function $f(x)$, we have

$$\int_{-\infty}^{x_{\max}} dx[\theta(x)\,q(x)]_+ f(x)\,, \\ = \int_0^{x_{\max}} dx\, q(x)\,[f(x)-f(0)] + f(0)\,Q(x_{\max})\,, \quad \text{(C3)}$$

for $x_{\max} > 0$.

For the special cases $q(x) = 1/x^{1-a}$ with $a > -1$ and $q(x) = \ln^n x/x$ with integer $n \geq 0$, we define:

$$\mathcal{L}^a(x) = \left[\frac{\theta(x)}{x^{1-a}}\right]_+\,, \quad \text{(C4)}$$

$$\mathcal{L}_n(x) = \left[\frac{\theta(x)\ln^n x}{x}\right]_+\,, \qquad n\geq 0\,. \quad \text{(C5)}$$

For convenience we also define

$$\mathcal{L}_{-1}(x) \equiv \delta(x)\,. \quad \text{(C6)}$$

The plus function $\mathcal{L}_n$ obeys the rescaling relation,

$$\lambda\,\mathcal{L}_n(\lambda x) = \sum_{k=0}^n \binom{n}{k}\ln^k\lambda\,\mathcal{L}_{n-k}(x) + \frac{\ln^{n+1}\lambda}{n+1}\,\delta(x), \quad \text{(C7)}$$

where $\lambda > 0$.

Appendix D: Renormalization Group Evolution

In this appendix we collect results relevant for resummation of the DIS 1-jettiness cross section Eq. (140) and its special cases Eqs. (147), (142), and (153) for $\tau_1^{a,b,c}$.

The RGE and anomalous dimension for the hard Wilson coefficient C in Eq. (154) for the two-quark operator are [36, 91]

$$\mu\frac{\mathrm{d}}{\mathrm{d}\mu}C(q^2,\mu) = \gamma_C^q(q^2,\mu)\,C(q^2,\mu)\,, \\ \gamma_C^q(q^2,\mu) = \Gamma^q_{\rm cusp}(\alpha_s)\ln\frac{-q^2}{\mu^2} + \gamma_C^q(\alpha_s)\,. \quad \text{(D1)}$$

The anomalous dimension for the hard function H in Eq. (155) is given by

$$\mu\frac{\mathrm{d}}{\mathrm{d}\mu}H(Q^2,\mu) = \gamma_H(Q^2,\mu)\,H(Q^2,\mu)\,, \\ \gamma_H(Q^2,\mu) = 2\Gamma^q_{\rm cusp}(\alpha_s)\ln\frac{Q^2}{\mu^2} + \gamma_H(\alpha_s)\,, \quad \text{(D2)}$$

where $\gamma_H = 2\gamma_C^q$. The expansions in α_s of $\Gamma^q_{\rm cusp}(\alpha_s)$ and $\gamma_C^q(\alpha_s)$ are given below in Eqs. (D28) and (D29).

The solution of the RGE in Eq. (D1) yields for the RG evolved hard function:

$$H(Q^2,\mu) = H(Q^2,\mu_0)\,U_H(Q^2,\mu_0,\mu)\,, \\ U_H(Q^2,\mu_0,\mu) = e^{K_H(\mu_0,\mu)}\Big(\frac{Q}{\mu_0}\Big)^{\eta_H(\mu_0,\mu)}\,, \\ K_H(\mu_0,\mu) = -4K_{\Gamma^q}(\mu_0,\mu) + K_{\gamma_H}(\mu_0,\mu)\,, \\ \eta_H(\mu_0,\mu) = 4\eta_{\Gamma^q}(\mu_0,\mu)\,, \quad \text{(D3)}$$

where the functions $K_{\Gamma^q}(\mu_0,\mu)$, $\eta_{\Gamma^q}(\mu_0,\mu)$ and K_γ are given below in Eqs. (D24) and (D26).

The quark beam function RGE is given by

$$\mu\frac{\mathrm{d}}{\mathrm{d}\mu}B_q(t,x,\mu) = \int \mathrm{d}t'\,\gamma_B^q(t-t',\mu)\,B_q(t',x,\mu)\,, \quad \text{(D4)}$$

$$\gamma_B^q(t,\mu) = -2\Gamma^q_{\rm cusp}(\alpha_s)\,\frac{1}{\mu^2}\mathcal{L}_0\Big(\frac{t}{\mu^2}\Big) + \gamma_B^q(\alpha_s)\,\delta(t)\,,$$

and its solution is [76, 99, 112, 113]

$$B_q(t,x,\mu) = \int \mathrm{d}t'\,B_q(t-t',x,\mu_0)\,U_{B_q}(t',\mu_0,\mu)\,, \\ U_{B_q}(t,\mu_0,\mu) = \frac{e^{K_{B_q}-\gamma_E\,\eta_{B_q}}}{\Gamma(1+\eta_{B_q})}\left[\frac{\eta_{B_q}}{\mu_0^2}\mathcal{L}^{\eta_{B_q}}\Big(\frac{t}{\mu_0^2}\Big) + \delta(t)\right], \\ K_{B_q}(\mu_0,\mu) = 4K_{\Gamma^q}(\mu_0,\mu) + K_{\gamma_B^q}(\mu_0,\mu)\,, \\ \eta_{B_q}(\mu_0,\mu) = -2\eta_{\Gamma^q}(\mu_0,\mu)\,. \quad \text{(D5)}$$

The solution of the RGE for B_q given by Eq. (D5) can be derived from the form of the solution Eq. (D3) for the hard function by first Laplace transforming the beam function:

$$\widetilde{B}_q(\nu,x,\mu) = \int_0^\infty dt\, e^{-\nu t}B_q(t,x,\mu)\,, \quad \text{(D6)}$$

which obeys the RGE

$$\mu\frac{d}{d\mu}\widetilde{B}_q(\nu,x,\mu) = \tilde{\gamma}_{B_q}(\nu,\mu)\widetilde{B}_q(\nu,x,\mu)\,, \quad \text{(D7)}$$

with the Laplace transformed anomalous dimension,

$$\tilde{\gamma}_B^q(\nu,\mu) = 2\Gamma^q_{\rm cusp}(\alpha_s)\ln(\mu^2\nu e^{\gamma_E}) + \gamma_B^q(\alpha_s)\,. \tag{D8}$$

The evolution of $\widetilde{B}_q$ in Eq. (D7) is multiplicative, of the same form as the hard function RGE Eq. (D2), and therefore its solution is just like the hard function Eq. (D3), given by

$$\widetilde{B}_q(\nu,x,\mu) = \widetilde{B}_q(\nu,x,\mu_0)\widetilde{U}_{B_q}(\nu,\mu_0,\mu)\,, \tag{D9}$$

where

$$\widetilde{U}_{B_q}(\nu,\mu_0,\mu) = e^{K_{B_q}(\mu_0,\mu)}(\mu_0^2\nu e^{\gamma_E})^{-\eta_{B_q}(\mu_0,\mu)}\,, \tag{D10}$$

with K_{B_q}, η_{B_q} given by the same expressions as in Eq. (D5). The inverse Laplace transform of the solution Eq. (D9) gives the momentum space solution for $B_q(t,x,\mu)$ in Eq. (D5).

The jet function obeys the same RGE as the beam function. They are defined by matrix elements of the same operator. The solution for the Laplace transformed jet function $\widetilde{J}_q(\nu,\mu)$ is given by the same form, Eqs. (D9) and (D10) with $B \to J$, and for the momentum-space jet function $J_q(t,\mu)$ by the same form Eq. (D5), with $B \to J$.

The hemisphere soft function in Eq. (160) obeys the RGE

$$\mu\frac{\rm d}{{\rm d}\mu}S_{\rm hemi}(k_J,k_B,\mu) = \int dk'_J dk'_B \times \gamma_S(k_J-k'_J,k_B-k'_B,\mu)S_{\rm hemi}(k'_J,k'_B,\mu)\,, \tag{D11}$$

where the dependence of the anomalous dimension on the two variables separates [108]:

$$\gamma_S(k_J,k_B,\mu) = \gamma_S(k_J,\mu)\delta(k_B) + \gamma_S(k_B,\mu)\delta(k_J)\,, \tag{D12}$$

with each piece of the anomalous dimension taking the form

$$\gamma_S(k,\mu) = 2\Gamma^q_{\rm cusp}(\alpha_s)\frac{1}{\mu}\mathcal{L}_0\Big(\frac{k}{\mu}\Big) + \gamma_S(\alpha_s)\delta(k)\,, \tag{D13}$$

where $\gamma_S = -\gamma_C^q - \gamma_B^q$. The solution to the soft RGE Eq. (D11) is given by

$$S_{\rm hemi}(k_J,k_B,\mu) = \int dk'_J dk'_B S_{\rm hemi}(k'_J,k'_B,\mu_0) \times U_S(k_J-k'_J,\mu_0,\mu)U_S(k_B-k'_B,\mu_0,\mu) \tag{D14}$$

where

$$\begin{aligned} U_S(k,\mu_0,\mu) &= \frac{e^{K_S-\gamma_E\,\eta_S}}{\Gamma(1+\eta_S)}\left[\frac{\eta_S}{\mu_0}\mathcal{L}^{\eta_S}\Big(\frac{k}{\mu_0}\Big) + \delta(k)\right], \\ K_S(\mu_0,\mu) &= -2K_{\Gamma^q}(\mu_0,\mu) + K_{\gamma_S}(\mu_0,\mu)\,, \\ \eta_S(\mu_0,\mu) &= 2\eta_{\Gamma^q}(\mu_0,\mu)\,. \end{aligned} \tag{D15}$$

This solution can be derived as for the beam and jet functions above by first taking the Laplace transform:

$$\widetilde{S}_{\rm hemi}(\nu_J,\nu_B,\mu) = \int_0^\infty dk_J \int_0^\infty dk_B\, e^{-\nu_J k_J - \nu_B k_B} S_{\rm hemi}(k_J,k_B,\mu)\,, \tag{D16}$$

which obeys the RGE

$$\mu\frac{d}{d\mu}\widetilde{S}_{\rm hemi}(\nu_J,\nu_B,\mu) = \widetilde{S}_{\rm hemi}(\nu_J,\nu_B,\mu) \times \left[\tilde{\gamma}_S(\nu_J,\mu) + \tilde{\gamma}_S(\nu_B,\mu)\right], \tag{D17}$$

where each part of the anomalous dimension takes the form

$$\tilde{\gamma}_S(\nu,\mu) = -2\Gamma^q_{\rm cusp}\ln(\mu\nu e^{\gamma_E}) + \gamma_S(\alpha_s)\,. \tag{D18}$$

Solving the soft RGE Eq. (D17), we obtain

$$\widetilde{S}_{\rm hemi}(\nu_J,\nu_B,\mu) = \widetilde{S}_{\rm hemi}(\nu_J,\nu_B,\mu_0) \times \widetilde{U}_S(\nu_J,\mu_0,\mu)\widetilde{U}_S(\nu_B,\mu_0,\mu)\,, \tag{D19}$$

where each soft evolution factor takes the form

$$\widetilde{U}_S(\nu,\mu_0,\mu) = e^{K_S(\mu_0,\mu)}(\mu_0\nu e^{\gamma_E})^{-\eta_S(\mu_0,\mu)}\,, \tag{D20}$$

where K_S, η_S are given by Eq. (D15). Taking the inverse Laplace transform of Eq. (D19) gives the solution to the RGE for the soft function in momentum space $S_{\rm hemi}(k_J,k_B,\mu)$ given in Eqs. (D14) and (D15).

In the 1-jettiness cross sections in this paper, we always encounter the soft function Eq. (D14) projected onto a function of a single variable k, according to Eq. (134). It obeys the RGE

$$\mu\frac{d}{d\mu}S_{\rm hemi}(k,\mu) = \int dk'\, 2\gamma_S(k-k',\mu)S_{\rm hemi}(k',\mu), \tag{D21}$$

where $\gamma_S(k,\mu)$ is given by Eq. (D13). In Laplace space,

$$\mu\frac{d}{d\mu}\widetilde{S}_{\rm hemi}(\nu,\mu) = 2\tilde{\gamma}_S(\nu,\mu)\widetilde{S}_{\rm hemi}(\nu,\mu)\,. \tag{D22}$$

The solutions to these RGEs are given by

$$S_{\rm hemi}(k,\mu) = \int dk' S_{\rm hemi}(k',\mu_0)U_S^2(k-k',\mu_0,\mu) \tag{D23a}$$

$$\widetilde{S}_{\rm hemi}(\nu,\mu) = \widetilde{S}_{\rm hemi}(\nu,\mu_0)\widetilde{U}_S(\nu,\mu_0,\mu)^2\,, \tag{D23b}$$

where $U_S^2(k,\mu_0,\mu)$ is given by Eq. (D15) with $K_S, \eta_S \to 2K_S, 2\eta_S$, and $\widetilde{U}_S(\nu,\mu_0,\mu)$ is given by Eq. (D20).

The functions $K_{\Gamma^q}(\mu_0,\mu)$, $\eta_{\Gamma^q}(\mu_0,\mu)$, $K_\gamma(\mu_0,\mu)$ in the above RGE solutions are defined as

$$\begin{aligned} K_{\Gamma^q}(\mu_0,\mu) &= \int_{\alpha_s(\mu_0)}^{\alpha_s(\mu)}\frac{{\rm d}\alpha_s}{\beta(\alpha_s)}\,\Gamma^q_{\rm cusp}(\alpha_s)\int_{\alpha_s(\mu_0)}^{\alpha_s}\frac{{\rm d}\alpha'_s}{\beta(\alpha'_s)}\,, \\ \eta_{\Gamma^q}(\mu_0,\mu) &= \int_{\alpha_s(\mu_0)}^{\alpha_s(\mu)}\frac{{\rm d}\alpha_s}{\beta(\alpha_s)}\,\Gamma^q_{\rm cusp}(\alpha_s)\,, \\ K_\gamma(\mu_0,\mu) &= \int_{\alpha_s(\mu_0)}^{\alpha_s(\mu)}\frac{{\rm d}\alpha_s}{\beta(\alpha_s)}\,\gamma(\alpha_s)\,. \end{aligned} \tag{D24}$$

Expanding the beta function and anomalous dimensions in powers of α_s,

$$\beta(\alpha_s) = -2\alpha_s\sum_{n=0}^\infty \beta_n\Big(\frac{\alpha_s}{4\pi}\Big)^{n+1}\,, \tag{D25}$$

$$\Gamma^q_{\rm cusp}(\alpha_s) = \sum_{n=0}^\infty \Gamma^q_n\Big(\frac{\alpha_s}{4\pi}\Big)^{n+1},\ \gamma(\alpha_s) = \sum_{n=0}^\infty \gamma_n\Big(\frac{\alpha_s}{4\pi}\Big)^{n+1},$$

their explicit expressions to NNLL accuracy are (suppressing the superscript q on Γ^q),

$$
\begin{aligned}
K_\Gamma(\mu_0,\mu) &= -\frac{\Gamma_0}{4\beta_0^2}\biggl\{\frac{4\pi}{\alpha_s(\mu_0)}\Bigl(1-\frac{1}{r}-\ln r\Bigr)+\Bigl(\frac{\Gamma_1}{\Gamma_0}-\frac{\beta_1}{\beta_0}\Bigr)(1-r+\ln r)+\frac{\beta_1}{2\beta_0}\ln^2 r \\
&\quad+\frac{\alpha_s(\mu_0)}{4\pi}\biggl[\Bigl(\frac{\beta_1^2}{\beta_0^2}-\frac{\beta_2}{\beta_0}\Bigr)\Bigl(\frac{1-r^2}{2}+\ln r\Bigr)+\Bigl(\frac{\beta_1\Gamma_1}{\beta_0\Gamma_0}-\frac{\beta_1^2}{\beta_0^2}\Bigr)(1-r+r\ln r)-\Bigl(\frac{\Gamma_2}{\Gamma_0}-\frac{\beta_1\Gamma_1}{\beta_0\Gamma_0}\Bigr)\frac{(1-r)^2}{2}\biggr]\biggr\}, \\
\eta_\Gamma(\mu_0,\mu) &= -\frac{\Gamma_0}{2\beta_0}\biggl[\ln r+\frac{\alpha_s(\mu_0)}{4\pi}\Bigl(\frac{\Gamma_1}{\Gamma_0}-\frac{\beta_1}{\beta_0}\Bigr)(r-1)+\frac{\alpha_s^2(\mu_0)}{16\pi^2}\Bigl(\frac{\Gamma_2}{\Gamma_0}-\frac{\beta_1\Gamma_1}{\beta_0\Gamma_0}+\frac{\beta_1^2}{\beta_0^2}-\frac{\beta_2}{\beta_0}\Bigr)\frac{r^2-1}{2}\biggr], \\
K_\gamma(\mu_0,\mu) &= -\frac{\gamma_0}{2\beta_0}\biggl[\ln r+\frac{\alpha_s(\mu_0)}{4\pi}\Bigl(\frac{\gamma_1}{\gamma_0}-\frac{\beta_1}{\beta_0}\Bigr)(r-1)\biggr].
\end{aligned}
\tag{D26}
$$

Here, $r=\alpha_s(\mu)/\alpha_s(\mu_0)$ and the running coupling is given to three-loop order by the expression

$$
\frac{1}{\alpha_s(\mu)}=\frac{X}{\alpha_s(\mu_0)}+\frac{\beta_1}{4\pi\beta_0}\ln X+\frac{\alpha_s(\mu_0)}{16\pi^2}\biggl[\frac{\beta_2}{\beta_0}\Bigl(1-\frac{1}{X}\Bigr)+\frac{\beta_1^2}{\beta_0^2}\Bigl(\frac{\ln X}{X}+\frac{1}{X}-1\Bigr)\biggr],
\tag{D27}
$$

where $X\equiv 1+\alpha_s(\mu_0)\beta_0\ln(\mu/\mu_0)/(2\pi)$. In our numerical analysis we use the full NNLL expressions for $K_{\Gamma,\gamma},\eta_\Gamma$ in Eq. (D26), but to be consistent with the value of $\alpha_s(\mu)$ used in the NLO PDFs we only use the two-loop truncation of Eq. (D27), dropping the β_2 and β_1^2 terms, to obtain numerical values for $\alpha_s(\mu)$. (The numerical difference between using the two-loop and three-loop α_s is numerically very small and well within our theory uncertainties.) Up to three loops, the coefficients of the beta function [114, 115] and cusp anomalous dimension [116, 117] in $\overline{\rm MS}$ are

$$
\begin{aligned}
\beta_0 &= \frac{11}{3}\,C_A-\frac{4}{3}\,T_F\,n_f\,, \\
\beta_1 &= \frac{34}{3}\,C_A^2-\Bigl(\frac{20}{3}\,C_A+4C_F\Bigr)\,T_F\,n_f\,, \\
\beta_2 &= \frac{2857}{54}\,C_A^3+\Bigl(C_F^2-\frac{205}{18}\,C_FC_A-\frac{1415}{54}\,C_A^2\Bigr)\,2T_F\,n_f+\Bigl(\frac{11}{9}\,C_F+\frac{79}{54}\,C_A\Bigr)\,4T_F^2\,n_f^2\,, \\
\Gamma_0^q &= 4C_F\,, \\
\Gamma_1^q &= 4C_F\Bigl[\Bigl(\frac{67}{9}-\frac{\pi^2}{3}\Bigr)\,C_A-\frac{20}{9}\,T_F\,n_f\Bigr]\,, \\
\Gamma_2^q &= 4C_F\Bigl[\Bigl(\frac{245}{6}-\frac{134\pi^2}{27}+\frac{11\pi^4}{45}+\frac{22\zeta_3}{3}\Bigr)C_A^2+\Bigl(-\frac{418}{27}+\frac{40\pi^2}{27}-\frac{56\zeta_3}{3}\Bigr)C_A\,T_F\,n_f \\
&\quad+\Bigl(-\frac{55}{3}+16\zeta_3\Bigr)C_F\,T_F\,n_f-\frac{16}{27}\,T_F^2\,n_f^2\Bigr]\,.
\end{aligned}
\tag{D28}
$$

The $\overline{\rm MS}$ non-cusp anomalous dimension $\gamma_H=2\gamma_C^q$ for the hard function H can be obtained [38, 118] from the IR divergences of the on-shell massless quark form factor $C(q^2,\mu)$ which are known to three loops [119],

$$
\begin{aligned}
\gamma_{C\,0}^q &= -6C_F\,, \\
\gamma_{C\,1}^q &= -C_F\Bigl[\Bigl(\frac{82}{9}-52\zeta_3\Bigr)C_A+(3-4\pi^2+48\zeta_3)C_F+\Bigl(\frac{65}{9}+\pi^2\Bigr)\beta_0\Bigr]\,, \\
\gamma_{C\,2}^q &= -2C_F\Bigl[\Bigl(\frac{66167}{324}-\frac{686\pi^2}{81}-\frac{302\pi^4}{135}-\frac{782\zeta_3}{9}+\frac{44\pi^2\zeta_3}{9}+136\zeta_5\Bigr)C_A^2 \\
&\quad+\Bigl(\frac{151}{4}-\frac{205\pi^2}{9}-\frac{247\pi^4}{135}+\frac{844\zeta_3}{3}+\frac{8\pi^2\zeta_3}{3}+120\zeta_5\Bigr)C_FC_A \\
&\quad+\Bigl(\frac{29}{2}+3\pi^2+\frac{8\pi^4}{5}+68\zeta_3-\frac{16\pi^2\zeta_3}{3}-240\zeta_5\Bigr)C_F^2+\Bigl(-\frac{10781}{108}+\frac{446\pi^2}{81}+\frac{449\pi^4}{270}-\frac{1166\zeta_3}{9}\Bigr)C_A\beta_0 \\
&\quad+\Bigl(\frac{2953}{108}-\frac{13\pi^2}{18}-\frac{7\pi^4}{27}+\frac{128\zeta_3}{9}\Bigr)\beta_1+\Bigl(-\frac{2417}{324}+\frac{5\pi^2}{6}+\frac{2\zeta_3}{3}\Bigr)\beta_0^2\Bigr]\,.
\end{aligned}
\tag{D29}
$$

As shown in [107], the anomalous dimension for the beam function equals that of the jet function, $\gamma_B^q=\gamma_J^q$, so the

non-cusp three-loop anomalous dimension for the jet and beam functions are both given by [38],

$$\begin{aligned}
\gamma^q_{B\,0} &= \gamma^q_{J\,0} = 6C_F\,,\\
\gamma^q_{B\,1} &= \gamma^q_{J\,1} = C_F\Big[\Big(\frac{146}{9} - 80\zeta_3\Big)C_A + (3 - 4\pi^2 + 48\zeta_3)C_F + \Big(\frac{121}{9} + \frac{2\pi^2}{3}\Big)\beta_0\Big]\,,\\
\gamma^q_{B\,2} &= \gamma^q_{J\,2} = 2C_F\Big[\Big(\frac{52019}{162} - \frac{841\pi^2}{81} - \frac{82\pi^4}{27} - \frac{2056\zeta_3}{9} + \frac{88\pi^2\zeta_3}{9} + 232\zeta_5\Big)C_A^2\\
&\quad + \Big(\frac{151}{4} - \frac{205\pi^2}{9} - \frac{247\pi^4}{135} + \frac{844\zeta_3}{3} + \frac{8\pi^2\zeta_3}{3} + 120\zeta_5\Big)C_AC_F\\
&\quad + \Big(\frac{29}{2} + 3\pi^2 + \frac{8\pi^4}{5} + 68\zeta_3 - \frac{16\pi^2\zeta_3}{3} - 240\zeta_5\Big)C_F^2 + \Big(-\frac{7739}{54} + \frac{325}{81}\pi^2 + \frac{617\pi^4}{270} - \frac{1276\zeta_3}{9}\Big)C_A\beta_0\\
&\quad + \Big(-\frac{3457}{324} + \frac{5\pi^2}{9} + \frac{16\zeta_3}{3}\Big)\beta_0^2 + \Big(\frac{1166}{27} - \frac{8\pi^2}{9} - \frac{41\pi^4}{135} + \frac{52\zeta_3}{9}\Big)\beta_1\Big]\,.
\end{aligned} \tag{D30}$$

The anomalous dimension for the soft function is obtained from $\gamma_S = -\gamma^q_C - \gamma^q_B$. At NNLL, we only need the one- and two-loop coefficients of $\gamma_{H,B,J,S}$. The three-loop coefficients are given for completeness. They would be required at N^{3}LL, along with the four-loop beta function and cusp anomalous dimension, the latter of which has not yet been calculated. In addition, the full N^{3}LL result would also require the two-loop fixed-order corrections, which are known for the hard function, but not yet for the beam and soft functions.

Appendix E: Coefficients in Momentum-Space Resummed Cross Section

The resummed cross sections for $\tau_1^{a,b,c}$ in Sec. VII are obtained by plugging the solutions to the RG equations for the hard function and for the momentum-space jet, beam, and soft functions given in App. D into the factorization theorems derived in Sec. V D. Performing the convolutions in these factorization theorems of the jet, beam, and soft evolution kernels given in App. D and fixed-order functions requires computing the convolutions of plus functions with each other. The results of these convolutions produce the expressions given in Eqs. (185) and (188), given in terms of coefficients J_n, I_n, S_n of the logs in the fixed-order jet, beam, and soft functions and coefficients V_k^{mn} and $V_k^n(a)$ that are the result of the convolutions of plus functions. In this Appendix we tabulate these coefficients. For more details see Refs. [14, 76].

1. Jet, Beam, and Soft Coefficients J_n, $I_n^{qq,qg}$, S_n

The fixed-order results at $\mathcal{O}(\alpha_s)$ of soft, jet, and beam functions can be written as sum of plus distributions as

$$G(t,\mu) = \frac{1}{\mu^{n_G}} \sum_{n=-1}^{1} G_n[\alpha_s(\mu)]\,\mathcal{L}_n\left(\frac{t}{\mu^{n_G}}\right)\,. \tag{E1}$$

where $G(t,\mu)$ represents the single-variable soft function $S(t,\mu)$ in Eq. (210), jet function $J(t,\mu)$ in Eq. (163), or the coefficient $I^{qq,qg}(t,z,\mu)$ inside the beam function in Eq. (171). The index $n_F = 1$ for the soft function and $n_F = 2$ for the jet and beam function. In the case of the beam function, the z dependence in $F(t,\mu)$ is implicit. The coefficients F_n in Eq. (E1) for the three functions are S_n, J_n, and $I_n^{qq,qg}$. The soft coefficients at order α_s are given by

$$\begin{aligned}
S_{-1}(\alpha_s) &= 1 + \frac{\alpha_s C_F}{4\pi}\frac{\pi^2}{3}\,,\\
S_0(\alpha_s) &= 0\,, \quad S_1(\alpha_s) = \frac{\alpha_s C_F}{4\pi}(-16)\,,
\end{aligned} \tag{E2}$$

the jet coefficients by

$$\begin{aligned}
J_{-1}(\alpha_s) &= 1 + \frac{\alpha_s C_F}{\pi}\left(\frac{7}{4} - \frac{\pi^2}{4}\right)\,,\\
J_0(\alpha_s) &= -\frac{\alpha_s C_F}{\pi}\frac{3}{4}\,, \quad J_1(\alpha_s) = \frac{\alpha_s C_F}{\pi}\,,
\end{aligned} \tag{E3}$$

and the beam function coefficients by

$$\begin{aligned}
I^{qq}_{-1}(\alpha_s,z) &= \mathcal{L}_{-1}(1-z) + \frac{\alpha_s C_F}{2\pi}\Big[\mathcal{L}_1(1-z)(1+z^2)\\
&\quad - \frac{\pi^2}{6}\mathcal{L}_{-1}(1-z) + \theta(1-z)\Big(1 - z - \frac{1+z}{1-z}\ln z\Big)\Big]\,,\\
I^{qq}_0(\alpha_s,z) &= \frac{\alpha_s C_F}{2\pi}\theta(z)\left(P_{qq}(z) - \frac{3}{2}\mathcal{L}_{-1}(1-z)\right)\,,\\
I^{qq}_1(\alpha_s,z) &= \frac{\alpha_s C_F}{2\pi}\,2\mathcal{L}_{-1}(1-z)\,,
\end{aligned} \tag{E4}$$

and

$$\begin{aligned}
I^{qg}_{-1}(\alpha_s,z) &= \frac{\alpha_s T_F}{2\pi}\theta(z)\Big[P_{qg}(z)\ln\frac{1-z}{z} + 2\theta(1-z)z(1-z)\Big]\,,\\
I^{qg}_0(\alpha_s,z) &= \frac{\alpha_s T_F}{2\pi}\theta(z)P_{qg}(z)\,,
\end{aligned} \tag{E5}$$

where the splitting functions $P_{qq,qg}(z)$ are given in Eq. (167).

The argument of the plus distributions $\mathcal{L}_n$ in Eq. (E1) can rescaled by using the identity Eq. (C7). Eq. (E1) can

be rewritten in terms of the rescaled distribution as

$$G(t,\mu) = \frac{1}{\lambda \mu^{n_G}} \sum_{n=-1}^{1} G_n[\alpha_s(\mu),\lambda]\, \mathcal{L}_n\left(\frac{\lambda^{-1} t}{\mu^{n_G}}\right), \quad \text{(E6)}$$

where the coefficents $G_n(\alpha_s,\lambda)$ in Eq. (E6) are expressed in terms of the coefficients in Eq. (E1) by using the rescaling identity in Eq. (C7) as

$$\begin{aligned} G_{-1}(\alpha_s,\lambda) &= G_{-1}(\alpha_s) + \sum_{n=0}^{\infty} G_n(\alpha_s) \frac{\ln^{n+1}\lambda}{n+1}\,, \\ G_n(\alpha_s,\lambda) &= \sum_{k=0}^{\infty} \frac{(n+k)!}{n!\,k!} G_{n+k}(\alpha_s) \ln^k \lambda\,, \end{aligned} \quad \text{(E7)}$$

where $G_n = \{S_n, J_n, I_n^{qq,qg}\}$. Explicit expressions for $S_n(\alpha_s,\lambda)$, $J_n(\alpha_s,\lambda)$, and $I_n^{qq,qg}(\alpha_s,\lambda)$ are obtained by inserting Eqs. (E2), (E3), (E4), and (E5) into Eq. (E7).

2. Results of convolving plus functions

Convolutions of plus distributions in the jet, beam, and soft evolution kernels and the fixed-order functions produce the functions $V_k^n(\Omega)$ and the coefficients V_k^{mn} in the resummed cross sections Eqs. (185) and (188). There are three types of convolutions of plus distribtions $\mathcal{L}_n$ and $\mathcal{L}^a$. and we write them in useful form as

$$\int dy \mathcal{L}_m(x-y)\mathcal{L}_n(y) = \sum_{\ell=-1}^{m+n+1} V_\ell^{mn} \mathcal{L}_\ell(x), \quad \text{(E8)}$$

$$\begin{aligned} &\int dy\, [a\mathcal{L}^a(x-y) + \delta(x-y)]\, [b\mathcal{L}^b(y) + \delta(y)] \\ &\qquad = \frac{\Gamma(1+a)\Gamma(1+b)}{\Gamma(1+a+b)} (a+b) \left[\mathcal{L}^{a+b}(x) + \delta(x)\right], \\ &\int dy\, [a\mathcal{L}^a(x-y) + \delta(x-y)]\, \mathcal{L}_n(y) = \sum_{k=-1}^{n+1} V_k^n(a)\, \mathcal{L}_k^a(x)\,. \end{aligned}$$

The coefficients $V_k^n(a)$ and V_k^{mn} are related to the Taylor series expansion of $V(a,b)$ around $a=0$ and $a=b=0$, where $V(a,b)$ is defined by

$$V(a,b) = \frac{\Gamma(a)\Gamma(b)}{\Gamma(a+b)} - \frac{1}{a} - \frac{1}{b}\,, \quad \text{(E9)}$$

which satisfies $V(0,0)=0$. The $V_k^n(a)$ for $n \geq 0$ are

$$V_k^n(a) = \begin{cases} a \left.\dfrac{\mathrm{d}^n}{\mathrm{d}b^n} \dfrac{V(a,b)}{a+b}\right|_{b=0}, & k=-1\,, \\ a \binom{n}{k} \left.\dfrac{\mathrm{d}^{n-k}}{\mathrm{d}b^{n-k}} V(a,b)\right|_{b=0} + \delta_{kn}\,, & 0 \leq k \leq n\,, \\ \dfrac{a}{n+1}\,, & k = n+1\,. \end{cases} \quad \text{(E10)}$$

The V_k^{mn} are symmetric in m and n, and for $m,n \geq 0$ they are

$$V_k^{mn} = \begin{cases} \left.\dfrac{\mathrm{d}^m}{\mathrm{d}a^m} \dfrac{\mathrm{d}^n}{\mathrm{d}b^n} \dfrac{V(a,b)}{a+b}\right|_{a=b=0}, & k=-1\,, \\ \displaystyle\sum_{p=0}^{m}\sum_{q=0}^{n} \delta_{p+q,k} \binom{m}{p}\binom{n}{q} \\ \qquad \times \left.\dfrac{\mathrm{d}^{m-p}}{\mathrm{d}a^{m-p}} \dfrac{\mathrm{d}^{n-q}}{\mathrm{d}b^{n-q}} V(a,b)\right|_{a=b=0}, & 0 \leq k \leq m+n\,, \\ \dfrac{1}{m+1} + \dfrac{1}{n+1}\,, & k = m+n+1\,. \end{cases} \quad \text{(E11)}$$

Using Eq. (C6) we can extend these definitions to include the cases $n=-1$ or $m=-1$. The relevant coefficients are

$$\begin{aligned} V_{-1}^{-1}(a) &= 1\,, \qquad V_0^{-1}(a) = a \\ V_{k\geq 1}^{-1}(a) &= 0\,, \qquad V_k^{-1,n} = V_k^{n,-1} = \delta_{nk}\,. \end{aligned} \quad \text{(E12)}$$

Appendix F: Resummed cross section from Laplace transforms

An alternative way [38, 80] to express the resummed cross sections in Sec. VII is to utilize the Laplace-transformed jet, beam, and soft functions given in App. D and their RGE solutions. The method avoids taking explicit convolutions of plus functions in the evolution factors and in the fixed-order jet, beam, and soft functions.

Each of the RGE solutions for the jet, beam, and soft functions is given by a function of the form

$$\widetilde{G}(\nu,\mu) = \widetilde{G}(\nu,\mu_0) e^{K_G(\mu_0,\mu)} [\mu_0 (\nu e^{\gamma_E})^{1/j_G}]^{-j_G \eta_G(\mu_0,\mu)}\,. \quad \text{(F1)}$$

For the jet and beam functions, $j_G = 2$, while for the soft function $j_G = 1$. The fixed-order expansion of $\widetilde{G}(\nu,\mu_0) \equiv \widetilde{G}(L_G,\mu_0)$ can be considered to be a function of the log $L_G \equiv \ln Q_G/\mu_0$, where $Q_G = (\nu e^{\gamma_E})^{-1/j_G}$. To $\mathcal{O}(\alpha_s^2)$,

$$\begin{aligned} \widetilde{G}(L_G,\mu_0) &= 1 + \frac{\alpha_s(\mu_0)}{4\pi}\Big(-\Gamma_G^0 L_G^2 - \gamma_G^0 L_G + c_G^1\Big) \quad \text{(F2)} \\ &\quad + \Big(\frac{\alpha_s(\mu_0)}{4\pi}\Big)^2 \Big[\frac{1}{2}(\Gamma_G^0)^2 L_G^4 + \Gamma_G^0\Big(\gamma_G^0 + \frac{2}{3}\beta_0\Big) L_G^3 \\ &\qquad + \Big(\frac{1}{2}(\gamma_G^0)^2 + \gamma_G^0\beta_0 - \Gamma_G^1 - c_G^1\Gamma_G^0\Big) L_G^2 \\ &\qquad - (\gamma_G^1 + c_G^1\gamma_G^0 + 2c_G^1\beta_0) L_G + c_G^2\Big]\,. \end{aligned}$$

Each power of L_G can be generated by taking derivatives with respect to η_G in Eq. (F1):

$$\widetilde{G}(\nu,\mu) = e^{K_G(\mu_0,\mu)} \tilde{g}(\partial_{\eta_F},\mu_0) \big[\mu_0 (\nu e^{\gamma_E})^{1/j_G}\big]^{-j_G \eta_G(\mu_0,\mu)}\,, \quad \text{(F3)}$$

where $\tilde{g}(\partial_\eta, \mu_0)$ is the operator constructed by replacing each L_G in Eq. (F2) with ∂_η / j_G:

$$\begin{aligned}\tilde{g}(\partial_\eta, \mu_0) = 1 + \frac{\alpha_s(\mu_0)}{4\pi}\Big(-\Gamma_G^0 \frac{\partial_\eta^2}{j_G^2} - \gamma_G^0 \frac{\partial_\eta}{j_G} + c_G^1\Big) \\ + \Big(\frac{\alpha_s(\mu_0)}{4\pi}\Big)^2 \Big[\frac{1}{2}(\Gamma_G^0)^2 \frac{\partial_\eta^4}{j_G^4} + \Gamma_G^0\Big(\gamma_G^0 + \frac{2}{3}\beta_0\Big)\frac{\partial_\eta^3}{j_G^3} \\ + \Big(\frac{1}{2}(\gamma_G^0)^2 + \gamma_G^0\beta_0 - \Gamma_G^1 - c_G^1\Gamma_G^0\Big)\frac{\partial_\eta^2}{j_G^2} \\ - (\gamma_G^1 + c_G^1\gamma_G^0 + 2c_G^1\beta_0)\frac{\partial_\eta}{j_G} + c_G^2\Big]\,.\end{aligned} \tag{F4}$$

Now it is easy to take the inverse Laplace transform of Eq. (F1),

$$\begin{aligned}G(t,\mu) &= \int_{c-i\infty}^{c+i\infty} \frac{d\nu}{2\pi i} e^{\nu t} \widetilde{G}(\nu,\mu) \\ &= e^{K_G(\mu_0,\mu)} \tilde{g}(\partial_{\eta_F}, \mu_0) \frac{e^{-\gamma_E \eta_G}}{\Gamma(\eta_G)} \frac{(t/\mu_0^{j_G})^{\eta_G}}{t}\,,\end{aligned} \tag{F5}$$

where $\eta_G \equiv \eta_G(\mu_0, \mu)$. The derivatives with respect to η_G automatically generate the results of taking convolutions of the logs inside $G(t, \mu_0)$ with the evolution kernel $U_G(t, \mu_0, \mu)$ in RGE solutions like Eqs. (D5) and (D14).

1. $\tau_1^{a,b}$ cross sections

Using the above formalism, we obtain for the Laplace transforms of the $\tau_1^{a,b}$ differential cross sections $(1/\sigma_0) d\sigma / d\tau_1^{a,b}$ in Eqs. (142) and (147),

$$\begin{aligned}\tilde{\sigma}(x, Q^2, \nu^{a,b}) = H(Q^2,\mu_H)\tilde{j}(\partial_{\eta_J},\mu_J)[L_q(x,Q^2)\tilde{b}_q^{a,b}(\partial_{\eta_B},x,\mu_B) + L_{\bar{q}}(x,Q^2)\tilde{b}_{\bar{q}}^{a,b}(\partial_{\eta_B},x,\mu_B)]\tilde{s}(\partial_{2\eta_S},\mu_S) \\ \times e^{K_H(\mu_H,\mu)+K_J(\mu_J,\mu)+K_B(\mu_B,\mu)+2K_S(\mu_S,\mu)} \\ \times \Big(\frac{Q}{\mu_H}\Big)^{\eta_H(\mu_H,\mu)} \Big(\frac{Q^2}{\mu_J^2 e^{\gamma_E}\nu^{a,b}}\Big)^{\eta_J(\mu_J,\mu)} \Big(\frac{Q^2}{\mu_B^2 e^{\gamma_E}\nu^{a,b}}\Big)^{\eta_B(\mu_B,\mu)} \Big(\frac{Q}{\mu_S e^{\gamma_E}\nu^{a,b}}\Big)^{2\eta_S(\mu_S,\mu)}\,.\end{aligned} \tag{F6}$$

Taking the inverse Laplace transform with respect to $\nu^{a,b}$ and taking the cumulant in Eq. (172), we easily obtain in momentum space,

$$\begin{aligned}\sigma_{\rm c}(x, Q^2, \tau_1^{a,b}) = H(Q^2,\mu_H)\Big(\frac{Q}{\mu_H}\Big)^{\eta_H(\mu_H,\mu)} \Big(\frac{Q^2\tau_1^{a,b}}{\mu_J^2}\Big)^{\eta_J(\mu_J,\mu)} \Big(\frac{Q^2\tau_1^{a,b}}{\mu_B^2}\Big)^{\eta_B(\mu_B,\mu)} \Big(\frac{Q\tau_1^{a,b}}{\mu_S}\Big)^{2\eta_S(\mu_S,\mu)-\Omega} \\ \times \Big[L_q^a(x,Q^2)\tilde{b}_q^{a,b}\Big(\partial_\Omega - \ln\frac{\mu_B^2}{Q\mu_S}, x, \mu_B\Big) + L_{\bar{q}}^a(x,Q^2)\tilde{b}_{\bar{q}}^{a,b}\Big(\partial_\Omega - \ln\frac{\mu_B^2}{Q\mu_S}, x, \mu_B\Big)\Big] \\ \times \tilde{j}\Big(\partial_\Omega - \ln\frac{\mu_J^2}{Q\mu_S}, \mu_J\Big)\tilde{s}\big(\partial_\Omega, \mu_S\big)\Big(\frac{Q\tau_1^{a,b}}{\mu_S e^{\gamma_E}}\Big)^{\Omega} \frac{\theta(\tau_1^{a,b})}{\Gamma(1+\Omega)} e^{\mathcal{K}(\mu_H,\mu_J,\mu_B,\mu_S,\mu)}\,,\end{aligned} \tag{F7}$$

with a sum over quark and antiquark flavors $q, \bar{q}$, and where the sums of evolution kernels $\mathcal{K}, \Omega$ are given by

$$\mathcal{K}(\mu_H,\mu_J,\mu_B,\mu_S,\mu) = K_H(\mu_H,\mu) + K_J(\mu_J,\mu) + K_B(\mu_B,\mu) + 2K_S(\mu_S,\mu) \tag{F8a}$$

$$\Omega \equiv \Omega(\mu_J,\mu_B,\mu_S,\mu) = \eta_J(\mu_J,\mu) + \eta_B(\mu_B,\mu) + 2\eta_S(\mu_S,\mu)\,, \tag{F8b}$$

where the individual evolution kernels $K_{H,J,B,S}, \eta_{J,B,S}$ are defined in App. D.

The fixed-order operators $\tilde{j}, \tilde{b}_{q,\bar{q}}, \tilde{s}$ in Eq. (F7) each take the form Eq. (F4), which in this paper we will truncate to $\mathcal{O}(\alpha_s)$, working to NNLL accuracy. In Eq. (F4), $\Gamma_F^n, \gamma_F^n, \beta_n$ are the coefficients in the fixed-order expansions Eq. (D25) of the anomalous dimensions and beta function, and where $j_G = 2$ for the jet function and $j_G = 1$ for the soft function, and the constants c_G^1 are given by

$$c_J^1 = (7-\pi^2)C_F - \frac{\Gamma_J^0}{4}\frac{\pi^2}{6}\,, \quad c_S^1 = \frac{\pi^2}{3}C_F - \Gamma_S^0\frac{\pi^2}{3}\,. \tag{F9}$$

Note that the cusp parts of the hard, jet/beam, and soft anomalous dimensions are related to the cusp anomalous dimension in Eq. (D25) by

$$\Gamma_H = 2\Gamma_{\rm cusp}^q\,, \quad \Gamma_{J,B} = -2\Gamma_{\rm cusp}^q\,, \quad \Gamma_S = 2\Gamma_{\rm cusp}^q\,. \tag{F10}$$

Meanwhile the beam function operators $\tilde{b}_q^{a,b}$ in the $\tau_1^{a,b}$ cross sections are given by

$$\begin{aligned}\tilde{b}_q^{a,b}(\partial_\Omega, x, \mu_B) = f_q(x,\mu_B)\Big\{1 + \frac{\alpha_s(\mu_B)}{4\pi}\Big(-C_F\frac{\pi^2}{3} - \frac{\Gamma_J^0}{4}\Big(\partial_\Omega^2 + \frac{\pi^2}{6}\Big) + \frac{\gamma_J^0}{2}\partial_\Omega\Big)\Big\} \\ + \frac{\alpha_s(\mu_B)}{2\pi}\int_x^1 \frac{dz}{z}\Big[C_F f_q\Big(\frac{x}{z},\mu_B\Big)F_q(z) + T_F f_g\Big(\frac{x}{z},\mu_B\Big)F_g(z)\Big] \\ + \frac{\alpha_s(\mu_B)}{2\pi}\int_x^1 \frac{dz}{z}\Big[C_F P_{qq}(z) f_q\Big(\frac{x}{z},\mu_B\Big) + T_F P_{qg}(z) f_g\Big(\frac{x}{z},\mu_B\Big)\Big]\big[\partial_\Omega + \delta b^{a,b}(z)\big]\,,\end{aligned} \tag{F11}$$

where $\tilde{b}_q^{a,b}$ differ only in the last term,

$$\delta b^a(z) = 0\,, \quad \delta b^b(z) = \ln z\,, \tag{F12}$$

and the functions $F_{q,g}$ are given by

$$F_q(z) \equiv (1+z^2)\left[\frac{\theta(1-z)\ln(1-z)}{1-z}\right]_+ + \theta(1-z)\Big(1 - z - \frac{1+z^2}{1-z}\ln z\Big) \tag{F13a}$$

$$F_g(z) \equiv P_{qg}(z)\Big(\ln\frac{1-z}{z} - 1\Big) + \theta(1-z)\,, \tag{F13b}$$

and $P_{qq,qg}$ are given by Eq. (167). The additional term $\delta b^b(z) = \ln z$ that appears in the final integrand in Eq. (F11) for $\tilde{b}^b$ is due to the nontrivial $\mathbf{k}_\perp^2$ dependent terms in Eq. (166) for the generalized beam function, which generate the $\delta b^b(z) = \ln z$ term upon integration over the transverse momentum in Eq. (142). Thus the difference the τ_1^a and τ_1^b cross sections will become more pronounced at smaller x, when the $\delta b^b(z) = \ln z$ term inside the integrand of Eq. (F11) can grow larger.

To evaluate the action of the fixed-order operators given by Eqs. (F4) and (F11) in the resummed cross section Eq. (F7), it is useful to tabulate the following relations:

$$\begin{aligned}\mathcal{G}(\Omega) &\equiv \Big(\frac{Q\tau_1}{\mu e^{\gamma_E}}\Big)^\Omega \frac{1}{\Gamma(1+\Omega)}\,, \\ \partial_\Omega\mathcal{G}(\Omega) &= \Big[-\ln\frac{\mu}{Q\tau_1} - H(\Omega)\Big]\mathcal{G}(\Omega)\,, \\ \partial_\Omega^2\mathcal{G}(\Omega) &= \Big[\Big(\ln\frac{\mu}{Q\tau_1} + H(\Omega)\Big)^2 - \psi^{(1)}(1+\Omega)\Big]\mathcal{G}(\Omega)\,,\end{aligned} \tag{F14}$$

where H is the harmonic number function, $H(\Omega) = \gamma_E + \psi^{(0)}(1+\Omega)$ and $\psi^{(n)}(x) = (d^n/dz^n)[\Gamma'(z)/\Gamma(z)]$ is the polygamma function. The result of taking these derivatives in the expression Eq. (F7) is equivalent to the results of convolving logs in the fixed-order jet, beam, and soft functions with the momentum-space evolution kernels in deriving the expression Eq. (185). The two formalisms yield equivalent expressions for the resummed cross section.

2. τ_1^c cross section

The resummed τ_1^c cross section obtained from RG evolution of the hard, jet, beam, and soft functions in Eq. (153) is given by

$$\begin{aligned}\sigma_c(x,Q^2,\tau_1^c) = H(Q^2,\mu_H)\Big(\frac{Q}{\mu_H}\Big)^{\eta_H(\mu_H,\mu)}\Big(\frac{Q^2}{\mu_J^2}\Big)^{\eta_J(\mu_J,\mu)}\Big(\frac{xQ^2}{\mu_B^2}\Big)^{\eta_B(\mu_B,\mu)}\Big(\frac{\sqrt{x}Q}{\mu_S}\Big)^{2\eta_S(\mu_S,\mu)-\Omega}\tilde{j}\Big(\partial_\Omega - \ln\frac{\sqrt{x}\mu_J^2}{Q\mu_S},\mu_J\Big) \\ \times\Big[L_q^c(Q^2)\tilde{b}_q^c\Big(\partial_\Omega - \ln\frac{\mu_B^2}{\sqrt{x}Q\mu_S},x,y,\tau_1^c,\mu_B\Big) + L_{\bar{q}}^c(Q^2)\tilde{b}_{\bar{q}}^c\Big(\partial_\Omega - \ln\frac{\mu_B^2}{\sqrt{x}Q\mu_S},x,y,\tau_1^c,\mu_B\Big)\Big] \\ \times\tilde{s}\big(\partial_\Omega,\mu_S\big)\Big(\frac{\sqrt{x}Q\,|\tau_1^c - 1 + y|}{\mu_S e^{\gamma_E}}\Big)^\Omega\frac{e^{\mathcal{K}(\mu_H,\mu_J,\mu_B,\mu_S,\mu)}}{\Gamma(1+\Omega)}\,,\end{aligned} \tag{F15}$$

where the operator $\tilde{b}_q^c$ is given by

$$\tilde{b}_q^c(\partial_\Omega, x, y, \tau_1^c, \mu_B) = \theta(\tau_1^c - 1 + y)\tilde{b}_q^a(\partial_\Omega, x, \mu_B) + \frac{\alpha_s(\mu_B)}{2\pi}\int_x^1 \frac{dz}{z}\left[C_F P_{qq}(z) f_q\Big(\frac{x}{z}, \mu_B\Big) + T_F P_{qg}(z) f_g\Big(\frac{x}{z}, \mu_B\Big)\right]$$
$$\times \left\{\theta(\tau_1^c - 1 + y)\left[\ln\left(\frac{z}{1-z}\frac{\tau_1^c - 1 + y}{x(1-y)}\right) - H(-\Omega) - \frac{1}{\Omega}\right] - \theta(1 - y - \tau_1^c)\frac{\pi}{\sin\pi\Omega}\right.$$
$$\left. + \frac{1}{\Omega}\left(\frac{(1-y)X}{|\tau_1^c - 1 + y|}\right)^{\Omega} {}_2\mathrm{F}_1\left(-\Omega, -\Omega, 1-\Omega; -\frac{\tau_1^c - 1 + y}{(1-y)X}\right)\right\}\theta\Big(\tau_1^c - (1-y)(1-X)\Big)\,, \quad \text{(F16)}$$

and similarly for $\tilde{b}_{\bar{q}}^c$. Here $X \equiv x(1-z)/(x+z-xz)$. The additional more complicated terms in $\tilde{b}_q^c$ are due to the nontrivial $\mathbf{p}_\perp$ integral in Eq. (153) which convolves the terms in the generalized beam function with nontrivial $\mathbf{p}_\perp^2$ dependence with the dependence of the jet function on $(\mathbf{q}_\perp + \mathbf{p}_\perp)^2$, with $\mathbf{q}_\perp \neq 0$ when $y < 1$. Note that the apparent singularities as $\Omega \to 0$ (the fixed-order limit) cancel in the sum of all terms. The result Eq. (F15) is equivalent to the expression Eq. (188) derived from RG evolution directly in momentum space.

3. Generic τ_1 cross section

In similar fashion we can form the resummed τ_1 cross section for an arbitrary definition Eq. (24) of the 1-jettiness. Using the generic factorization theorem Eq. (140)

$$\sigma_{\mathrm{c}}(x, Q^2, \tau_1) = H(Q^2, \mu_H)\Big(\frac{Q}{\mu_H}\Big)^{\eta_H(\mu_H,\mu)}\Big(\frac{s_J}{\mu_J^2}\Big)^{\eta_J(\mu_J,\mu)}\Big(\frac{s_B}{\mu_B^2}\Big)^{\eta_B(\mu_B,\mu)}\Big(\frac{Q_R}{\mu_S}\Big)^{2\eta_S(\mu_S,\mu)-\Omega}$$
$$\times \left[L_q(q_J, q_B, Q^2)\tilde{b}_q\Big(\partial_\Omega - \ln\frac{\mu_B^2 Q_R}{s_B\mu_S}, q_J, q_B, \tau_1, \mu_B\Big) + L_{\bar{q}}(q_J, q_B, Q^2)\tilde{b}_{\bar{q}}\Big(\partial_\Omega - \ln\frac{\mu_B^2 Q_R}{s_B\mu_S}, q_J, q_B, \tau_1, \mu_B\Big)\right] \quad \text{(F17)}$$
$$\times \tilde{j}\Big(\partial_\Omega - \ln\frac{\mu_J^2 Q_R}{s_J\mu_S}, \mu_J\Big)\tilde{s}\big(\partial_\Omega, \mu_S\big)\left(\frac{Q_R\,|\tau_1 - \tau_q|}{\mu_S e^{\gamma_E}}\right)^{\Omega}\frac{e^{\mathcal{K}(\mu_H,\mu_J,\mu_B,\mu_S,\mu)}}{\Gamma(1+\Omega)}\,,$$

where the operator $\tilde{b}_q$ is given by

$$\tilde{b}_q(\partial_\Omega, q_J, q_B, \tau_1, \mu_B) = \theta(\tau_1 - \tau_q)\tilde{b}_q^a(\partial_\Omega, x, \mu_B) + \frac{\alpha_s(\mu_B)}{2\pi}\int_x^1 \frac{dz}{z}\left[C_F P_{qq}(z) f_q\Big(\frac{x}{z}, \mu_B\Big) + T_F P_{qg}(z) f_g\Big(\frac{x}{z}, \mu_B\Big)\right]$$
$$\times \left\{\theta(\tau_1 - \tau_q)\left[\ln\left(\frac{1 - X_q}{X_q}\frac{\tau_1 - \tau_q}{\tau_q}\right) - H(-\Omega) - \frac{1}{\Omega}\right] - \theta(\tau_q - \tau_1)\frac{\pi}{\sin\pi\Omega}\right. \quad \text{(F18)}$$
$$\left. + \frac{1}{\Omega}\left(\frac{\tau_q X_q}{|\tau_1 - \tau_q|}\right)^{\Omega} {}_2\mathrm{F}_1\left(-\Omega, -\Omega, 1-\Omega; -\frac{\tau_1 - \tau_q}{\tau_q X_q}\right)\right\}\theta\Big(\tau_1 - \tau_q(1 - X_q)\Big)\,,$$

and similarly for $\tilde{b}_{\bar{q}}^c$. In Eqs. (F17) and (F18), τ_q and X_q are given by

$$\tau_q \equiv \frac{\mathbf{q}_\perp^2}{Q_J \bar{n}_J \cdot q} = \frac{\mathbf{q}_\perp^2}{s_J}\,, \qquad X_q \equiv \frac{-q_J \cdot q(1-z)}{[z q_B - (1-z)q_J]\cdot q}\,. \quad \text{(F19)}$$

Appendix G: $\mathcal{O}(\alpha_s)$ fixed-order cross sections

1. τ_1^c cross section

The fixed-order τ_1^c cross section at $\mathcal{O}(\alpha_s)$ is easily obtained from Eq. (F15) by taking the limit $\mu_{H,J,B,S} = \mu$, which turns off all the resummation. We plug the $\mathcal{O}(\alpha_s)$ hard function Eq. (155), the $\mathcal{O}(\alpha_s)$ jet and soft operators given by Eq. (F4), and the $\mathcal{O}(\alpha_s)$ beam function operator Eq. (F16) into the expression Eq. (F15). We use Eq. (F14) to

evaluate the action of these operators in Eq. (F15), and finally take the $\mathcal{K}, \Omega, \eta_{H,J,B,S} \to 0$ limit. The result is:

$$\begin{aligned}
\sigma_{\rm c}(x,Q^2,\tau_1^c) &= \theta(\tau_1^c-1+y)\int_x^1 \frac{dz}{z}\big[L_q^c(Q^2)f_q(x/z,\mu)+L_{\bar q}^c(Q^2)f_{\bar q}(x/z,\mu)\big] \\
&\quad\times\Bigg\{\delta(1-z)\bigg[1-\frac{\alpha_s(\mu)C_F}{4\pi}\Big(9+\frac{2\pi^2}{3}+3\ln[x(\tau_1^c-1+y)^2]+4\ln[x(\tau_1^c-1+y)]\ln(\tau_1^c-1+y)\Big)\bigg] \\
&\qquad+\frac{\alpha_s(\mu)C_F}{2\pi}\bigg[P_{qq}(z)\ln\frac{xQ^2(\tau_1^c-1+y)}{\mu^2}+F_q(z)\bigg]\Bigg\} \\
&\quad+\frac{\alpha_s(\mu)T_F}{2\pi}\big(L_q^c+L_{\bar q}^c\big)(Q^2)\theta(\tau_1^c-1+y)\int_x^1\frac{dz}{z}f_g\Big(\frac{x}{z},\mu\Big)\Big[P_{qg}(z)\ln\frac{xQ^2(\tau_1^c-1+y)}{\mu^2}+F_g(z)\Big] \\
&\quad+\frac{\alpha_s(\mu)}{2\pi}\int_x^1\frac{dz}{z}\Big\{C_FP_{qq}(z)\big[L_q^c(Q^2)f_q(x/z,\mu)+L_{\bar q}^c(Q^2)f_{\bar q}(x/z,\mu)\big]+T_FP_{qg}(z)(L_q+L_{\bar q})(Q^2)f_g(x/z,\mu)\Big\} \\
&\qquad\times\bigg[\theta(\tau_1^c-1+y)\ln\frac{z}{x+z-xz}+\theta(1-y-\tau_1^c)\theta\Big(\tau_1^c-\frac{z(1-y)}{x+z-xz}\Big)\ln\frac{(1-y)X}{1-y-\tau_1^c}\bigg].
\end{aligned} \tag{G1}$$

In the last line we used that in the $\Omega \to 0$ limit, the hypergeometric function in Eq. (F16) behaves like [120, 121]:

$${}_2\mathrm{F}_1(-\Omega,-\Omega,1-\Omega;-T) = 1+\Omega^2\,\mathrm{Li}_2(-T)+\cdots\,, \tag{G2}$$

In the $\Omega \to 0$ limit in Eq. (F16), only the first term in this expansion survives.

2. Generic τ_1 cross section

The fixed-order $\mathcal{O}(\alpha_s)$ cross section is similarly obtained from Eq. (F17) by taking the limit of equal scales $\mu = \mu_H = \mu_J = \mu_B = \mu_S$, and thus $\mathcal{K}, \Omega, \eta_{H,J,B,S} \to 0$. For the cumulant to $\mathcal{O}(\alpha_s)$, we obtain:

$$\begin{aligned}
\sigma_{\rm c}(x,Q^2,\tau_1) &= \theta(\tau_1-\tau_q)\int_x^1\frac{dz}{z}\big[L_q(q_J,q_B,Q^2)f_q(x/z,\mu)+L_{\bar q}(q_J,q_B,Q^2)f_{\bar q}(x/z,\mu)\big] \\
&\quad\times\Bigg\{\delta(1-z)\bigg[1-\frac{\alpha_s(\mu)C_F}{4\pi}\Big(9+\frac{2\pi^2}{3}+3\ln\frac{Q_R^2(\tau_1-\tau_q)^2}{Q^2}+4\ln\frac{Q_R^2(\tau_1-\tau_q)}{s_B}\ln\frac{Q_R^2(\tau_1-\tau_q)}{s_J}\Big)\bigg] \\
&\qquad+\frac{\alpha_s(\mu)C_F}{2\pi}\bigg[P_{qq}(z)\ln\frac{s_B(\tau_1-\tau_q)}{\mu^2}+F_q(z)\bigg]\Bigg\} \\
&\quad+\frac{\alpha_s(\mu)T_F}{2\pi}\big(L_q+L_{\bar q}\big)(q_J,q_B,Q^2)\theta(\tau_1-\tau_q)\int_x^1\frac{dz}{z}f_g\Big(\frac{x}{z},\mu\Big)\Big[P_{qg}(z)\ln\frac{s_B(\tau_1-\tau_q)}{\mu^2}+F_g(z)\Big] \\
&\quad+\frac{\alpha_s(\mu)}{2\pi}\int_x^1\frac{dz}{z}\Big\{C_FP_{qq}(z)\Big[L_qf_q\Big(\frac{x}{z},\mu\Big)+L_{\bar q}f_{\bar q}\Big(\frac{x}{z},\mu\Big)\Big]+T_FP_{qg}(z)(L_q+L_{\bar q})f_g\Big(\frac{x}{z},\mu\Big)\Big\} \\
&\qquad\times\bigg[\theta(\tau_1-\tau_q)\ln(1-X_q)+\theta(\tau_q-\tau_1)\theta\Big(\tau_1-\tau_q(1-X_q)\Big)\ln\frac{\tau_qX_q}{\tau_q-\tau_1}\bigg],
\end{aligned} \tag{G3}$$

where we have used the relation in Eq. (59), $s_Js_B/Q_R^2 = Q^2$ to leading order in λ, to simplify the arguments of the logs on the second line.

[1] R. E. Taylor, Rev.Mod.Phys. **63**, 573 (1991).
[2] H. W. Kendall, Rev.Mod.Phys. **63**, 597 (1991).
[3] J. I. Friedman, Rev.Mod.Phys. **63**, 615 (1991).
[4] J. Bjorken, Phys.Rev. **179**, 1547 (1969).
[5] D. Gross and F. Wilczek, Phys.Rev.Lett. **30**, 1343 (1973).

[6] H. Politzer, Phys.Rev.Lett. **30**, 1346 (1973).
[7] S. Bethke, A. H. Hoang, S. Kluth, J. Schieck, I. W. Stewart, et al. (2011), 1110.0016.
[8] A. Gehrmann-De Ridder, T. Gehrmann, E. W. N. Glover, and G. Heinrich, Phys. Rev. Lett. **99**, 132002 (2007), 0707.1285.
[9] A. Gehrmann-De Ridder, T. Gehrmann, E. W. N. Glover, and G. Heinrich, JHEP **12**, 094 (2007), 0711.4711.
[10] S. Weinzierl, Phys. Rev. Lett. **101**, 162001 (2008), 0807.3241.
[11] S. Weinzierl, JHEP **06**, 041 (2009), 0904.1077.
[12] T. Becher and M. D. Schwartz, JHEP **07**, 034 (2008), 0803.0342.
[13] Y.-T. Chien and M. D. Schwartz, JHEP **1008**, 058 (2010), 1005.1644.
[14] R. Abbate, M. Fickinger, A. H. Hoang, V. Mateu, and I. W. Stewart, Phys. Rev. **D83**, 074021 (2011), 1006.3080.
[15] V. Antonelli, M. Dasgupta, and G. P. Salam, JHEP **0002**, 001 (2000), hep-ph/9912488.
[16] S. Catani and M. Seymour, Nucl.Phys. **B485**, 291 (1997), hep-ph/9605323.
[17] D. Graudenz (1997), hep-ph/9710244.
[18] C. W. Bauer, S. Fleming, and M. E. Luke, Phys. Rev. **D63**, 014006 (2000), hep-ph/0005275.
[19] C. W. Bauer, S. Fleming, D. Pirjol, and I. W. Stewart, Phys. Rev. **D63**, 114020 (2001), hep-ph/0011336.
[20] C. W. Bauer and I. W. Stewart, Phys. Lett. **B516**, 134 (2001), hep-ph/0107001.
[21] C. W. Bauer, D. Pirjol, and I. W. Stewart, Phys. Rev. **D65**, 054022 (2002), hep-ph/0109045.
[22] C. W. Bauer, S. Fleming, D. Pirjol, I. Z. Rothstein, and I. W. Stewart, Phys. Rev. **D66**, 014017 (2002), hep-ph/0202088.
[23] M. D. Schwartz, Phys. Rev. **D77**, 014026 (2008), 0709.2709.
[24] A. Hornig, C. Lee, and G. Ovanesyan, Phys. Lett. **B677**, 272 (2009), 0901.1897.
[25] A. Hornig, C. Lee, and G. Ovanesyan, JHEP **05**, 122 (2009), 0901.3780.
[26] I. W. Stewart, F. J. Tackmann, and W. J. Waalewijn, Phys. Rev. Lett. **106**, 032001 (2011), 1005.4060.
[27] I. W. Stewart, F. J. Tackmann, and W. J. Waalewijn, Phys. Rev. Lett. **105**, 092002 (2010), 1004.2489.
[28] C. F. Berger, C. Marcantonini, I. W. Stewart, F. J. Tackmann, and W. J. Waalewijn, JHEP **1104**, 092 (2011), 1012.4480.
[29] T. T. Jouttenus, I. W. Stewart, F. J. Tackmann, and W. J. Waalewijn (2013), 1302.0846.
[30] C. Adloff et al. (H1 Collaboration), Phys.Lett. **B406**, 256 (1997), hep-ex/9706002.
[31] C. Adloff et al. (H1 Collaboration), Eur.Phys.J. **C14**, 255 (2000), hep-ex/9912052.
[32] A. Aktas et al. (H1 Collaboration), Eur.Phys.J. **C46**, 343 (2006), hep-ex/0512014.
[33] J. Breitweg et al. (ZEUS Collaboration), Phys.Lett. **B421**, 368 (1998), hep-ex/9710027.
[34] S. Chekanov et al. (ZEUS Collaboration), Eur.Phys.J. **C27**, 531 (2003), hep-ex/0211040.
[35] S. Chekanov et al. (ZEUS Collaboration), Nucl.Phys. **B767**, 1 (2007), hep-ex/0604032.
[36] A. V. Manohar, Phys. Rev. **D68**, 114019 (2003), hep-ph/0309176.
[37] J. Chay and C. Kim, Phys.Rev. **D75**, 016003 (2007), hep-ph/0511066.
[38] T. Becher, M. Neubert, and B. D. Pecjak, JHEP **01**, 076 (2007), hep-ph/0607228.
[39] P.-y. Chen, A. Idilbi, and X.-d. Ji, Nucl.Phys. **B763**, 183 (2007), hep-ph/0607003.
[40] S. Fleming and O. Zhang (2012), 1210.1508.
[41] S. Catani, Y. L. Dokshitzer, M. Olsson, G. Turnock, and B. R. Webber, Phys. Lett. **B269**, 432 (1991).
[42] S. Catani, Y. L. Dokshitzer, M. H. Seymour, and B. R. Webber, Nucl. Phys. **B406**, 187 (1993).
[43] S. D. Ellis and D. E. Soper, Phys. Rev. **D48**, 3160 (1993), hep-ph/9305266.
[44] Y. L. Dokshitzer, G. D. Leder, S. Moretti, and B. R. Webber, JHEP **08**, 001 (1997), hep-ph/9707323.
[45] G. P. Salam and G. Soyez, JHEP **05**, 086 (2007), 0704.0292.
[46] M. Cacciari, G. P. Salam, and G. Soyez, JHEP **04**, 063 (2008), 0802.1189.
[47] M. Dasgupta and G. P. Salam, Phys. Lett. **B512**, 323 (2001), hep-ph/0104277.
[48] M. Dasgupta and G. P. Salam, JHEP **0208**, 032 (2002), hep-ph/0208073.
[49] M. Dasgupta and G. P. Salam, JHEP **0203**, 017 (2002), hep-ph/0203009.
[50] A. Banfi, G. Marchesini, and G. Smye, JHEP **08**, 006 (2002), hep-ph/0206076.
[51] R. Appleby and M. Seymour, JHEP **0212**, 063 (2002), hep-ph/0211426.
[52] Y. Delenda, R. Appleby, M. Dasgupta, and A. Banfi, JHEP **0612**, 044 (2006), hep-ph/0610242.
[53] A. Banfi, M. Dasgupta, K. Khelifa-Kerfa, and S. Marzani, JHEP **1008**, 064 (2010), 1004.3483.
[54] A. Hornig, C. Lee, J. R. Walsh, and S. Zuberi, JHEP **1201**, 149 (2012), 1110.0004.
[55] F. J. Tackmann, J. R. Walsh, and S. Zuberi, Phys.Rev. **D86**, 053011 (2012), 1206.4312.
[56] A. Banfi and M. Dasgupta, Phys.Lett. **B628**, 49 (2005), hep-ph/0508159.
[57] K. Khelifa-Kerfa, JHEP **1202**, 072 (2012), 1111.2016.
[58] R. Kelley, J. R. Walsh, and S. Zuberi, JHEP **1209**, 117 (2012), 1202.2361.
[59] R. Kelley, J. R. Walsh, and S. Zuberi (2012), 1203.2923.
[60] R. Kelley, M. D. Schwartz, R. M. Schabinger, and H. X. Zhu, Phys.Rev. **D84**, 045022 (2011), 1105.3676.
[61] A. Hornig, C. Lee, I. W. Stewart, J. R. Walsh, and S. Zuberi, JHEP **1108**, 054 (2011), 1105.4628.
[62] X. Liu and F. Petriello, Phys.Rev. **D87**, 014018 (2013), 1210.1906.
[63] Y. Delenda and K. Khelifa-Kerfa, JHEP **1209**, 109 (2012), 1207.4528.
[64] E. Farhi, Phys. Rev. Lett. **39**, 1587 (1977).
[65] J. Thaler and K. Van Tilburg (2011), 1108.2701.
[66] Z.-B. Kang, S. Mantry, and J.-W. Qiu, Phys.Rev. **D86**, 114011 (2012), 1204.5469.
[67] I. W. Stewart, F. J. Tackmann, and W. J. Waalewijn, Phys. Rev. **D81**, 094035 (2010), 0910.0467.
[68] S. Mantry and F. Petriello, Phys.Rev. **D81**, 093007 (2010), 0911.4135.
[69] G. Salam and D. Wicke, JHEP **0105**, 061 (2001), hep-ph/0102343.
[70] C. Lee and G. Sterman (2006), hep-ph/0603066.
[71] C. Lee and G. Sterman, Phys. Rev. **D75**, 014022 (2007), hep-ph/0611061.

[72] V. Mateu, I. W. Stewart, and J. Thaler, Phys.Rev. **D87**, 014025 (2013), 1209.3781.

[73] Y. L. Dokshitzer and B. R. Webber, Phys. Lett. **B352**, 451 (1995), hep-ph/9504219.

[74] R. Akhoury and V. I. Zakharov, Phys. Lett. **B357**, 646 (1995), hep-ph/9504248.

[75] G. P. Korchemsky and G. Sterman, Nucl. Phys. **B437**, 415 (1995), hep-ph/9411211.

[76] Z. Ligeti, I. W. Stewart, and F. J. Tackmann, Phys. Rev. **D78**, 114014 (2008), 0807.1926.

[77] J. Dudek, R. Ent, R. Essig, K. Kumar, C. Meyer, et al., Eur.Phys.J. **A48**, 187 (2012), 1208.1244.

[78] A. Accardi, J. Albacete, M. Anselmino, N. Armesto, E. Aschenauer, et al. (2012), 1212.1701.

[79] J. Abelleira Fernandez et al. (LHeC Study Group), J.Phys. **G39**, 075001 (2012), 1206.2913.

[80] T. Becher and M. Neubert, Phys. Rev. Lett. **97**, 082001 (2006), hep-ph/0605050.

[81] T. T. Jouttenus, I. W. Stewart, F. J. Tackmann, and W. J. Waalewijn, Phys.Rev. **D83**, 114030 (2011), 1102.4344.

[82] M. Dasgupta and G. P. Salam, J.Phys.G **G30**, R143 (2004), hep-ph/0312283.

[83] J. Chay and C. Kim, Phys. Rev. **D65**, 114016 (2002), hep-ph/0201197.

[84] A. V. Manohar, T. Mehen, D. Pirjol, and I. W. Stewart, Phys. Lett. **B539**, 59 (2002), hep-ph/0204229.

[85] C. W. Bauer, S. Fleming, C. Lee, and G. Sterman, Phys. Rev. **D78**, 034027 (2008), 0801.4569.

[86] N. A. Sveshnikov and F. V. Tkachov, Phys. Lett. **B382**, 403 (1996), hep-ph/9512370.

[87] G. P. Korchemsky, G. Oderda, and G. Sterman (1997), hep-ph/9708346.

[88] A. V. Belitsky, G. P. Korchemsky, and G. Sterman, Phys. Lett. **B515**, 297 (2001), hep-ph/0106308.

[89] C. M. Arnesen, J. Kundu, and I. W. Stewart, Phys. Rev. **D72**, 114002 (2005), hep-ph/0508214.

[90] J. Chay, C. Kim, Y. G. Kim, and J.-P. Lee, Phys. Rev. **D71**, 056001 (2005), hep-ph/0412110.

[91] C. W. Bauer, C. Lee, A. V. Manohar, and M. B. Wise, Phys. Rev. **D70**, 034014 (2004), hep-ph/0309278.

[92] S. Fleming, A. H. Hoang, S. Mantry, and I. W. Stewart, Phys. Rev. **D77**, 074010 (2008), hep-ph/0703207.

[93] S. Mantry and F. Petriello, Phys.Rev. **D84**, 014030 (2011), 1011.0757.

[94] A. Jain, M. Procura, and W. J. Waalewijn, JHEP **1204**, 132 (2012), 1110.0839.

[95] X.-d. Ji and F. Yuan, Phys.Lett. **B543**, 66 (2002), hep-ph/0206057.

[96] J. C. Collins, Acta Phys. Polon. **B34**, 3103 (2003), hep-ph/0304122.

[97] A. Idilbi and I. Scimemi, Phys.Lett. **B695**, 463 (2011), 1009.2776.

[98] I. Feige, M. D. Schwartz, I. W. Stewart, and J. Thaler, Phys.Rev.Lett. **109**, 092001 (2012), 1204.3898.

[99] S. Fleming, A. H. Hoang, S. Mantry, and I. W. Stewart, Phys. Rev. **D77**, 114003 (2008), 0711.2079.

[100] P. F. Monni, T. Gehrmann, and G. Luisoni, JHEP **1108**, 010 (2011), 1105.4560.

[101] S. D. Ellis, A. Hornig, C. Lee, C. K. Vermilion, and J. R. Walsh, Phys. Lett. **B689**, 82 (2010), 0912.0262.

[102] S. D. Ellis, C. K. Vermilion, J. R. Walsh, A. Hornig, and C. Lee, JHEP **11**, 101 (2010), 1001.0014.

[103] C. W. Bauer, F. J. Tackmann, J. R. Walsh, and S. Zuberi, Phys.Rev. **D85**, 074006 (2012), 1106.6047.

[104] C. W. Bauer and A. V. Manohar, Phys. Rev. **D70**, 034024 (2004), hep-ph/0312109.

[105] T. Becher and M. Neubert, Phys.Lett. **B637**, 251 (2006), hep-ph/0603140.

[106] S. Fleming, A. K. Leibovich, and T. Mehen, Phys.Rev. **D74**, 114004 (2006), hep-ph/0607121.

[107] I. W. Stewart, F. J. Tackmann, and W. J. Waalewijn, JHEP **09**, 005 (2010), 1002.2213.

[108] A. H. Hoang and I. W. Stewart, Phys. Lett. **B660**, 483 (2008), 0709.3519.

[109] G. P. Korchemsky and S. Tafat, JHEP **10**, 010 (2000), hep-ph/0007005.

[110] A. Martin, W. Stirling, R. Thorne, and G. Watt, Eur.Phys.J. **C63**, 189 (2009), 0901.0002.

[111] Z.-B. Kang, X. Liu, S. Mantry, and J.-W. Qiu (2013), 1303.3063.

[112] C. Balzereit, T. Mannel, and W. Kilian, Phys. Rev. **D58**, 114029 (1998), hep-ph/9805297.

[113] M. Neubert, Eur.Phys.J. **C40**, 165 (2005), hep-ph/0408179.

[114] O. Tarasov, A. Vladimirov, and A. Y. Zharkov, Phys.Lett. **B93**, 429 (1980).

[115] S. Larin and J. Vermaseren, Phys.Lett. **B303**, 334 (1993), hep-ph/9302208.

[116] G. P. Korchemsky and A. V. Radyushkin, Nucl. Phys. **B283**, 342 (1987).

[117] S. Moch, J. Vermaseren, and A. Vogt, Nucl.Phys. **B688**, 101 (2004), hep-ph/0403192.

[118] A. Idilbi, X.-d. Ji, and F. Yuan, Nucl.Phys. **B753**, 42 (2006), hep-ph/0605068.

[119] S. Moch, J. Vermaseren, and A. Vogt, JHEP **0508**, 049 (2005), hep-ph/0507039.

[120] T. Huber and D. Maitre, Comput.Phys.Commun. **175**, 122 (2006), hep-ph/0507094.

[121] T. Huber and D. Maitre, Comput.Phys.Commun. **178**, 755 (2008), 0708.2443.